Square-planar Co(III) in $\{O_4\}$ Coordination: Large ZFS and Reactivity with ROS

Supporting Information

Jennifer L. Steele, Laleh Tahsini, Chen Sun, Jessica K. Elinburg, Christopher M. Kotyk, James McNeely, Sebastian A. Stoian, Alina Dragulescu-Andrasi, Andrew Ozarowski, M. Ozerov, J. Krzystek, Joshua Telser, Jeffrey W. Bacon, James A. Golen, Arnold L. Rheingold, and Linda H. Doerrer

Table of Contents

Experimental

Synthetic procedures.

All methods to produce $[Co^{II}(Hpfa)]^{2-}$ were completed in air under ambient conditions, and the syntheses to produce $[Co^{III}(pin^F)_2]^-$ were carried out using standard Schlenk and glove box techniques. CH_3CN, Et_2O, and EtOH used for the syntheses completed in air were used without further purification. CH_3CN used for air-free syntheses was distilled twice, once from P_2O_5 and once from CaH_2, and then stored over molecular sieves. The anhydrous solvents CH_2Cl_2 and THF, used for air-free synthesis, were dried in an alumina-based solvent purification system (SPS) under Ar, piped directly into a N_2-filled MBraun glovebox, and stored over molecular sieves. Hydrogen peroxide, $OC(CF_3)_2{\cdot}3H_2O$, $[Me_4N][OH]{\cdot}5H_2O$, $[^nBu_4N][PF_6]$, and CoI_2 were obtained commercially and used without any further purification. Ultra-high purity O_2 was supplied by Airgas for O_2 studies. $[Me_4N]_2[Co(pin^F)_2]$ was prepared as previously reported.[1, 2] UV-vis data were collected with a Shimadzu UV-3600 spectrometer. NMR spectra were measured using Varian 400 and 500 MHz spectrometers and prepared in CD_3CN which was stored over sieves under N_2. Solution phase magnetic susceptibilities were determined via the Evans method[3, 4] in CD_3CN and reported after appropriate diamagnetic corrections. Elemental analyses were performed by Atlantic Microlabs, Inc. (Norcross, Georgia). Electrochemical data was collected using a three-electrode cell connected to an external CHI 630C potentiostat run by a personal computer with CHI software. Unless otherwise noted, all data were collected using a glassy carbon electrode (0.5 mm diameter) as the working electrode, $Ag/AgNO_3$ as the reference electrode, a platinum counter electrode, and $TBAPF_6$ as the electrolyte. IR spectra were collected on a Nicolet FT-IR with ATR attachment.

$[Me_4N]_2[Co(Hpfa)_4]$ (3). *Method A: Synthesis from $[Me_4N]_2[Co(pin^F)_2$ in CH_3CN under ambient conditions*. $[Me_4N]_2[Co(pin^F)_2]$ (142 mg, 0.163 mmol) was dissolved in CH_3CN (10 mL) under ambient conditions. After several days, the unstirred solution turned from magenta to orange and finally to purple. Solvent was then removed on a rotary evaporator. The purple residue was extracted with CH_3CN and layered with Et_2O. A purple crystalline solid was obtained in 61% yield (93.1 mg) after lowering temperature to 10 °C.

Method B: Direct synthesis from CoI_2. H_2pfa (1.00 mL, 7.17 mmol) and $Me_4NOH{\cdot}5H_2O$ (1.27 g, 7.01 mmol) in EtOH (10mL) were combined in EtOH (20 mL) and stirred for 0.5 h. This mixture was then added dropwise to anhydrous CoI_2 (553 mg, 1.77 mmol) dissolved in EtOH (20 mL). The solution was stirred for 2 h and then filtered. The purple precipitate was extracted with CH_3CN

and layered with Et_2O. A purple crystalline solid was obtained in 41% yield (684 mg) after recrystallization overnight at 10 °C, and pure material was obtained after a second crystallization from CH_3CN and Et_2O. Anal. Calculated: $C_{20}H_{28}N_2O_8F_{24}Co$: C 25.57; H 3.00; F 48.54. Found: C 25.46; H 3.02; F 48.31. ^1H NMR (CD_3CN, 20 °C) δ 2.17 (s, OH, 4H), 3.02 (s, Me_4N, 12H). μ_{eff} (CD_3CN, 20 °C): 4.75 μ_B. IR (cm^{-1}) 3150 (br), 1488 m, 1311 m, 1288 m, 1186 s, 1074 s, 959 s, 720 m. UV-vis (λ_{max}, nm (ε, M^{-1} cm^{-1})):481 (133), 567 (165).

Samples of $(Me_4N)[Co(Hpfa)_4]$, **3**, with ^{18}O incorporated were prepared as above by method A except as described below.

For reaction with $H_2(^{18}O)$, $[Me_4N]_2[Co(pin^F)_2]$ (97 mg, 0.11 mmol) was dissolved in dry MeCN (3 mL) in an N_2-filled glovebox, fitted with a rubber septum, and transferred to a Schlenk line. 50 μL of $H_2(^{18}O)$ (2.5 mmol) stored in a sealed vial were added by syringe transfer. An O_2-filled balloon (natural abundance) was fitted to the stirred reaction for one hour. The balloon was removed and the reaction was sealed and allowed to stir overnight at room temperature. The resulting purple solution was layered with Et_2O and stored at 15 °C overnight to produce $(Me_4N)[Co(Hpfa)_4]$ as purple crystals.

For reaction with $^{18}O_2$, $[Me_4N]_2[Co(pin^F)_2]$ (105 mg, 0.121 mmol) was dissolved in dry MeCN (3 mL) in an N_2-filled glovebox, fitted with a rubber septum, and transferred to a Schlenk line. 50 μL of degassed H_2O (2.5 mmol) were added by syringe transfer. An $^{18}O_2$-filled balloon was fitted to the stirred reaction for 15 min. The balloon was removed and the reaction was sealed and allowed to stir overnight at room temperature. The resulting purple solution was layered with Et_2O and stored at 15 °C overnight to produce $(Me_4N)[Co(Hpfa)_4]$ as purple crystals.

$[Me_4N][Co(pin^F)_2]$ (2). A solution of $[Me_4N]_2[Co(pin^F)_2]$ (102 mg, 0.117 mmol) in a mixture of THF (7 mL) and CH_3CN (2 mL) was added to a solution of $AgPF_6$ (29 mg, 0.115 mmol) in THF (3 mL). The pink solution was allowed to stir for 1 hour under inert atmosphere while minimizing exposure to light. Solvent was then removed *in vacuo*, and the resulting orange residue was extracted with THF. Yellow-orange crystals were obtained in 54% yield (50 mg) by layering the THF solution onto CH_2Cl_2 and lowering the temperature to -20°C overnight. Anal. Calculated: $C_{16}H_{12}NO_4F_{24}Co$: C 24.10; H 1.52; N 1.76; F 57.20. Found: C 24.32; H 1.47; N 1.89; F 57.06. ^1H NMR (CD_3CN, 20 °C) δ 3.05 (s, Me_4N, 12H). μ_{eff} (CD_3CN, 20 °C): 3.63 μ_B. IR (cm^{-1}): 1489 w, 1256 m, 1226 s, 1196 s, 1151 m, 1079 m, 1046 w, 990 w, 950 m, 876 m, 766 m, 735 w, 726 w, 709 s. UV-vis (λ_{max}, nm (ε, M^{-1} cm^{-1})): 406 (3790).

$(Me_4N)[Co(Pin^F)_2]$ generation from the reaction of 2 with H_2O_2.

To a solution of $(Me_4N)_2[Co(pin^F)_2]$ (2.61 mg, 1.00 mM) in dry CH_3CN (3 mL), 15.0 µL of a stock solution (200 mM) of H_2Pin^F in H_2O was added. After collecting the spectral data, 15.0 µL of a stock solution (200 mM) of H_2O_2 in H_2O was introduced and the spectra were collected over an hour (Figure 2). To this solution, Me_4NOH (0.54 mg, 1.00 mM) was then added in dry CH_3CN and the spectral changes due to the formation of **3** were recorded for one hour (Figure S3).

X-ray Crystallography

Data for **2** were collected at 100K using a Bruker Proteum-R diffractometer with Cu K_α radiation (λ = 1.54178 Å). A multi-scan absorption correction was applied using SADABS.[5] Non-hydrogen atoms were located using atom-independent direct methods.[6] The $(Me_4N)^+$ cation was located on a mirror plane and refined using the PART -1 instruction with bond distance and angle restraints in SHELXL.[7] Hydrogen atoms were located via difference Fourier synthesis and refined using a riding model. Crystal data and refinement details are given in Table S2.

For **3**, a purple crystal of LT-I-24B was mounted on a Cryoloop with Paratone-N oil and data were collected on a Bruker APEX II CCD system using Mo K_α radiation at -183°C. Data were corrected for absorption with SADABS and the structure was solved by direct methods. All non-hydrogen atoms were refined anisotropically by full matrix least squares on F^2. Hydrogen atoms on O5, O6, O7, O8, and O9 were found from a Fourier difference map and were refined with fixed distance of 0.86 Å. All other hydrogen atoms were placed in calculated positions with appropriate riding models. Structural refinement and solution indicates a merohedral twin with monoclinic unit cell with β angle of 90.009º. The twin law of -1 0 0 , 0 -1 0 , 0 0 1 was employed with BASF ratio of 50.94 / 49.06.

Mass Spectrometry

Samples were run using either negative mode electrospray (ESI) or Direct Analysis in Real Time (DART) on an AccuTOF time-of-flight (TOF) mass spectrometer (JEOL USA, Inc., Peabody, MA, USA). The resolving power was ~6000 (FWHM definition), measured using Fomblin Y (Sigma Aldrich) for DART or PEG 600 for ESI measurements.

Samples for DART were sampled directly by dipping the closed end of a melting point capillary into a sample solution and positioning the sample-coated tube between the DART ion source and the detector inlet. The DART ion source was operated with helium gas (Airgas, Cambridge, MA, USA) at 400°C.

Samples analyzed by ESI were introduced using a syringe fitted with a luer lock fitting directly into the top of the ESI capillary using a zero volume fitting. A mass spectrum of Fomblin Y was obtained with each data acquisition for DART and PEG 600 for ESI to help aid potentially drifts in calibration. Orifice 1 operated at varying voltages in order to minimize fragmentation, orifice 2 = 5 V, and ring lens =3 V were constant for all measurements.

The RF ion guide voltage was generally set to 800 V, to allow detection of ions greater than *m/z* 80.

Magnetic Measurements. Direct-current (dc) magnetic susceptibility and low-temperature (2-30 K) magnetization data were obtained using a quantum interference device (SQUID) magnetometer (MPMS-XL, Quantum Design). The susceptibility was measured in an applied-field of 0.1 T from 1.8 K to RT at a cooling/warming rate of 2 K/min. The experimental data was corrected for the contributions of the sample holder and for that of the intrinsic diamagnetism. The later value, χ_{dia} = -319 cm^3/mol, was obtained using the tabulated Pascal constants.[8] The fit of the magnetic susceptibility was obtained using the JulX program written by Dr. Eckard Bill. The reduced-magnetization data was simulated using an in-house written program.

FIRMS. Far InfraRed Magnetic Spectroscopy was performed at the National High Magnetic Field Laboratory on a 17 T vertical-bore superconducting magnet using a Bruker Vertex 80v Fourier-transform infrared spectrometer. The evacuated (~4 mBar) optical beamline was used for their coupling and the experimental set-up was equipped with a mercury lamp and a composite silicon bolometer (Infrared Laboratories) as a THz radiation source and detector, respectively. Eicosane pellets containing the studied compound were measured in the spectral region between 18 and 730 cm^{-1} (0.55 – 22 THz) with a resolution of 0.3 cm^{-1} (9 GHz). Both sample and bolometer were cooled by low-pressure helium gas to a temperature of 4.6 K. Transmittance spectra were calculated as the THz intensity spectrum at each magnetic field divided by the THz intensity spectrum averaged for all fields.

Computational Methods

General Computational Considerations

The ORCA electronic structure suite, version 4.0, was used for all calculations.[9, 10] The highly efficient resolution of identity (RI) and "chain of spheres" (COSX) approximations for the Coulomb and Exchange integrals respectively were employed (RIJCOSX[11-13]). The cc-pVDZ/cc-pVTZ[14-16] basis sets were employed for all DFT calculations along with an automatically generated auxiliary basis set for the RI calculations, which is the so-called "AutoAux" technique in ORCA parlance. All CASSCF and NEVPT2 calculations were performed with the scalar relativistic DKH Hamiltonian,[17] the relativistically recontracted DKH-def2-TZVP basis set,[18] and an "AutoAux" auxiliary basis set. Picture change effects were included in the calculation of the spin-orbit coupling

All DFT calculations employed the PBE0[19] hybrid functional. The CASSCF wave functions were converged to the default energy tolerance of $1.00 * 10^{-7}$ Hartree and an orbital gradient of 0.001. Dynamic correlation was introduced with the strongly contracted version of N-electron valence perturbation theory (SC-NEVPT2) and the quasi-degenerate NEVPT2 (QD-NEVPT2) approaches. None of the orbitals were frozen for the NEVPT2 calculations. Spin Hamiltonian parameters were extracted from the *ab-initio* results using the Effective Hamiltonian approach.[2, 20]

We also note here that throughout the rest of this document, the $^3B_2$ and $^3B_3$ labels are used to describe the first and second excited triplet states for **2**. These labels are derived from the pseudo-D_2 symmetry for the inner coordination sphere of the metal center.

DFT Calculations

Geometries were optimized at the PBE0/cc-pVTZ/RIJCOSX level. The equilibrium structures are shown in Tables S20-S22. Each of the equilibrium structures was confirmed as a local minimum

based on inspection of the calculated harmonic vibrational frequencies. The experimental structure (**2**) has the best agreement with the equilibrium structure for the triplet geometry (^{3}**2**). The relevant structural parameters are shown in Table S4.

The energies of ^{3}**2**, ^{1}**2**, and ^{5}**2** also confirm that **2** is best described as an intermediate spin triplet. The energies at the PBE0/cc-pVTZ/RIJCOSX level are E (^{3}**2**) = 0.0 kcal/mol < E (^{5}**2**) = 15.8 kcal/mol < E (^{1}**2**) = 38.9 kcal/mol.

The ground state PBE0/cc-pVTZ/RIJCOSX spin density for ^{3}**2** is shown in Figure S8. Figure S8 clearly shows that the magnetic orbitals are best described as $3d_{xz}$ and $3d_{yz}$. The $3d_{x^2-y^2}$ and $3d_{z^2}$ orbitals are doubly occupied and the $3d_{xy}$ orbital is unoccupied. The quasi-restricted [21] valence space is shown in Figure S9.

State-Specific Active Space

A number of state-specific CASSCF active spaces were sampled to investigate the interactions between the PIN^F ligands and the Co(III) center in **2**. We have started with a minimal active space consisting solely of the metal d-orbitals correlated with six electrons for a CASSCF(6,5) active space. Next, a σ orbital was introduced that partnered with the antibonding $3d_{xy}$ orbital for a CASSCF(8,6) calculation. Then a full double d-shell was added to help address some dynamic correlation for the metal d-orbitals for a so-called CASSCF(8,11) calculation. Following this calculation, the orbitals in the double shell that balanced the weakly occupied 3d orbitals ($3d_{xy}$, $3d_{xz}$, $3d_{yz}$) were removed for a CASSCF(8,8) calculation. Next, a pair of π-bonding orbitals were added to balance the π^* $3d_{xz}$ and $3d_{yz}$ orbitals for a CASSCF(12,10) calculation. Finally, the full double-shell was re-introduced for a CASSCF(12,13) calculation. The natural orbitals for the different active spaces are shown in Figures S20-S25 along with the natural orbital occupation numbers (NOON) and the metal contribution to the NOs based on Löwdin population analysis.

These calculations were also performed for ^{3}**2**, and the resulting wave functions were very similar (ΔNOON $\leq$ 0.01, ΔCo% $\leq$ 0.5). A summary of the Löwdin charges and spin populations is shown in Table S5.

With the exception of the σ^* ($^{3}d_{xy}$) NO, the d-shell NOs are highly ionic throughout the range of active spaces. Upon introduction of a σ-bonding counterpart to the active space, the cobalt percentage of the σ^* NO drops from 81.1 to 74.6, and it remains between 70% and 75% for the rest of the active spaces sampled.

One of the non-bonding d-shell NOs ($^{3}d_{x^2-y^2}$) contains approximately constant cobalt composition throughout as expected. The other non-bonding d-shell NO ($^{3}d_{z^2}$) becomes slightly more ionic when a double d-shell is added to the active space. This increase in cobalt composition is accompanied by a reduction in hybridization (4s contribution drops from 5 to 2 %), presumably because the double d-shell ($^{4}d_{z^2}$) competes with the non-bonding NO for the 4s orbital. It appears that this reduction in hybridization prevents the orbital from interacting as effectively.

The magnetic π^* d-shell NOs ($^{3}d_{xz}$ and $^{3}d_{yz}$) are unaffected by the introduction of the double d-shell NOs, but they have a slight increase in covalency when their π-bonding counterparts are added to the active space. While this affect is small for the ground state, it might impact the excited states and thus the magnetic properties of the system, so these extended active spaces were also tested for the calculation of magnetic properties

NEVPT2 State-Averaged Over Three Lowest Roots

NEVPT2 calculations were performed on top of CASSCF(12,10) and CASSCF(12,13) averaged over the three lowest triplet roots on **2**. The description of the excited states is included in the main text, and the natural orbitals (NO) are shown in Figure S16 along with NOONs for CASSCF(12,10). The energies of the $^3B_2$ and $^3B_3$ calculated at this level are shown in Table S15.

Inspection of Tables S13 and S14 does show some noticeable differences between the two methods. Although the SA(3)-NEVPT2(12,13) calculations were closer to the experiment with regard to g_{iso} and D, the SA(3)-NEVPT2(12,10) was able to reproduce the rhombicity more accurately. We have chosen to report the SA(3)-NEVPT2(12,10) results due to this technique's great economy relative to the SA(3)-NEVPT2(12,13) calculations, and because of its superior treatment of the rhombicity, and 'suitable' treatment of the ***g***-tensor and axial ZFS parameter D.

CASSCF/NEVPT2 Averaging Regime

The active space and averaging regime reported in the main text were chosen with care. While the previous section convinced us the minimal active space (CASSCF(6,5)) is sufficient to describe the ground state electronic structure of the system, the magnetic properties of the system were still calculated using extended active spaces described in the previous section. The minimal active space should, however, suffice to explore the averaging regime used for subsequent calculations. We have thus explored the magnetic properties of **2** calculated via NEVPT2 on top of CASSCF(6,5) reference wave functions under different averaging regimes. The active space will be extended once again following the choice of averaging.

The first, and the most obvious, choice of averaging was a "full" average over all 5 quintet states, 45 triplet states, and 50 singlet states (herein referred to as SA(5,45,50)-NEVPT2(6,5). The contributions to the spin-orbit coupling from each of these states are shown in Table S6.

It can clearly be seen from Table S6 that the quintet block and many of the higher-lying excited roots in the singlet and triplet block contribute very little to the ZFS for **2**. As a first reduction in the averaging space, we have eliminated 15 of the singlet roots and 10 of the triplet roots, which corresponds to eliminating the second set of the free ion ^{3}P, ^{3}F, ^{1}G, ^{1}D, and ^{1}S terms. This results in an averaging of 5 quintet states, 35 triplet states, and 35 singlet states. The

contribution of these states to the ZFS calculated at the SA(5,35,35)-NEVPT2(6,5) level is shown in Table S7. The discrepancy between the two averaging regimes is shown in Table S8.

The discrepancy is significant, and is predominately due to the contributions from the first and second excited triplet states. Although there is a significant discrepancy, the total ZFS calculated with each regime is of the same order of magnitude. It is presumed that some of the higher-lying roots worsen the description of the first and second excited triplet states. Therefore, we further moved to eliminate more roots before expanding the active space.

We have thus chosen to only include the lowest free ion states (^{5}D, ^{3}H, ^{1}I) in the averaging for a SA(5,11,13)-NEVPT2(6,5) calculation. This reduction serves three purposes: 1) The SC-NEVPT2 calculations using canonical orbitals for each state is far cheaper; 2) As has already been shown, the main contributions to the ZFS in **2** arise from the $^3B_2$ and $^3B_3$ states that should be described more accurately with a reduced averaging regime; 3) When the active space is expanded in the following section, a reduced averaging regime will prevent charge-transfer excited states from entering the conversation, and should allow for more direct comparison between different active spaces. The resulting contributions to the ZFS and discrepancy with the SA(5,45,50)-NEVPT2(6,5) calculations are shown in Tables S8 and S9.

Finally, we have chosen to reduce the averaging regime to the three lowest triplet roots that are the main source of the ZFS observed in the system. The contributions of each root in the SA(3)-NEVPT2(6,5) calculation is shown in Table S11.

The magnetic parameters calculated with each of the four averaging regimes are summarized in Table S12 along with the experimental parameters. Table S13 shows the relative energies of the two lowest excited triplet states ($^3B_2$, $^3B_3$) calculated with the four different regimes.

Table S12 shows that each of the averaging regimes over-estimates the isotropic g-value. This is a common deficiency of CASSCF wave functions that tend to describe metal centers as being too ionic. The magnitude of the experimental ZFS agrees best with the "full" state-averaging [SA(5,45,50)]. However, we have proceeded under the notion that the relative inaccuracy of the smaller averaging regime [SA(5,11,13)] will be reduced when the reference CASSCF wave function is described more accurately by expanding the active space. As will be shown below, this is exactly what happened.

State-Averaged CASSCF/NEVPT2 Active Space Choice

In the previous section, we showed that upon reducing the number of states averaged in the CASSCF calculation, the ZFS parameters and isotropic *g*-value systematically get larger. It was also shown, however, that most of the high-lying states in both the triplet and singlet blocks only gave miniscule contributions to the ZFS. We therefore posit that the enhanced agreement between the experimental results and the SA(5,45,50)-NEVPT2(6,5) was fortuitous. The inferior description of the first and second excited triplet states using the SA(5,45,50)-NEVPT2 calculation helped push up the energies of the $^3d_{xz}$ and $^3d_{yz}$ orbitals, which mimics the action of including a π-bonding counterpart to these orbitals in the active space.

In this section, we will show that upon expanding the active space to CASSCF(12,10)/CASSCF(12,13), the SH parameters averaged over 5 quintet, 11 triplet, and 13 singlet states/3 triplet states were in much better agreement with experiment than the SA(5,11,13)/SA(3)-NEVPT2(6,5) results. Table S14 shows the magnetic parameters calculated at the SA(5,11,13)-NEVPT2(6,5), SA(5,11,13)-NEVPT2(8,6), SA(5,11,13)-NEVPT2(8,8), SA(5,11,13)-NEVPT2(8,11), SA(5,11,13)-NEVPT2(12,10), SA(5,11,13)-NEVPT2(12,13) ,

SA(3)-NEVPT2(12,10), and SA(3)-NEVPT2(12,13) levels. The energies of the $^3B_2$ and $^3B_3$ states are shown in Table S15.

The information in Tables S13 and S14 provides an interesting story. When a σ-bonding orbital is added to the active space that couples with the $^3d_{xy}$ orbital, which is formally unoccupied in single-reference methods, the calculated SOC is slightly increased. This is accompanied by a stabilization of both the $^3B_2$ and $^3B_3$ states. It can also be seen from Figures S20 and S21 that the cobalt magnetic orbitals are slightly more ionic in the ground state after this expansion. All of this matches well with the observed increase in ZFS when going from SA(5,11,13)-NEVPT2(6,5) to SA(5,11,13)-NEVPT2(8,6).

The ZFS and energies of the $^3B_2$ and $^3B_3$ states are very similar in the SA(5,11,13)-NEVPT2(8,8) and SA(5,11,13)-NEVPT2(8,11) calculations although there is a reversal in sign in *D*. In each case the magnitude of the ZFS is reduced, but the isotropic *g*-value is increased. It can also be seen that the energies of the both $^3B_2$ and $^3B_3$ states are significantly reduced, but the $^3B_3$ state is reduced to a far larger extent (> 650 cm^{-1}). One would expect, therefore, that the axial ZFS would go up and the rhombicity would be reduced, but the opposite effect is observed. It is also observed that when introducing the double d-shell, the ground state multiplicity as predicted by CASSCF changes from the quintet to the triplet block. This confirms that the introduction of the double d-shell accounts for some correlation effects in the zeroth order non-relativistic wave function which should improve the treatment with NEVPT2.

When we move ahead to the SA(5,11,13)-NEVPT2(12,10) calculation, there is an abrupt decrease in the ZFS and principal *g*-values accompanied by an increase in the energies of the $^3B_2$ and $^3B_3$ states. This change is even more enhanced when moving to the SA(5,11,13)-NEVPT2(12,13) results. This confirms that the inclusion of the π-bonding counterpart to the

magnetic $3d_{xz}$ and $3d_{yz}$ orbitals is essential to accurately describe the $^3B_2$ and $^3B_3$ states. The source of the discrepancy between the SH parameters calculated with the SA(5,11,13)-NEVPT2(12,10) and SA(5,11,13)-NEVPT2(12,13) is evident in the ground state wavefunctions displayed in Figures S23 and S24. There is an increased amount of π-covalency in the CASSCF(12,13) wave function, which is expected to push up the energies of the $^3B_2$ and $^3B_3$ states, which should in turn decrease the ZFS. As mentioned before, with the results from CASSCF(12,13) zeroth-order wave functions might be more accurate, the benefit(s) from their use is easily outweighed by the extreme cost of the calculations. The contributions of each state to the ZFS are shown in Tables S15 and S16, with the contributions for SA(3)-NEVPT2(12,10)/SA(3)-NEVPT2(12,13) shown in Tables S17 and S18.

These observations all point to the necessity of including the π-bonding orbitals in the active space. Given the large magnitude of the SOC observed in this system, very small changes in electronic structure have a large effect on the ZFS. A forthcoming publication will address the electronic structure, magnetostructural correlations, and computational guidelines of this and related systems in greater detail.

QD-NEVPT2

Quasi-degenerate strongly-contracted N-electron valence perturbation theory (QD-NEVPT2[22]) was employed to try and improve the theoretical description of the ***g***-tensor for **2**. These calculations were performed on top of CASSCF(12,10) averaged over 5 quintet, 11, triplet, and 13 singlet states [SA(5,11,13)-CASSCF(12,10)]. These calculations used a non-Hermitian effective Hamiltonian and default CI truncation and linear dependency thresholds. The susceptibility curves estimated with 'direct' QD-NEPVT2 and SC-NEVPT2 were nearly identical, and are therefore not

shown. The energies of the $^3B_2$ and $^3B_3$ states calculated at the QD-NEVPT2 level are 2202 and 3930 cm^{-1} respectively, as compared with 2223 and 3883 cm^{-1} at the SC-NEVPT2 level.

Ab Initio Ligand Field Theory (AILFT)

Ab initio ligand field theory,[23, 24] recently implemented in ORCA, was used to relate the computational results to standard inorganic parameters and look at the ligand field splitting in **2**. Unfortunately, the calculations were unsuccessful. There was high error in the agreement between the ligand field energies and the ab-initio energies (0.72 eV total RMS error). The ligand field splitting that was calculated was in qualitative disagreement with the ground state electronic structure calculated using DFT, state-specific NEVPT2, and SA(3)-NEVPT2(12,10). We are currently assessing the source of the observed error, but one possibility is anisotropic π-donation from the PIN^F ligands.

Basis Set, Structural, and Relativistic Checks

Shown in Table S20 are the SH parameters calculated with a number of different basis sets both with and without scalar relativistic effects. We have also performed SA(5,11,13/3)-NEVPT2(12,10) calculations on a model of **2** that included the counter-cation. Little variation in the magnetic parameters is observed with the introduction of the counter-ion to the model. It can also be seen that for the SA(3)-NEVPT2(12,10) calculations, little is gained by moving from the DKH-DEF2-TZVP to DKH-DEF2-QZVPP level.

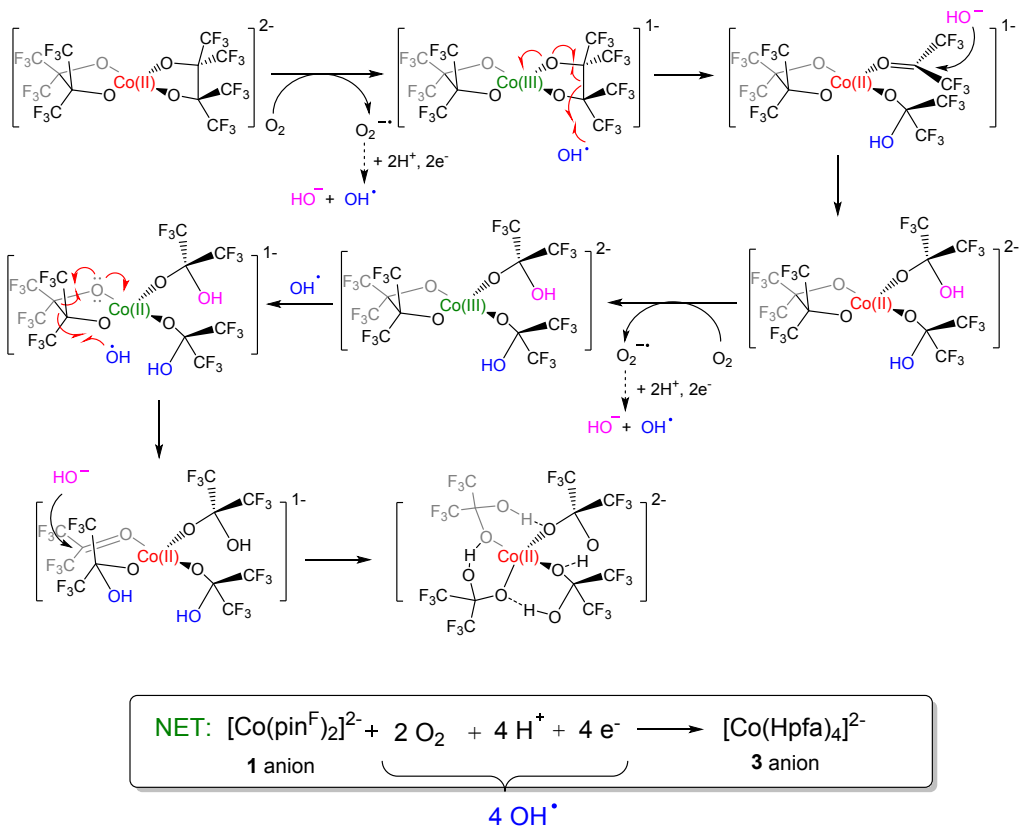

Scheme S1. Proposed role of hydroxyl radical in formation of **3** from **1** via **2.**

Scheme S1. One possible mechanism of oxidative cleavage. This process is proposed to begin with outer sphere electron transfer from **1** (i.e., Co(II)) to O_2 or H_2O_2 forming **2** (i.e., Co(III)). The superoxide anion, $O_2^{\bullet-}$, is readily protonated and reduced, and can then decompose to give a hydroxyl radical and alkoxide anion. Alternatively, when H_2O_2 is reduced by one electron, spontaneous cleavage to a hydroxyl radical and hydroxide anion could occur. Whatever the source, a hydroxyl radical can attack the relatively weak C-C bond of $[pin^F]^{2-}$, effecting C-C cleavage and forming hexafluoroacetone (along with $(CF_3)_2C(OH)O^-$; see upper right structure). This ketone is susceptible to nucleophilic attack by hydroxide to form the second $[Hpfa]^-$ ligand. Repeating the oxidation, hydroxyl, and hydroxide additions on the other $[pin^F]^{2-}$ ligand results in formation of $[Co^{II}(Hpfa)_4]^{2-}$, the anion of **3** (see last structure). Thus the two $[pinF]^{2-}$ ligands are converted to four $[Hpfa]^-$ ligands, as shown in the net reaction (at bottom). The mechanism may not include exclusively hydroxyl radicals as the key ROS, as $HO^{\bullet}$ has a very short lifetime under the observed conditions, but it is likely that ROS are responsible for overall C-C bond cleavage and C-O bond formation.

References:

1. L. Tahsini, S. E. Specht, J. S. Lum, J. J. M. Nelson, A. F. Long, J. A. Golen, A. L. Rheingold and L. H. Doerrer, *Inorganic Chemistry*, 2013, **52**, 14050-14063.
2. V. Vallet, L. Maron, C. Teichteil and J.-P. Flament, *J. Chem. Phys.*, 2000, **113**, 1391-1402.
3. D. F. Evans, *J. Chem. Soc.*, 1959, 2003-2005.
4. S. K. Sur, *J. Magn. Reson.* , 1989, **82**, 169-173.
5. L. Krause, R. Herbst-Irmer, G. M. Sheldrick and D. Stalke, *J. Appl. Crystallogr.*, 2015, **48**, 3-10.
6. G. M. Sheldrick, *Acta Crystallogr., Sect. A: Found. Crystallogr.*, 2008, **64**, 112-122.
7. G. M. Sheldrick, *Acta Crystallogr., Sect. C: Struct. Chem.*, 2015, **71**, 3-8.
8. E. Bill, *JulX*, https://cec.mpg.de/en/research/molecular-theory-and-spectroscopy/dr-eckhard-bill/
9. F. Neese, *ORCA – An Ab Initio, DFT and Semiempirical SCF-MO Package, Ver. 4.0*, Max Planck Institute for Chemical Energy Conversion, Mülheim a. d. Rurh, Germany, 2017, pp.
10. F. Neese, *WIREs Comput Mol Sci*, 2012, **2**, 73-78.
11. D. Ganyushin, N. Gilka, P. R. Taylor, C. M. Marian and F. Neese, *J. Chem. Phys.*, 2010, **132**, 144111.
12. S. Kossmann and F. Neese, *Chem. Phys. Lett.*, 2009, **481**, 240-243.
13. F. Neese, F. Wennmohs, A. Hansen and U. Becker, *Moving Frontiers in Quantum Chemistry:*, 2009, **356**, 98-109.
14. N. B. Balabanov and K. A. Peterson, *J. Chem. Phys.*, 2006, **125**, 074110.
15. N. B. Balabanov and K. A. Peterson, *J. Chem. Phys.*, 2005, **123**, 064107.
16. T. H. Dunning, *J. Chem. Phys.*, 1989, **90**, 1007-1023.
17. B. A. Hess, *Phys. Rev. A*, 1986, **33**, 3742-3748.
18. D. A. Pantazis, X.-Y. Chen, C. R. Landis and F. Neese, *J. Chem. Theory Comput.*, 2008, **4**, 908-919.
19. A. D. Becke, *J. Chem. Phys.*, 1993, **98**, 1372-1377.
20. R. Maurice, R. Bastardis, C. d. Graaf, N. Suaud, T. Mallah and N. Guihéry, *J. Chem. Theory Comput.*, 2009, **5**, 2977-2984.
21. F. Neese, *J. Am. Chem. Soc.*, 2006, **128**, 10213-10222.
22. C. Angeli, S. Borini, M. Cestari and R. Cimiraglia, *J. Chem. Phys.*, 2004, **121**, 4043-4049.
23. M. Atanasov, J. M. Zadrozny, J. R. Long and F. Neese, *Chem. Sci.*, 2013, **4**, 139-156.
24. M. Atanasov, D. Ganyushin, K. Sivalingam and F. Neese, in *Molecular Electronic Structures of Transition Metal Complexes II*, eds. D. M. P. Mingos, P. Day and J. P. Dahl, Springer Berlin Heidelberg, Berlin, Heidelberg, 2012, pp. 149-220.
25. B. Ramdhanie, L. N. Zakharov, A. L. Rheingold and D. P. Goldberg, *Inorg. Chem.*, 2002, **41**, 4105-4107.
26. L. H. Doerrer, M. T. Bautista and S. J. Lippard, *Inorg. Chem.*, 1997, **36**, 3578-3579.
27. S. E. Harnung and E. Larsen, *Inorg. Chem.*, 2007, **46**, 5166-5173.
28. P. J. M. W. L. Birker, J. J. Bour and J. J. Steggerda, *Inorg. Chem.*, 1973, **12**, 1254-1259.
29. M. A. García-Monforte, I. Ara, A. Martín, B. Menjón, M. Tomás, P. J. Alonso, A. B. Arauzo, J. I. Martínez and C. Rillo, *Inorg. Chem.*, 2014, **53**, 12384-12395.

30. F. L. Benedito, T. Petrenko, E. Bill, T. Weyhermüller and K. Wieghardt, *Inorg. Chem.*, 2009, **48**, 10913-10925.
31. P. O. Lagaditis, B. Schluschaß, S. Demeshko, C. Würtele and S. Schneider, *Inorg. Chem.*, 2016, **55**, 4529-4536.
32. J. Bendix, M. Brorson and C. E. Schäffer, *Inorg. Chem.*, 1993, **32**, 2838-2849.
33. J. Krzystek, J. Telser, L. A. Pardi, D. P. Goldberg, B. M. Hoffman and L.-C. Brunel, *Inorg. Chem.*, 1999, **38**, 6121-6129.

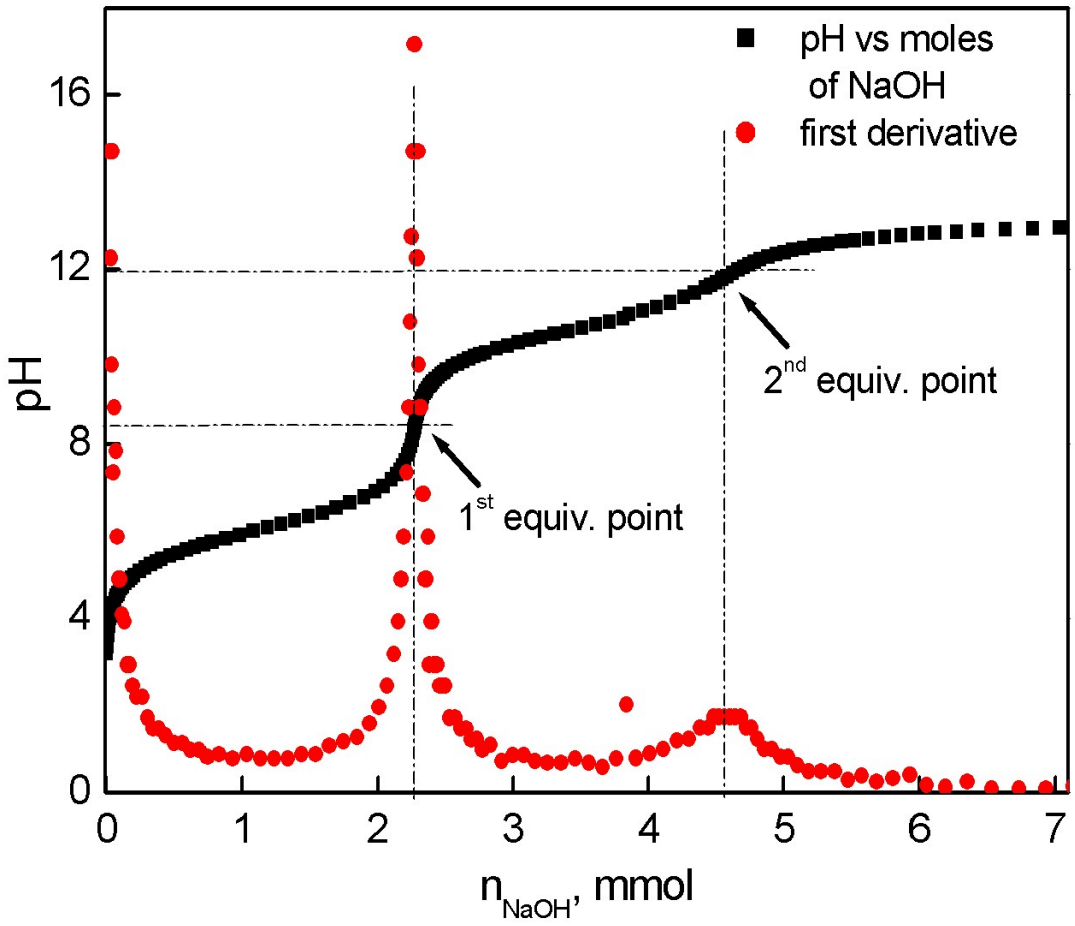

Figure S1. Titration of H_2Pin^F with NaOH.

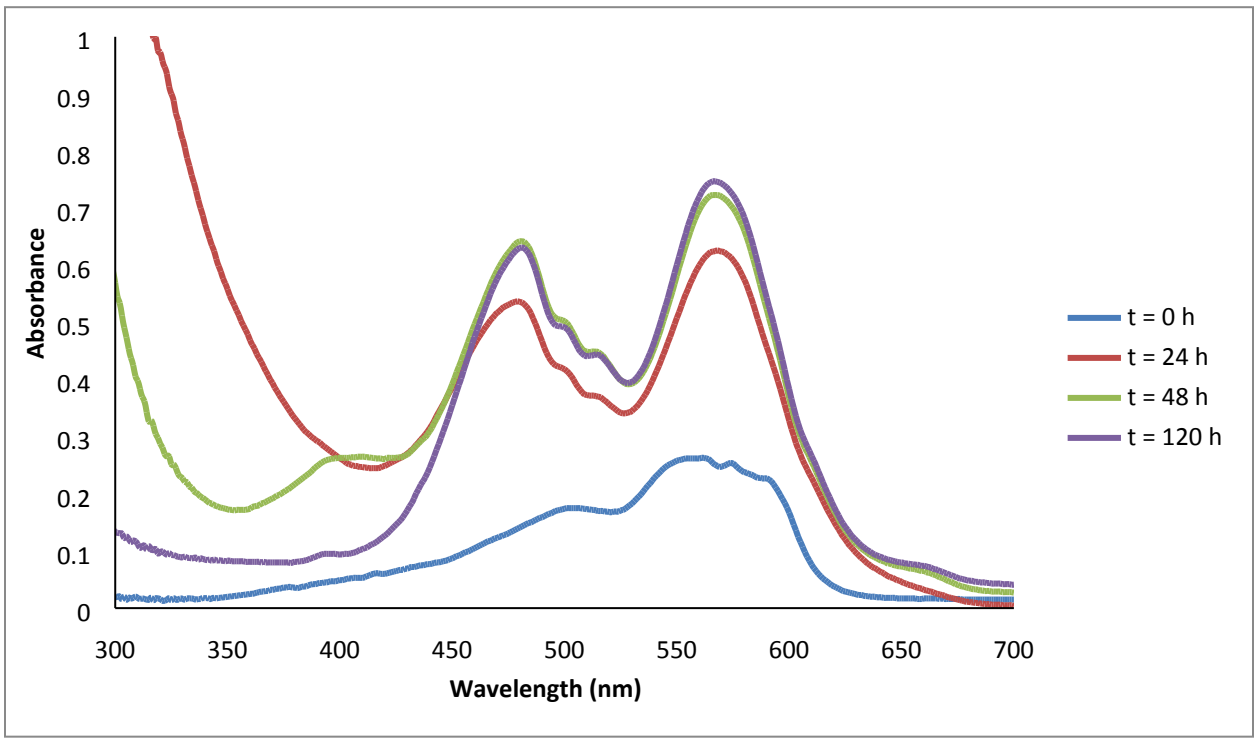

Figure S2. UV-vis spectra of conversion of $[Co(pin^F)_2]^{-2}$ (**1**) (5 mM) to compounds **3** and **2** in distilled MeCN exposed to ambient conditions. Blue shows **1**; Green and Red show a mixture of **3** and **2**; Purple shows **3**.

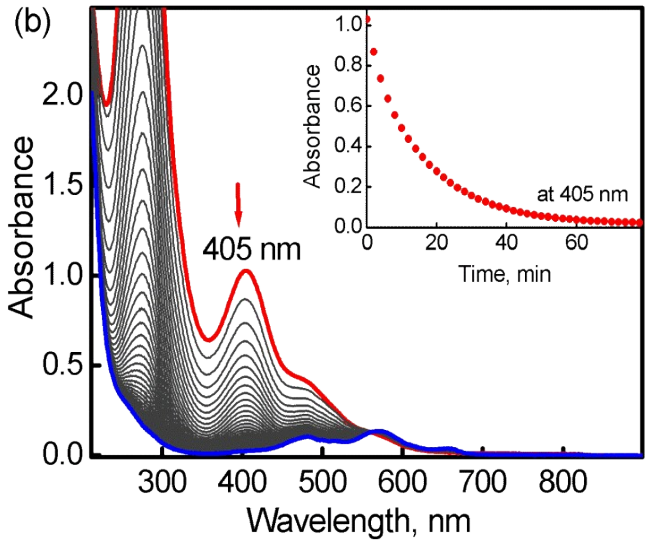

Figure S3. UV-vis spectral changes of conversion of **2** to **3** effected by Me_4NOH in CH_3CN solution.

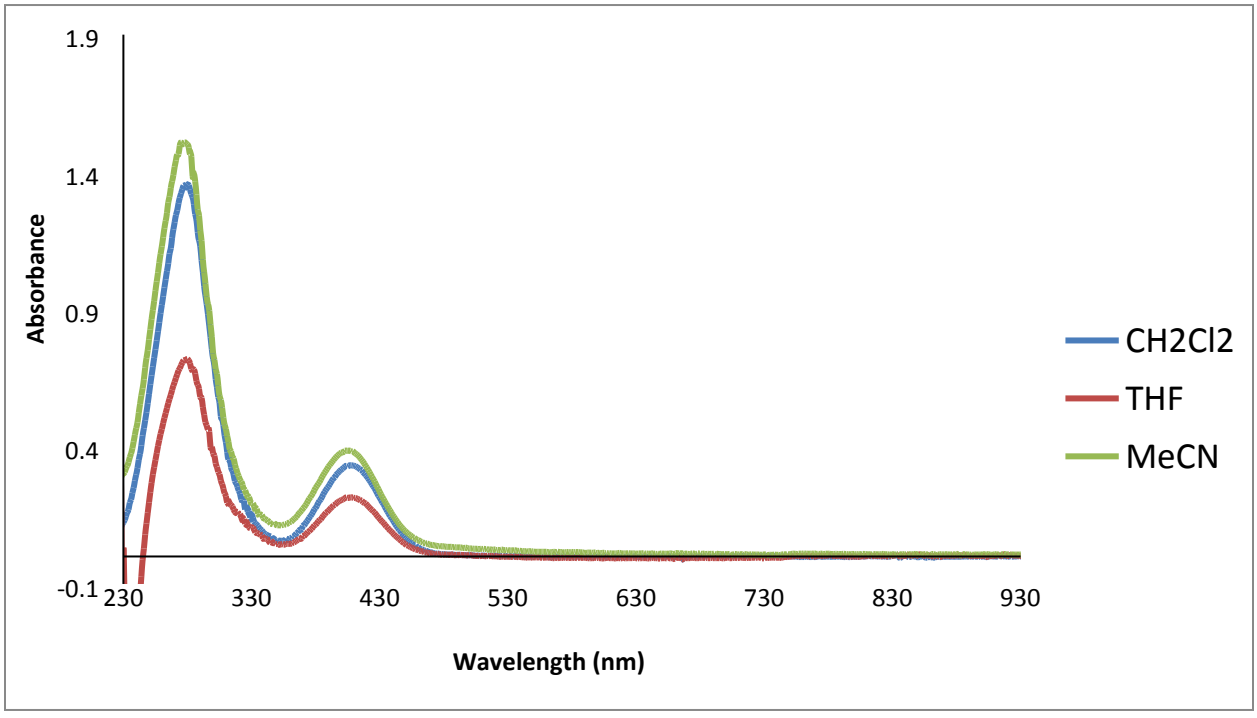

Figure S4. UV-vis spectra of **2** in CH_2Cl_2, THF, CH_3CN show unchanged λ_{max} in coordinating and non-coordinating solvents.

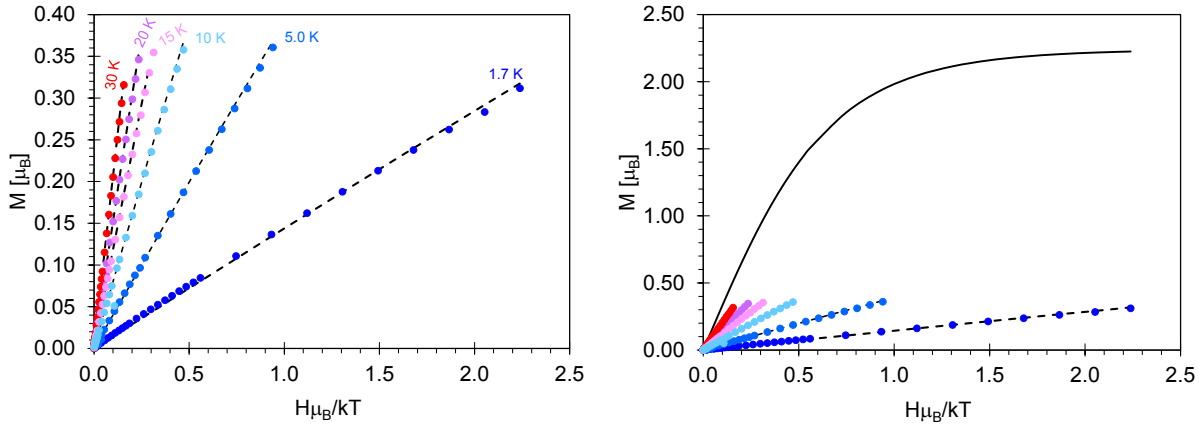

Figure S5. Reduced magnetization data collected for **2** at 1.7 K, 5 K, 10 K, 15 K, 20 K, and 30 K for fields from 0 to 7 T. The dotted black lines are simulations obtained for $S = 1$ using $D = 65$ cm^{-1}, E/D = 0.33, $g_{iso} = 2.24$. The solid black line of the plot shown on the right was obtained using a Brillouin function for which $S = 1$ and $g_{iso} = 2.24$. This curve highlights the expected behavior of an $S = 1$ without ZFS, i.e., $D = E/D = 0$. Thus, this plot demonstrates that the first term of the spin Hamiltonian $\hat{H} = D\left[\hat{S}_z^2 - \frac{2}{3} + \frac{E}{D}\left(\hat{S}_x^2 - \hat{S}_y^2\right)\right] + g_{iso}\hat{S} \cdot \vec{B}$ is dominant.

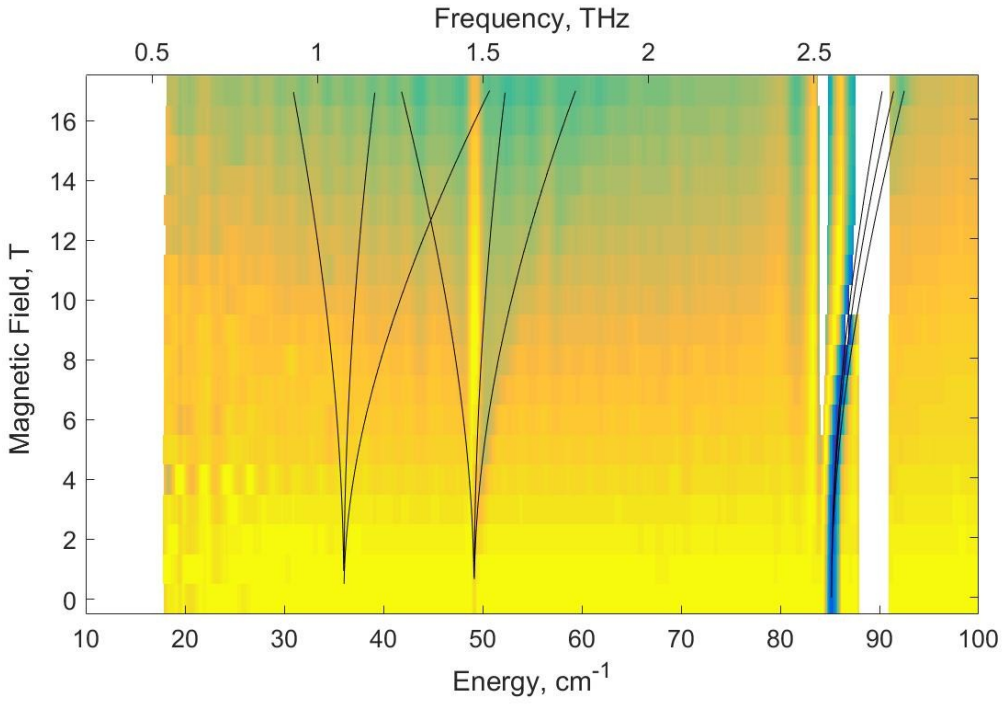

Figure S6. A false-colour map of FIRMS resonances (same as in Figure 4 in the main text) with superimposed simulations of the turning points in the triplet state powder pattern. The simulation ZFS parameters were $|D|$ = 67.2 cm^{-1}, $|E|$ = 18.0 cm^{-1} (E/D = 0.27). Note that turning points originating from the 2$|E|$ zero-field transition (36 cm^{-1}) do not show up in the experiment suggesting positive sign of D.

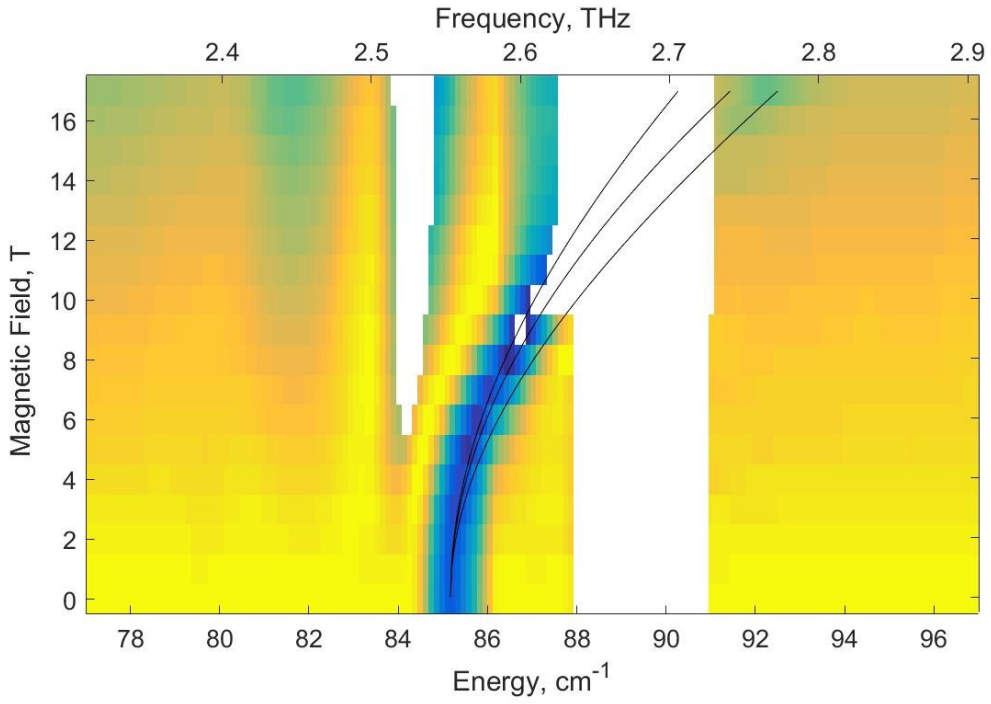

Figure S7. The *D*+*E* transition region of the FIRMS spectra with superimposed simulations of the turning points in the powder spectra. Adjusting anisotropic *g*-values yielded $g_{\perp} = 2.10 \pm 0.05$, $g_{\parallel} = 2.25 \pm 0.05$. The blank areas such as the one between 88 and 91 cm^{-1} are regions where the sample was non-transparent (100% absorption).

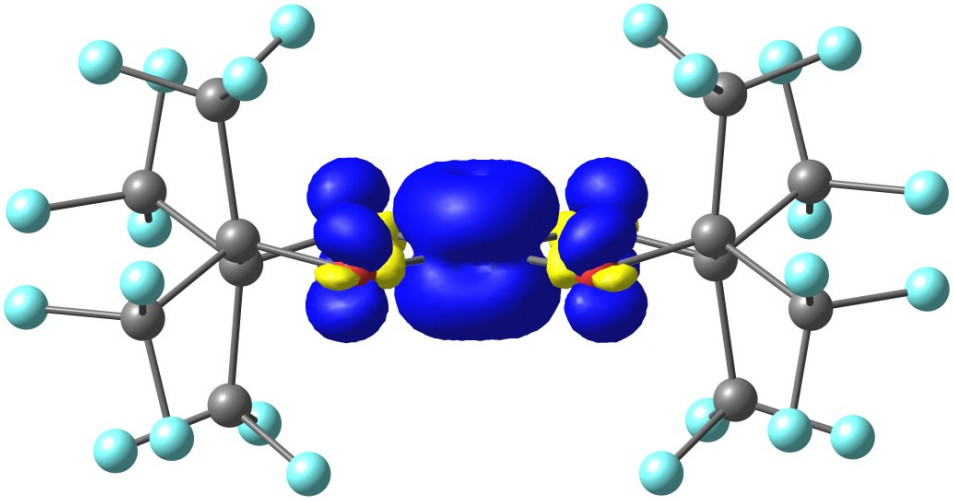

Figure S8. Spin density for ^{3}**2** calculated at the PBE0/cc-pVTZ/RIJCOSX level with isosurface of 0.005.

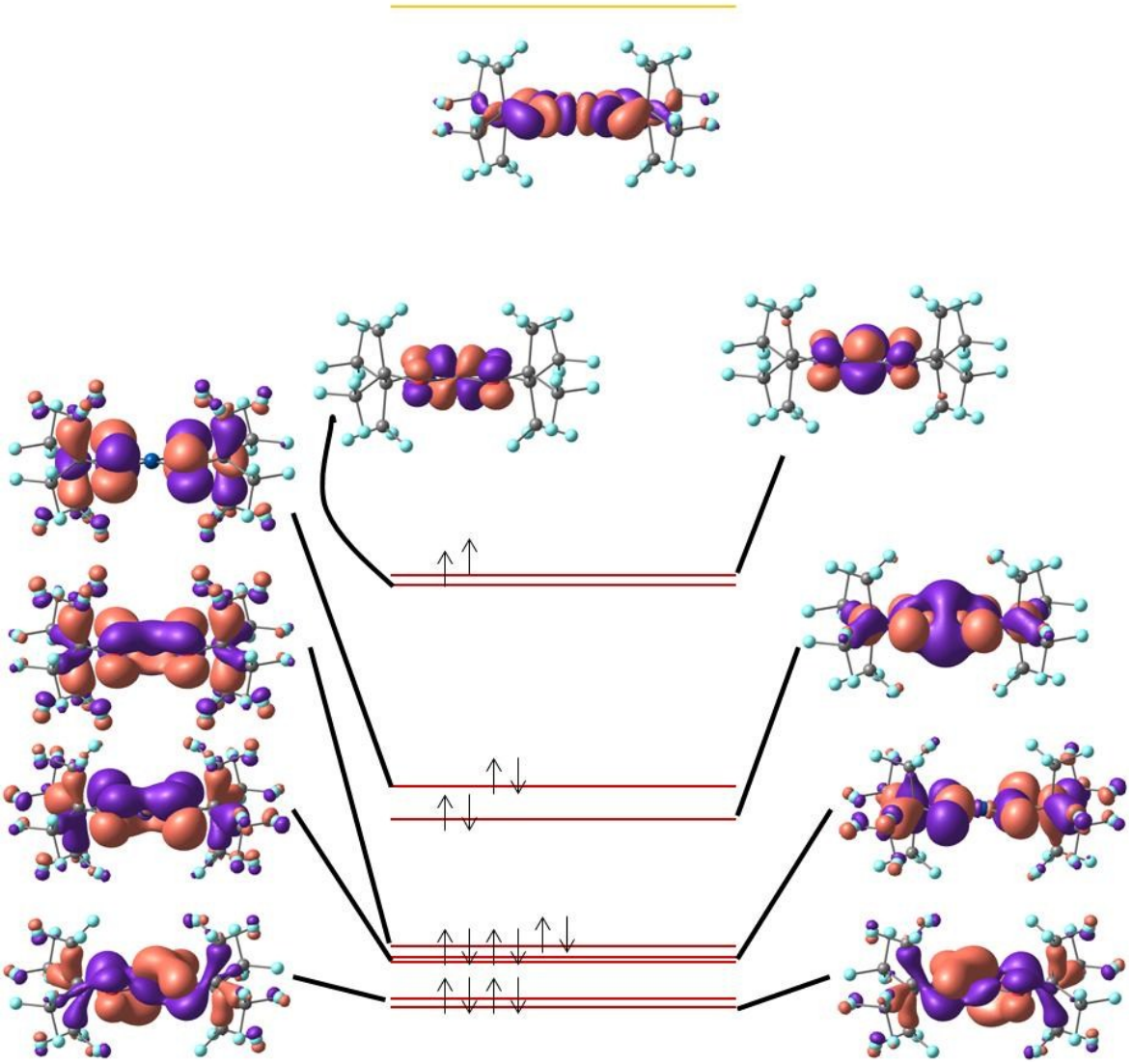

Figure S9. Quasi-restricted valence orbitals (QRO) for ^{3}**2** with qualitative energy scale.

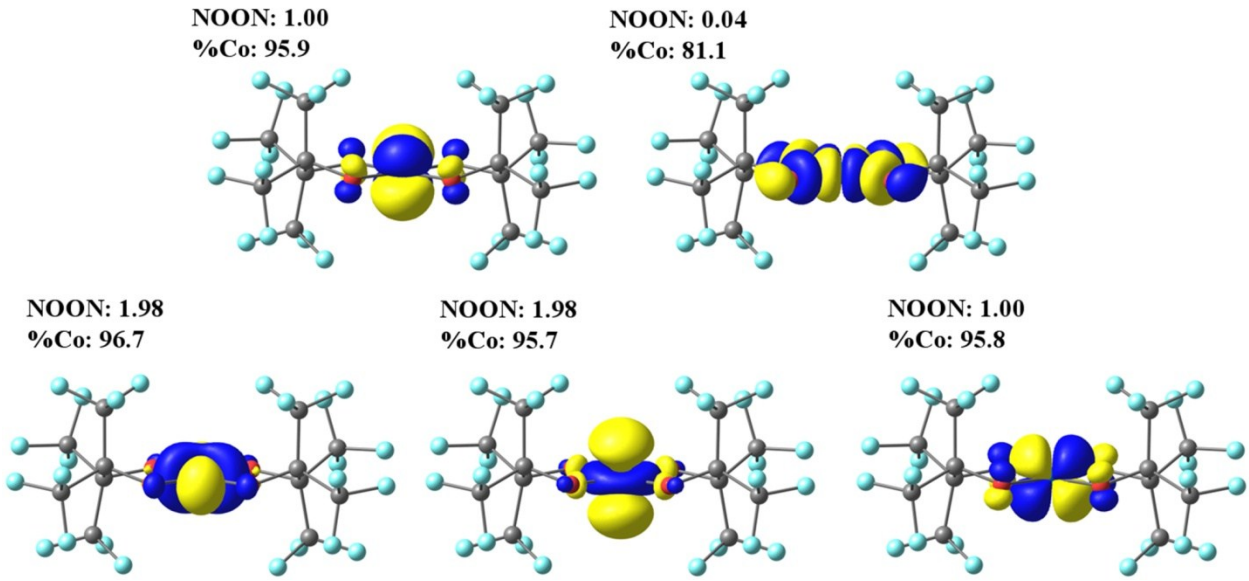

Figure S10. Natural orbitals, NOONs, and metal contributions for state-specific CASSCF(6,5) wave function for **2**.

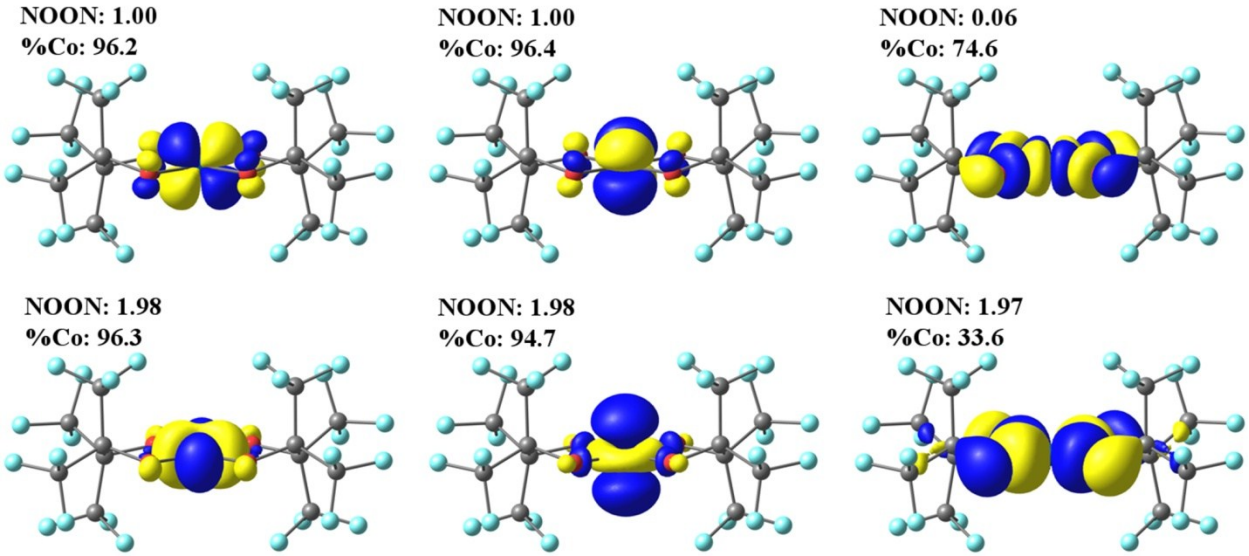

Figure S11. Natural orbitals, NOONs, and metal contributions for state-specific CASSCF(8,6) wave function for **2**.

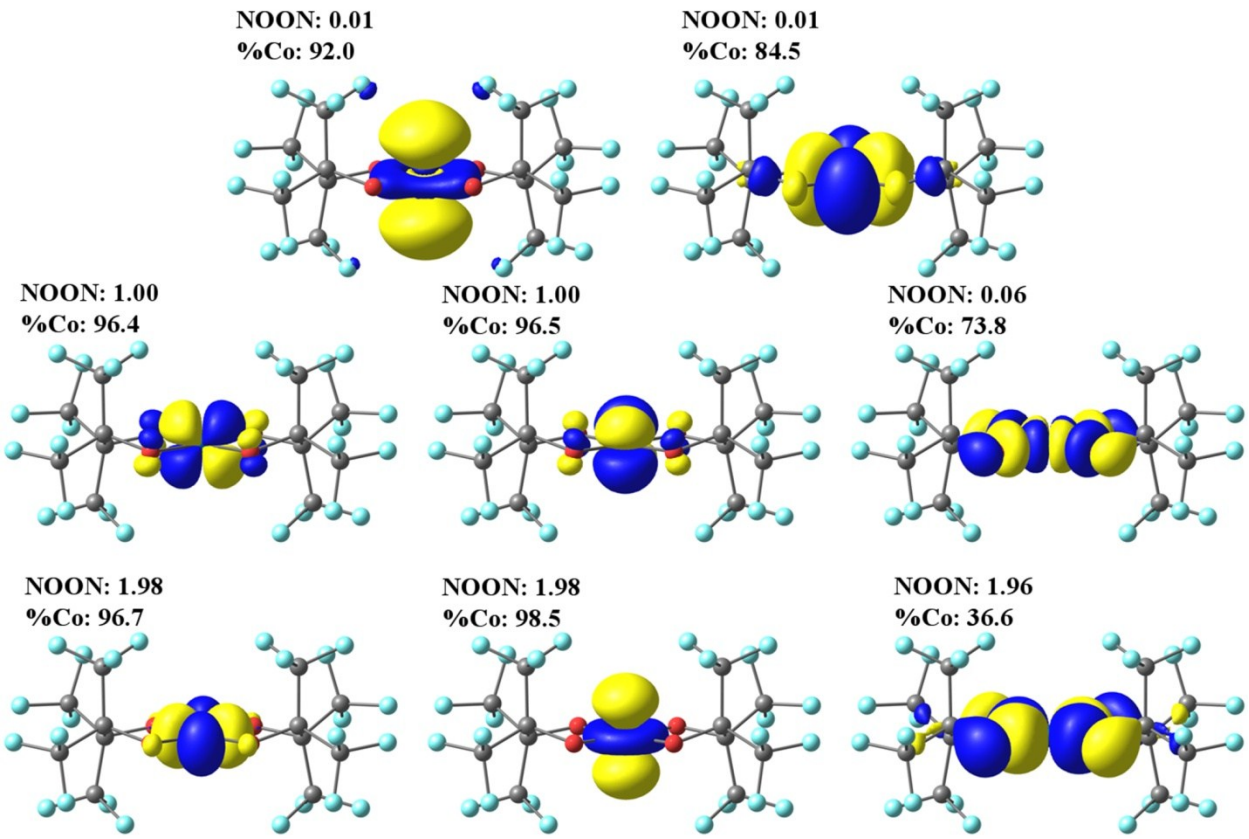

Figure S12. Natural orbitals, NOONs, and metal contributions for state-specific CASSCF(8,8) wave function for **2**.

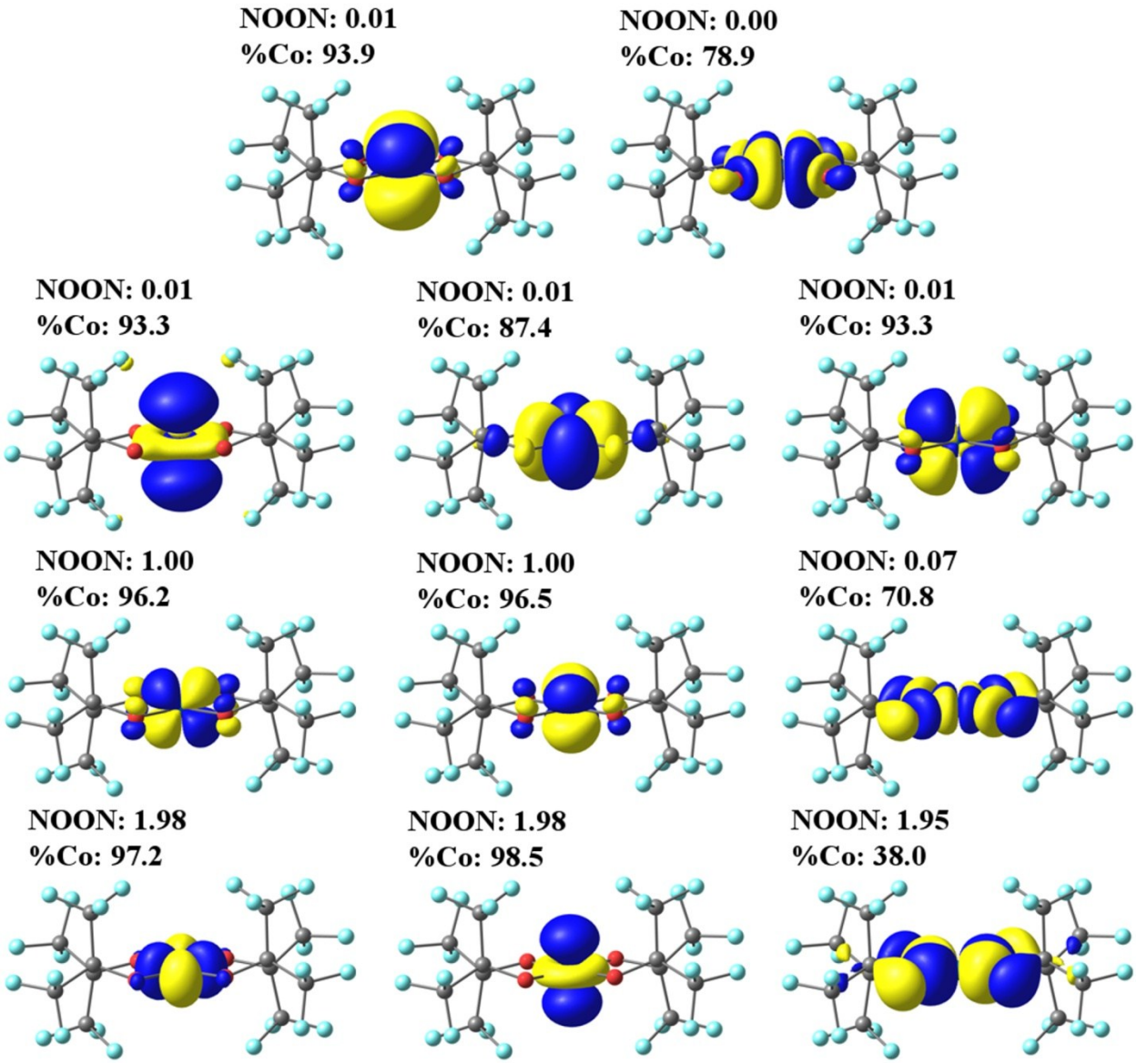

Figure S13. Natural orbitals, NOONs, and metal contributions for state-specific CASSCF(8,11) wave function for **2**.

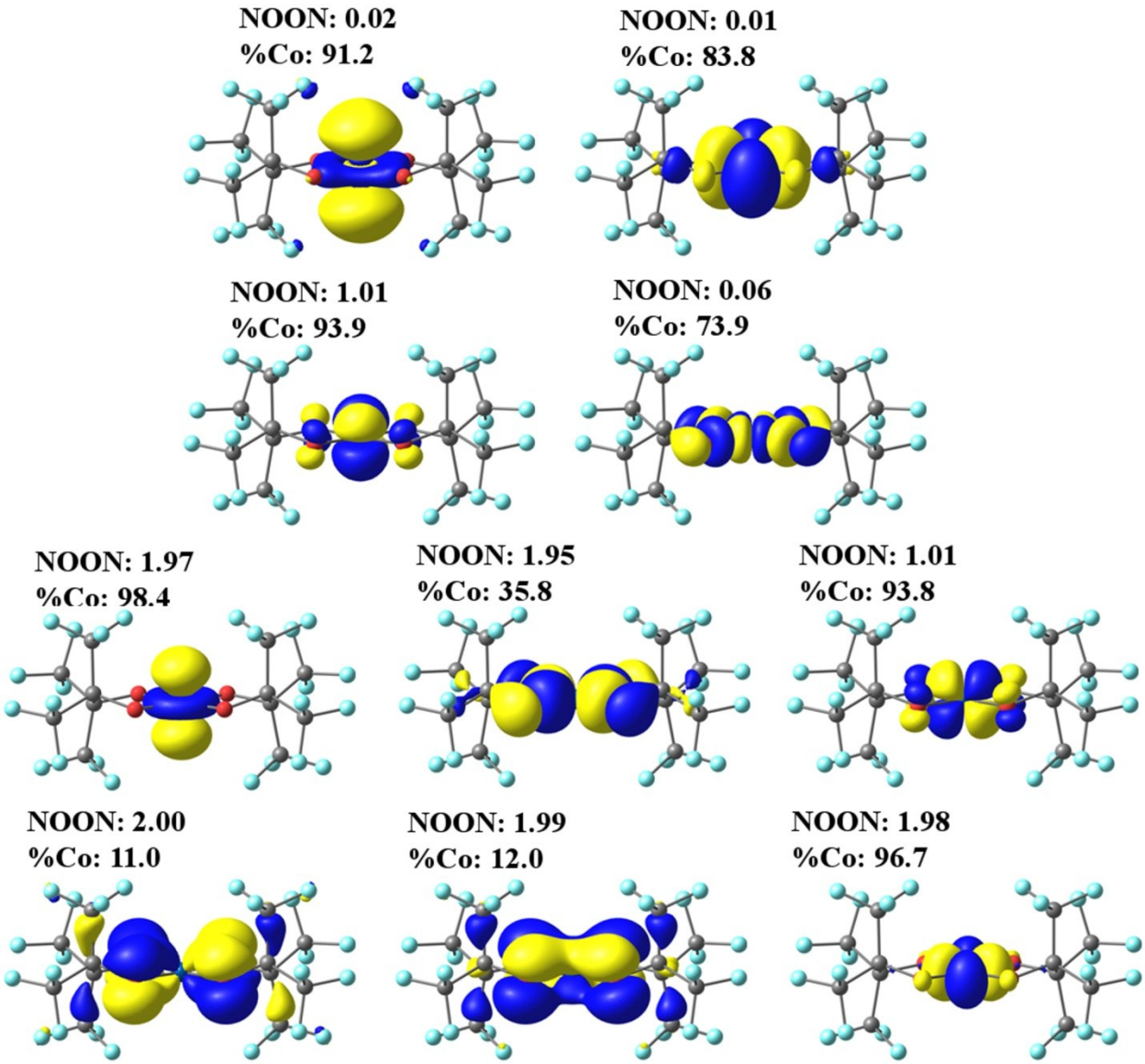

Figure S14. Natural orbitals, NOONs, and metal contributions for state-specific CASSCF(12,10) wave function for **2**.

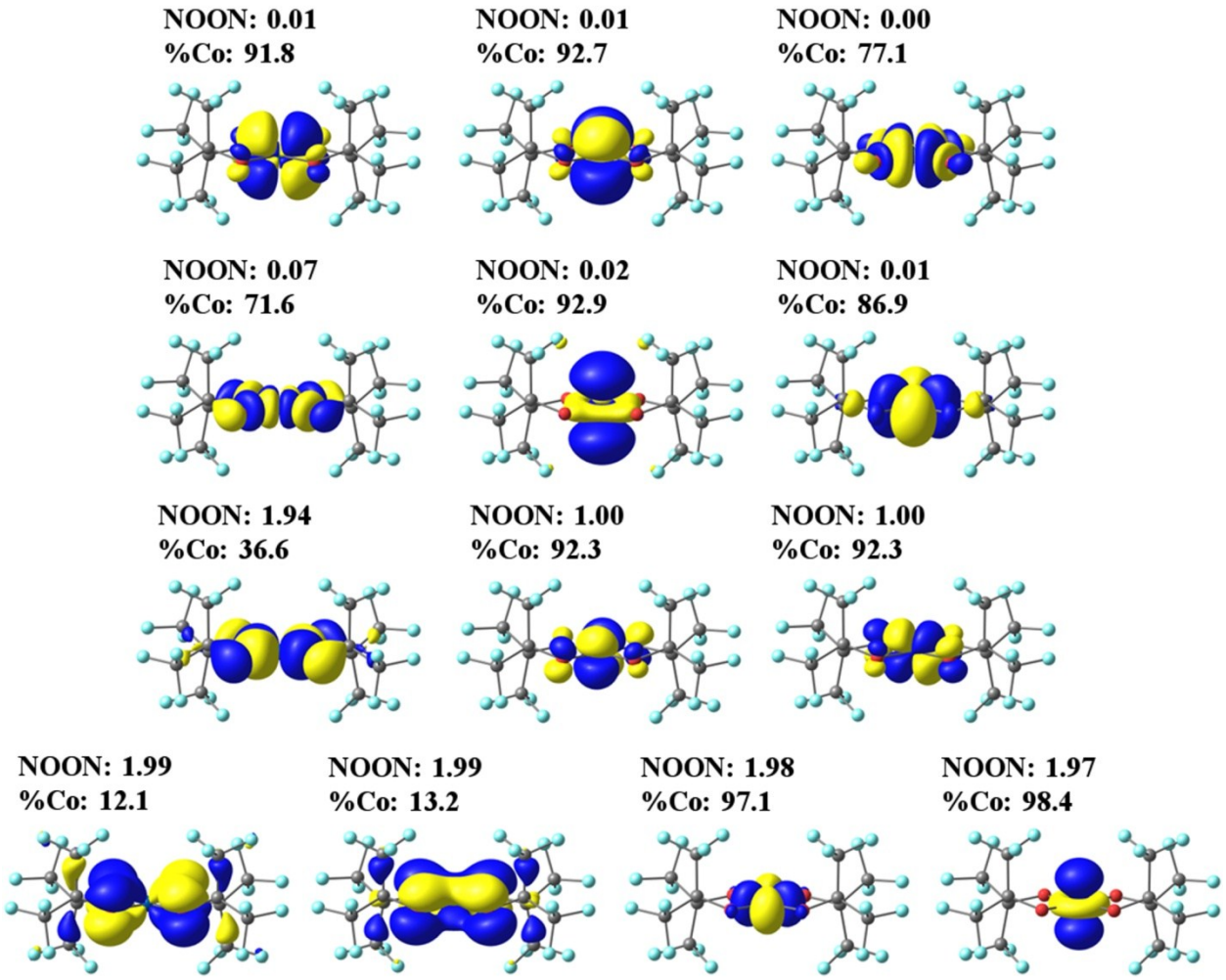

Figure S15. Natural orbitals, NOONs, and metal contributions for state-specific CASSCF(12,13) wave function for **2**.

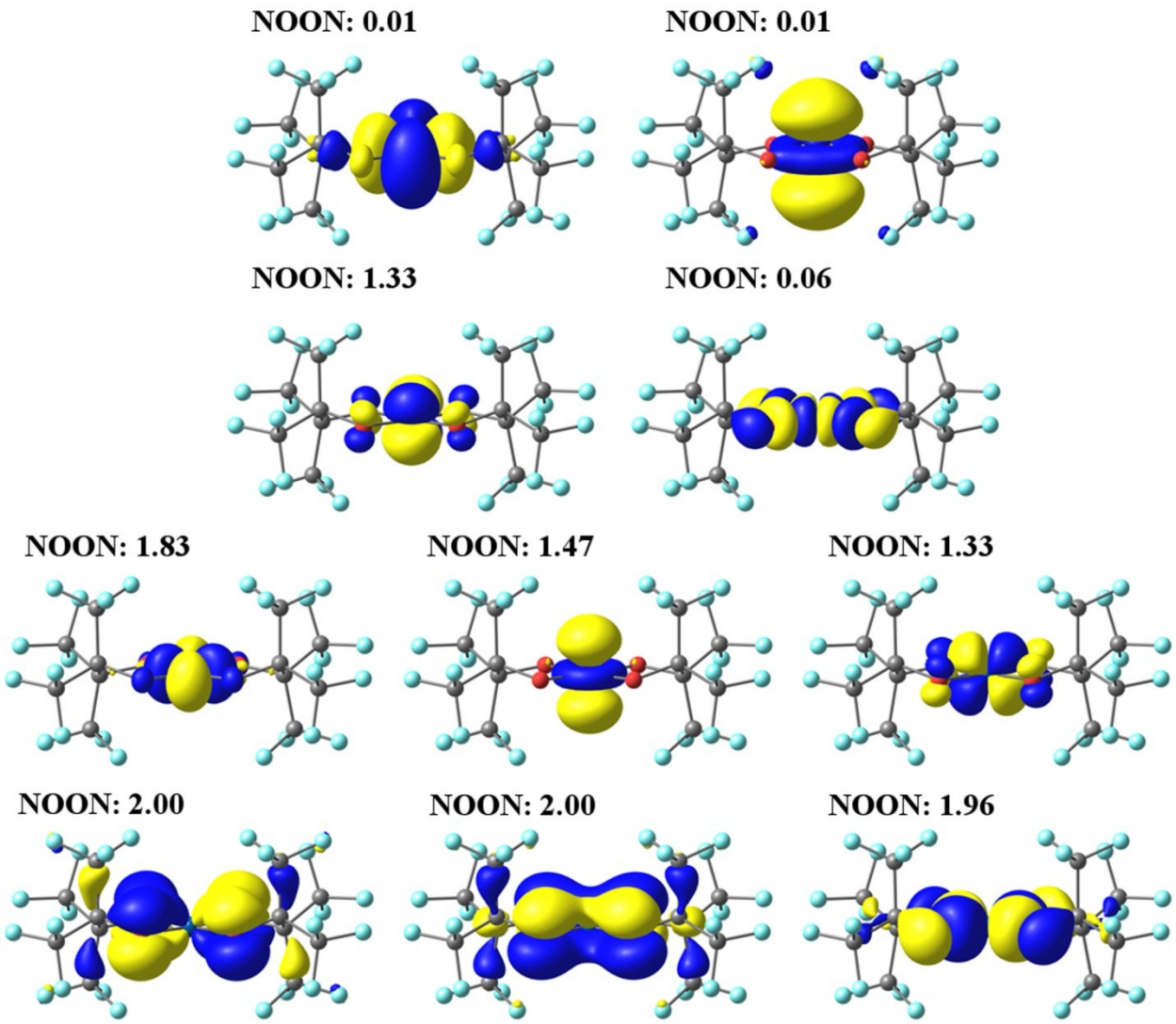

Figure S16. Natural orbitals and NOONs for SA(3)-NEVPT2(12,10) for **2**.

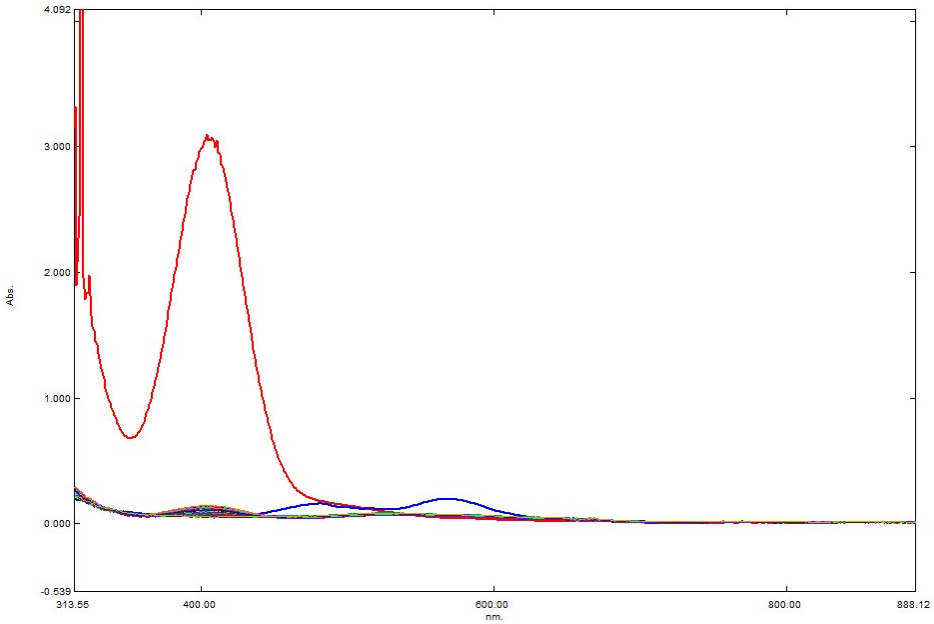

Figure S17. Time dependent UV-vis spectra of reaction of **1** with O_2 in the presence of H_2pin^F Multiple colors leading to red trace of **3** after 4 days and **2** (blue trace) after 7 days.

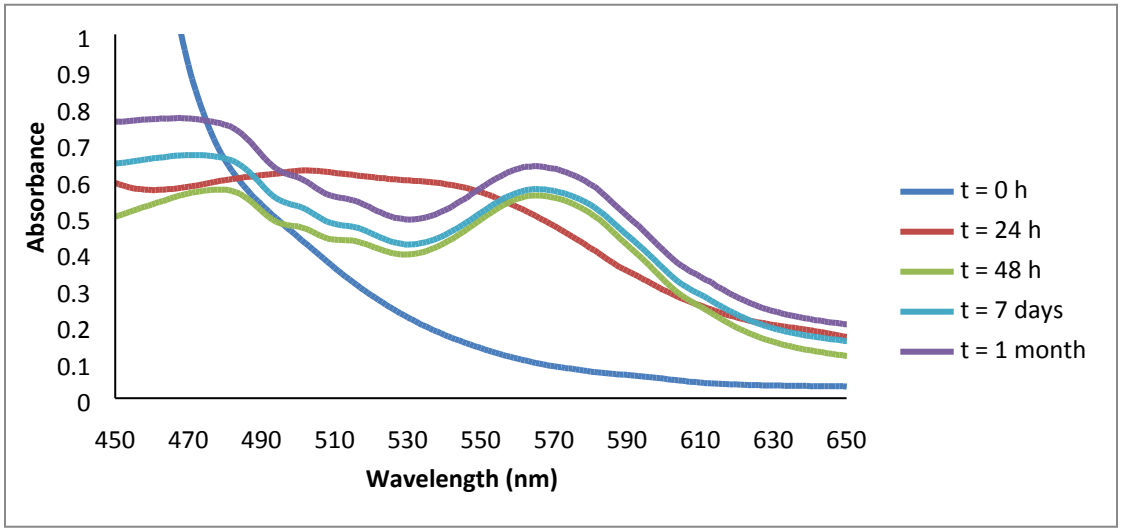

Figure S18. UV-vis of air exposure of **2** (5mM) in CH_3CN with $TBAPF_6$ (5mM). At t = 0 h, **2** is only component in solution (dark blue); at t = 24 h (red), **1** is observed; past t = 48 h, only **3** is in solution.

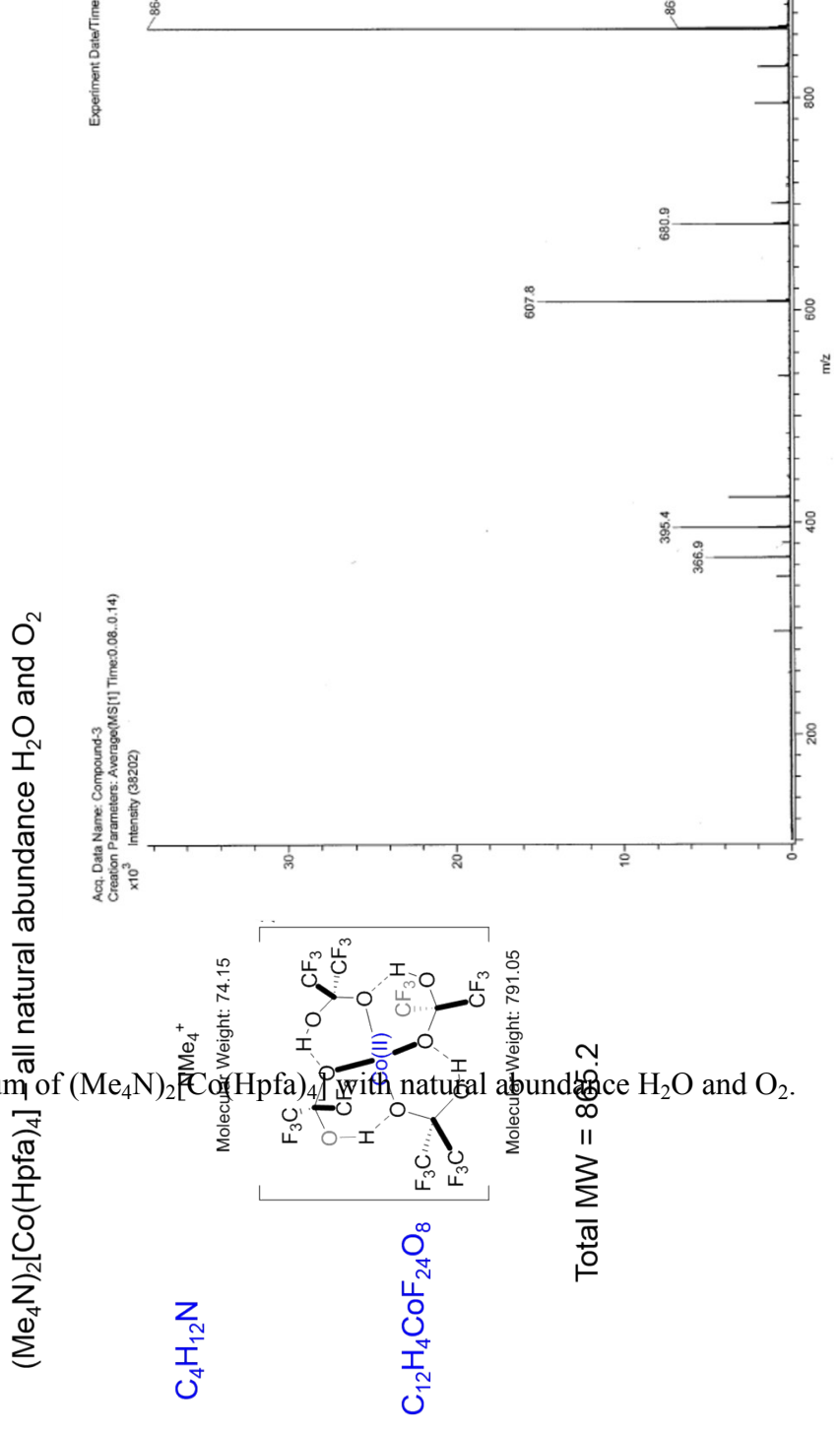

Figure S19. ESI Mass Spectrum of $(Me_4N)_2[Co(Hpfa)_4]$ with natural abundance H_2O and O_2.

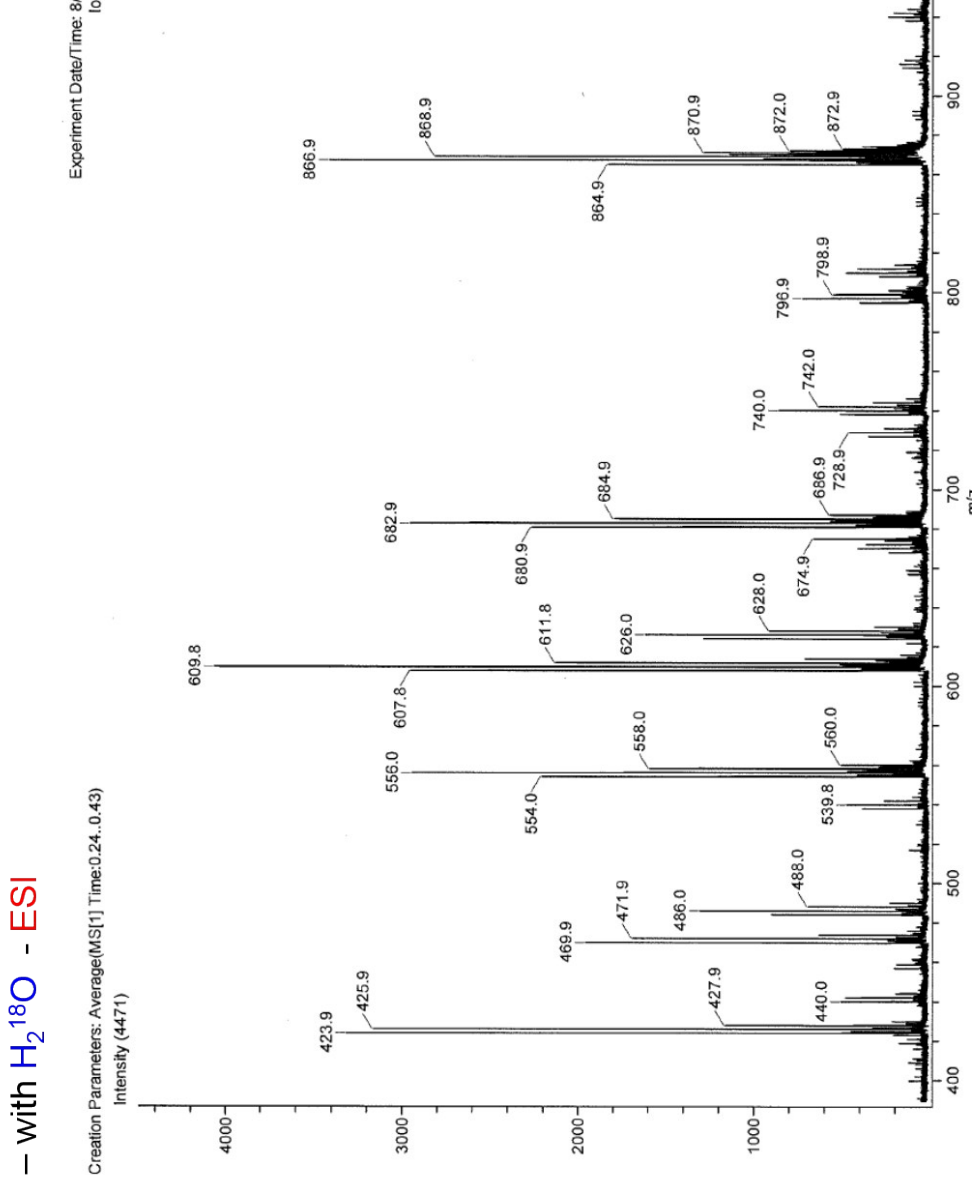

Figure S20. ESI Mass Spectrum of $(Me_4N)_2[Co(Hpfa)_4]$ – made with $H_2{}^{18}O$.

Figure S21. ESI Mass Spectrum of $(Me_4N)_2[Co(Hpfa)_4]$ – made with $^{18}O_2$.

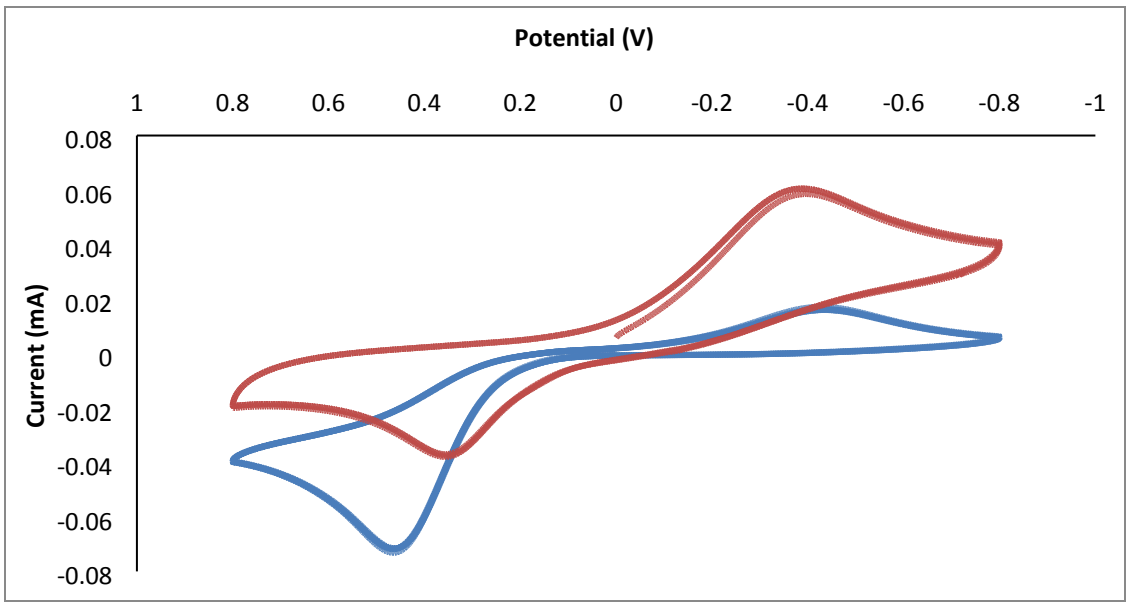

Figure S22. Cyclic voltammograms of **1** (blue) and **2** (red) in CH_3CN with $(^nBu_4N)PF_6$ (working electrode: GCE, counter electrode: Pt, and reference electrode: $Ag/AgNO_3$). [Co] = 5 mM [TBAPF6] = 0.1 M

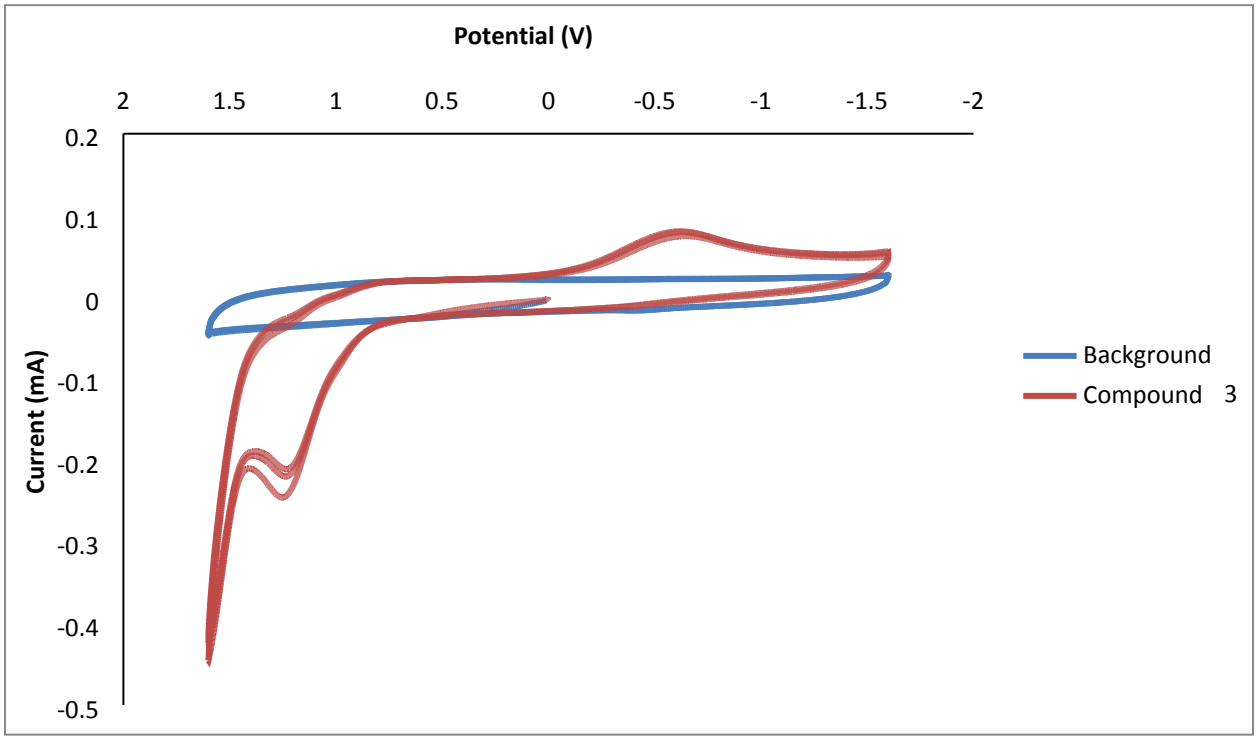

Figure S23. Cyclic voltammogram (red) of **3** in dry CH_3CN. ($TBAPF_6$ working electrode: GCE, counter electrode: Pt, and reference electrode: $Ag/AgNO_3$ and scan rate 800 mV/s.)

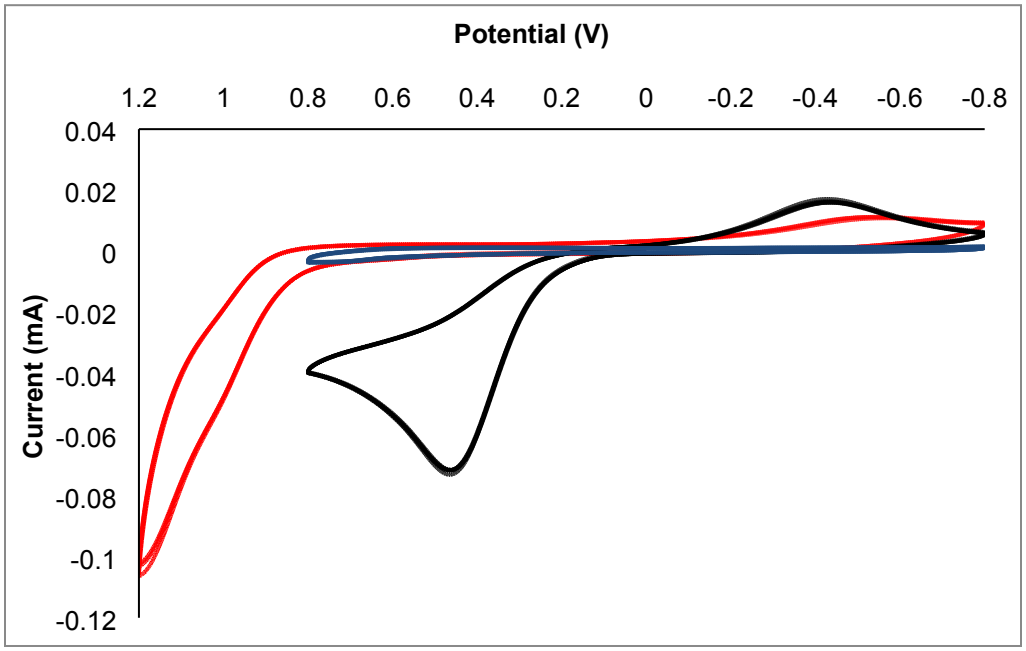

Figure S24: Cyclic voltammograms of conversion of **1** to **3** in MeCN with air ($TBAPF_6$ working electrode: GCE, counter electrode: Pt, and reference electrode: $Ag/AgNO_3$). (blue = background; black $t = 0$; red $t = 3.5$ h).

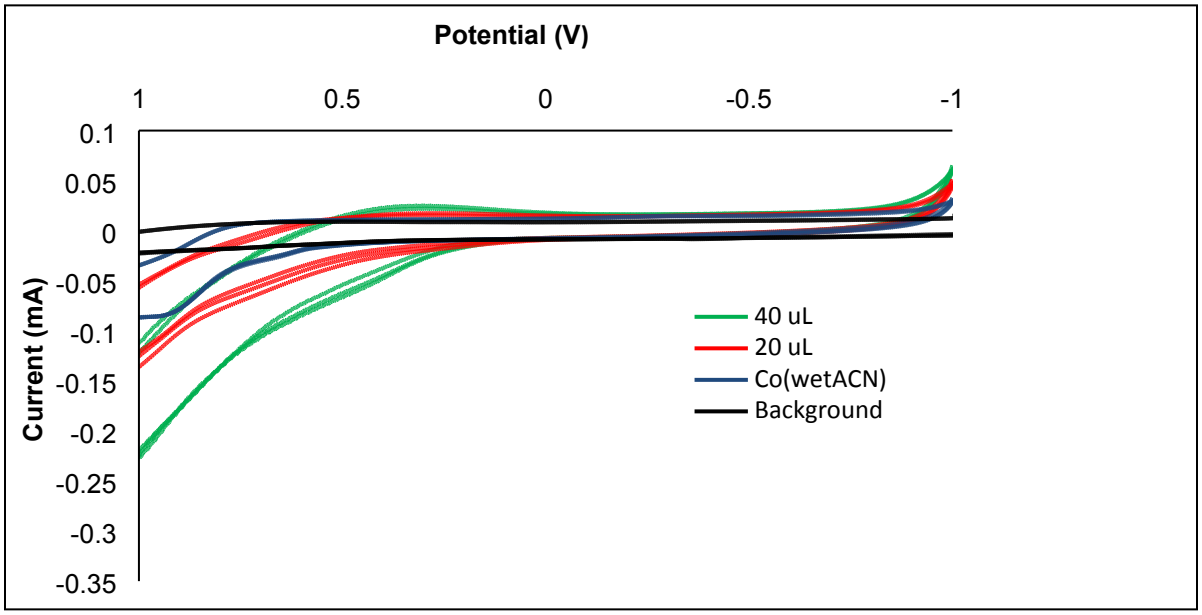

Figure S25. Cyclic voltammogram of **3** in wet CH_3CN with $TBAPF_6$ electrolyte. Also shown with additional aliquots of water (black = background, blue = 0 µL H_2O; red = 20 µL H_2O; green = 40 µL H_2O).

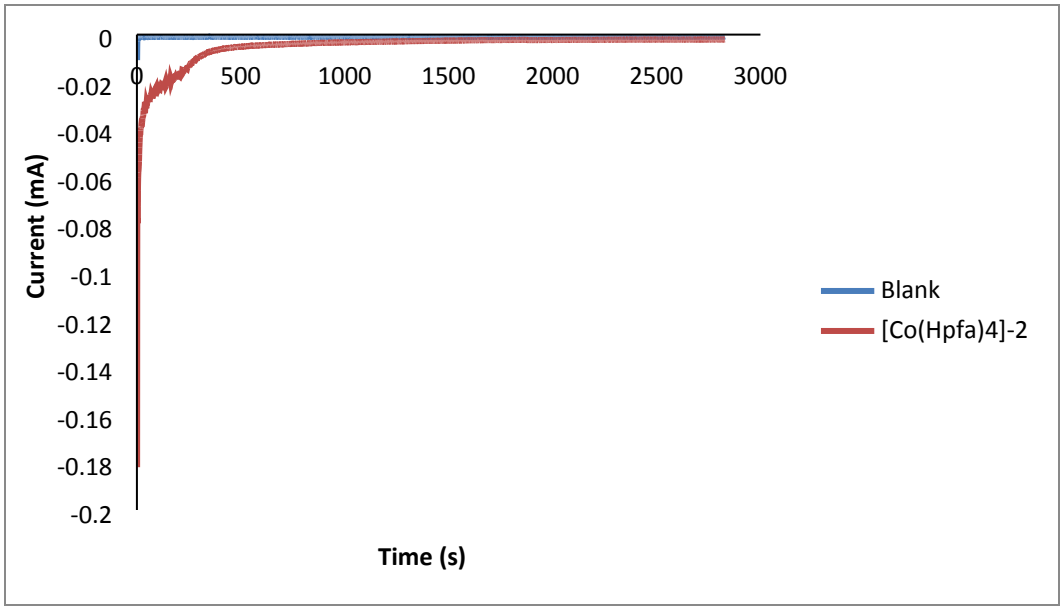

Figure S26. CPE of **3** in undistilled CH_3CN. Aliquots of water added at t = 0 s and t = 1800 s. [Co] = 4.2 mM; [$TBAPF_6$] = 0.1 M; additional V_{H2O} = 50 µL (initial) and 100 µL (final).

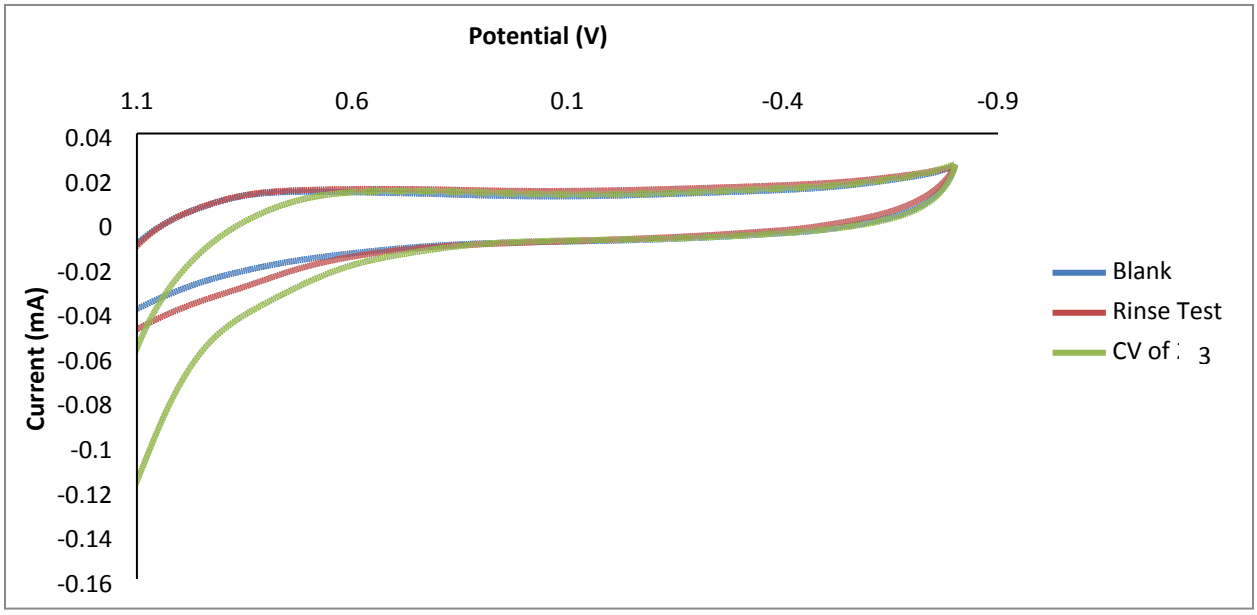

Figure S27. Rinse test after CPE of **3**. Background on polished electrode; rinse test performed on unpolished electrode after CPE; and sample run after polishing electrode on CPE solution. Only segments 4-5 shown.

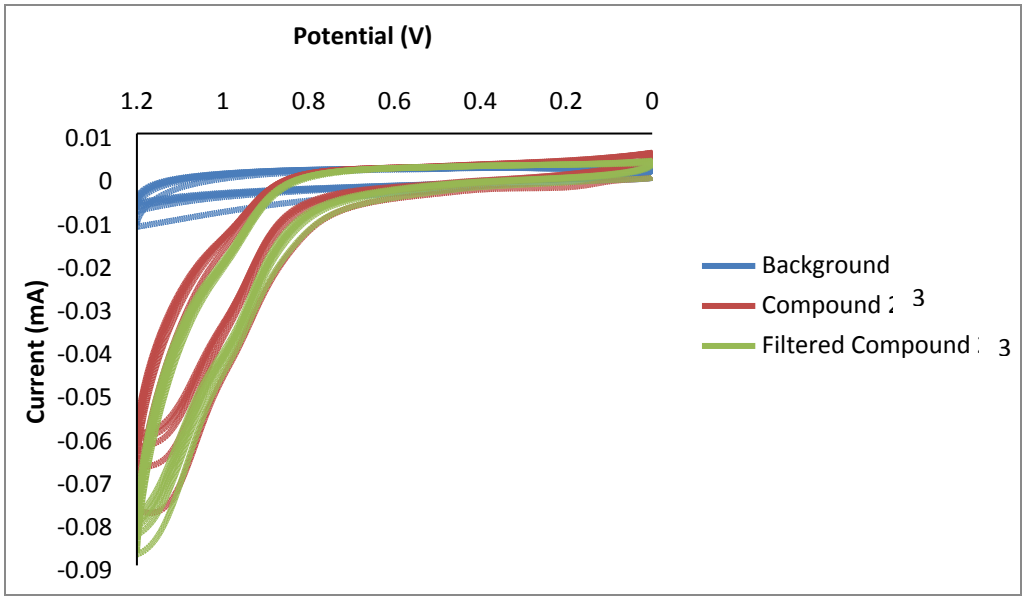

Figure S28. Oxidative half of cyclic voltammogram of **3** before and after filtration. Blue: background; Red: **3**; Green: **3** after filtration

Table S1. Comparison of four-coordinate {Co(III)} $S = 1$ ground state systems

Complex	Donors	D/k_B (K)	D (cm^{-1})	g	Reference
Compound 3	$\{CoO_4\}$		67.2	g_{iso} = 2.24	this work
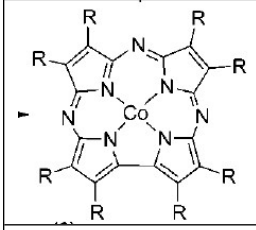	$\{CoN_4\}$		Not reported	- -	[25]
$[Co(TC\text{-}3,3)]^+$ 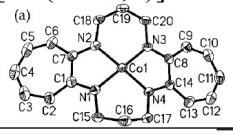	$\{CoN_4\}$		Not reported		[26]
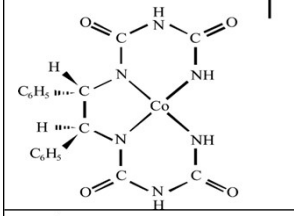	$\{CoN_4\}$		Not reported		[27]
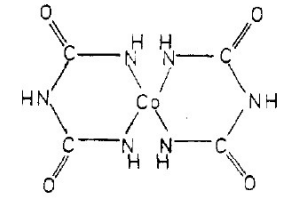	$\{CoN_4\}$		40	g_x=g_y=2	[28]
$[Co(C_6F_5)_4]^{1-}$	$\{CoC_4\}$	208(6)	144.6	3.20 ($g_\perp$)	[29]
$[Co(C_6Cl_5)_4]^{1-}$	$\{CoC_4\}$	134(9)	93.1	2.62 ($g_\perp$)	[29]
$[Co(mnt)_2]^-$ 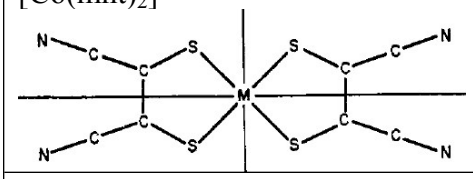	$\{CoS_4\}$		Not reported	g_{iso} = 2.255	
$(nBu_4N)[Co(S\hat{}S)_2)]$ 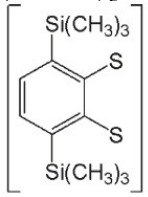	$\{CoS_4\}$		+35	2.094	[30]
$[CoCl\{L_3^{tBu}\}]$	$\{CoNPN\}Cl$		+79	$g_x = g_y$ = 2.28; g_z = 2.41	[31]

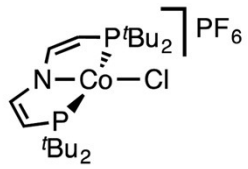					

Table S2. X-ray Crystallographic Data Collection and Refinement Parameters

	2	**3**
Chemical formula	$C_{16}H_{12}CoF_{24}O_4N$	$C_{20}H_{30}CoF_{24}N_2O_9$
M_r	797.20	957.39
Crystal system	Orthorhombic	Monoclinic
Space group	*Pnma*	$P2_1/c$
Temperature (K)	100	90(2)
a (Å)	17.2160 (8)	18.9087(17)
b (Å)	20.2934 (9)	9.8278(8)
c (Å)	7.1911 (4)	18.7047(17)
β (°)		90.009(2)
V (Å^3)	2512.4 (2)	3475.9(5)
Z	4	4
Radiation type	Cu *K*α	Mo *K*α
μ (mm^{-1})	7.35	0.670
Crystal size (mm)	0.12 × 0.05 × 0.05	0.15 x 0.20 x 0.25
T_{min}, T_{max}	0.468, 0.753	0.8503, 0.9061
Measured, independent, and observed [$I > 2\sigma(I)$] reflections	14534, 2229, 2058	20027, 6349, 5641
R_{int}	0.057	0.0290
$R[F^2 > 2\sigma(F^2)]$, $wR(F^2)$, S	0.041, 0.109, 1.05	0.039, 0.0754, 1.047
No. of reflections	2229	6349
No. of parameters	236	532
No. of restraints	220	7
$\Delta\rho_{max}$, $\Delta\rho_{min}$ (e Å^{-3})	0.69, −0.45	0.520, -0.290

Table S3. Important interatomic distances and angles in **2** and **3**

Bond Lengths (Å)			
$[Me_4N][Co(pin^F)_2]$ (**2**)		$[Me_4N]_2[Co(Hpfa)_4]$ (**3**)	
Co(1)-O(1)	1.8020(17)	Co(1)-O(1)	1.9554(18)
Co(1)-O(2)	1.7995(18)	Co(1)-O(2)	1.961(2)
C(1)-C(4)	1.596(4)	Co(1)-O(3)	1.961(2)
		Co(1)-(O4)	1.941(2)
		O(1)…O(8)	2.640(3)
		O(2)…O(5)	2.627(3)
		O(3)…O(6)	2.677(3)
		O(4)…O(7)	2.659(3)

Bond Angles (º)			
$[Me_4N][Co(pin^F)_2]$ (**2**)		$[Me_4N]_2[Co(Hpfa)_4]$ (**3**)	
$O(1)^i$—Co(1)—O(1)	91.37(11)	O(1)-Co(1)-O(2)	98.43(8)
O(2)—Co(1)—$O(1)^i$	178.20 (9)	O(1)-Co(1)-O(4)	98.64(8)
O(2)—Co(1)—O(1)	88.14 (8)	O(2)-Co(1)-O(4)	130.07(8)
$O(2)^i$—Co(1)—O(2)	92.30(11)	O(1)-Co(1)-O(3)	140.04(8)
		O(2)-Co(1)-O(3)	98.33(8)
		O(3)-Co(1)-O(4)	97.77(8)

Table S4. Selected structural parameters for the singlet (^{1}**2**), triplet (^{3}**2**), quintet (^{5}**2**), and experimental (**2**) structures. All distances in Å and angles in degrees.

	^{1}**2 (singlet)**	^{5}**2 (quintet)**	^{3}**2 (triplet)**	**2 (expt.)**
Co-O (avg)	1.802*	1.869	1.804**	1.800
(F_6C_2O)C-C(OC_2F_6)	1.614	1.640	1.605	1.596
C-F (avg)	1.333	1.334	1.333	1.330
O-Co-O [1] (avg)	87.7	83.3	87.3	88.1
O-Co-O [2] (avg)	92.3	96.8	92.7	91.8
τ_4	0.004	0.03	0.0001	0.03

*_cis_ Co-O distances 1.854 and 1.750

**_cis_ Co-O distances 1.802 and 1.806

Table S5. Löwdin atomic charges^Q and spin populations$^\rho$ for DFT and CASSCF wave functions sampled for **2**, with values for ^{3}**2** shown in parentheses.

	Co^ρ	Co^Q	O^Q_{avg}	$O\text{-}C^Q_{avg}$	$F\text{-}C^Q_{avg}$	F^Q_{avg}
PBE0	1.80 (1.80)	-0.47 (-0.44)	0.16 (0.17)	-0.333 (-0.341)	-0.817 (-0.805)	0.279 (0.273)
CASSCF(6,5)	1.92 (1.92)	0.659 (0.680)	-0.087 (-0.077)	-0.275 (-0.282)	-0.557 (-0.546)	0.177 (0.172)
CASSCF(8,6)	1.99	0.603	-0.075	-0.273	-0.557	0.177
CASSCF(8,8)	2.01	0.560	-0.066	-0.273	-0.557	0.177
CASSCF(8,11)	2.02	0.538	-0.062	-0.272	-0.557	0.177
CASSCF(12,10)	1.94 (1.95)	0.524 (0.543)	-0.059 (-0.048)	-0.272 (-0.280)	-0.557 (-0.545)	0.177 (0.172)
CASSCF(12,13)	1.91	0.489	-0.052	-0.271	-0.557	0.177

Table S6. Contributions (cm^{-1}) to the spin-orbit coupling of **2** as calculated with SA-NEVPT2(6,5) averaged over 5 quintet, 45 triplet, and 50 singlet states [SA(5,45,50)-NEVPT2(6,5)].

$S = 0$						$S = 1$						$S = 2$		
Root	*D*	*E*	Root	*D*	*E*	Root	*D*	*E*	Root	*D*	*E*	Root	*D*	*E*
0	-0.01	0.01	25	0.00	0.00	0	-6.79	-6.79	25	0.00	0.00	0	0.00	0.00
1	18.14	0.00	26	0.00	0.00	1	-103.11	-0.04	26	0.00	0.00	1	0.00	0.00
2	-1.98	-2.00	27	0.00	0.00	2	26.87	-26.88	27	0.00	0.00	2	0.00	0.00
3	-7.77	7.77	28	0.00	0.00	3	-0.12	-0.07	28	-0.02	0.00	3	0.00	0.00
4	0.02	-0.24	29	-0.01	-0.01	4	0.02	-0.02	29	0.00	0.00	4	0.00	0.00
5	-4.49	-4.57	30	-0.04	-0.04	5	0.10	0.12	30	0.00	0.00			
6	-0.01	-0.07	31	0.00	0.00	6	-0.03	0.03	31	-0.03	0.00			
7	-1.48	1.48	32	0.01	0.00	7	0.00	0.00	32	0.01	-0.01			
8	1.67	0.00	33	0.00	0.00	8	0.09	-0.09	33	0.00	0.00			
9	-0.02	0.02	34	0.00	0.00	9	-0.14	0.09	34	0.00	0.00			
10	0.00	0.00	35	-0.01	-0.01	10	0.07	-0.07	35	-0.03	0.00			
11	-0.11	-0.11	36	0.02	0.00	11	-0.04	0.11	36	0.01	-0.01			
12	-2.64	-2.64	37	-0.01	0.01	12	0.14	-0.14	37	0.00	0.00			
13	-0.01	0.01	38	0.01	0.00	13	-0.37	0.13	38	0.00	0.00			
14	0.02	0.00	39	-0.01	0.01	14	0.52	-0.52	39	0.00	0.00			
15	0.00	0.00	40	0.00	0.00	15	-0.91	0.02	40	0.00	0.00			
16	-0.01	0.01	41	0.00	0.00	16	2.17	2.18	41	0.00	0.00			
17	0.05	-0.02	42	0.00	0.00	17	0.01	-0.01	42	-0.03	0.00			
18	-0.23	0.23	43	0.00	0.00	18	0.01	-0.01	43	0.02	-0.02			
19	0.44	-0.02	44	0.00	0.00	19	-0.01	0.01	44	0.00	0.00			
20	0.00	0.00	45	0.02	0.00	20	0.34	-0.34						
21	0.00	0.00	46	-0.01	0.01	21	-0.42	0.00						
22	-0.36	-0.37	47	0.00	0.00	22	0.10	0.10						
23	0.00	0.00	48	0.00	0.00	23	0.01	-0.01						
24	0.00	0.00	49	0.00	0.00	24	0.42	0.44						

Table S7. Contributions (cm^{-1}) to the spin-orbit coupling of **2** as calculated with SA-NEVPT2(6,5) averaged over 5 quintet, 35 triplet, and 35 singlet states [SA(5,35,35)-NEVPT2(6,5)].

$S = 0$						$S = 1$						$S = 2$		
Root	*D*	*E*	Root	*D*	*E*	Root	*D*	*E*	Root	*D*	*E*	Root	*D*	*E*
0	-0.01	0.01	18	-0.24	0.24	0	-7.01	-7.01	18	0.01	-0.01	0	0.00	0.00
1	18.59	0.00	19	0.46	-0.02	1	-113.50	-0.05	19	-0.02	0.00	1	0.00	0.00
2	-2.02	-2.04	20	0.00	0.00	2	29.22	-29.22	20	0.35	-0.35	2	0.00	0.00
3	-7.96	7.96	21	-0.01	0.01	3	-0.12	-0.07	21	-0.44	0.00	3	0.00	0.00
4	-0.07	-0.33	22	-0.36	-0.36	4	0.02	-0.02	22	0.08	0.08	4	0.00	0.00
5	-4.48	-4.56	23	0.00	0.00	5	0.09	0.12	23	0.02	-0.02			
6	-0.03	-0.08	24	0.00	0.00	6	-0.03	0.03	24	0.41	0.44			
7	-1.50	1.50	25	0.00	0.00	7	0.00	0.00	25	0.00	0.00			
8	1.68	0.00	26	0.00	0.00	8	0.08	-0.08	26	0.00	0.00			
9	-0.02	0.02	27	0.00	0.00	9	-0.14	0.09	27	0.00	0.00			
10	0.00	0.00	28	0.00	0.00	10	0.07	-0.07	28	-0.02	0.00			
11	-0.15	-0.15	29	-0.02	-0.02	11	0.00	0.13	29	0.00	0.00			
12	-2.64	-2.65	30	-0.03	-0.03	12	-0.34	0.12	30	0.00	0.00			
13	-0.01	0.01	31	0.00	0.00	13	0.15	-0.15	31	-0.03	0.00			
14	0.02	0.00	32	0.01	0.00	14	0.50	-0.50	32	0.01	-0.01			
15	0.00	0.00	33	0.00	0.00	15	-0.95	0.01	33	0.00	0.00			
16	-0.01	0.01	34	0.00	0.00	16	2.22	2.23	34	0.00	0.00			
17	0.04	-0.02				17	0.01	-0.01						

Table S8. Discrepancy between the SA(5,45,50)-NEVPT2(6,5) and SA(5,35,35)-NEVPT2(6,5) contributions to the ZFS (cm^{-1}) for **2**.

	$S = 0$					$S = 1$						$S = 2$		
Root	ΔD	ΔE	Root	ΔD	ΔE	Root	ΔD	ΔE	Root	ΔD	ΔE	Root	ΔD	ΔE
0	0.00	0.00	18	-0.01	0.01	0	-0.22	-0.22	18	0.00	0.00	0	0.00	0.00
1	0.45	0.00	19	0.02	0.00	1	-10.39	-0.01	19	-0.01	-0.01	1	0.00	0.00
2	-0.04	-0.04	20	0.00	0.00	2	2.35	-2.34	20	0.01	-0.01	2	0.00	0.00
3	-0.19	0.19	21	-0.01	0.01	3	0.00	0.00	21	-0.02	0.00	3	0.00	0.00
4	-0.09	-0.09	22	0.00	0.01	4	0.00	0.00	22	-0.02	-0.02	4	0.00	0.00
5	0.01	0.01	23	0.00	0.00	5	-0.01	0.00	23	0.01	-0.01			
6	-0.02	-0.01	24	0.00	0.00	6	0.00	0.00	24	-0.01	0.00			
7	-0.02	0.02	25	0.00	0.00	7	0.00	0.00	25	0.00	0.00			
8	0.01	0.00	26	0.00	0.00	8	-0.01	0.01	26	0.00	0.00			
9	0.00	0.00	27	0.00	0.00	9	0.00	0.00	27	0.00	0.00			
10	0.00	0.00	28	0.00	0.00	10	0.00	0.00	28	0.00	0.00			
11	-0.04	-0.04	29	-0.01	-0.01	11	0.04	0.02	29	0.00	0.00			
12	0.00	-0.01	30	0.01	0.01	12	-0.48	0.26	30	0.00	0.00			
13	0.00	0.00	31	0.00	0.00	13	0.52	-0.28	31	0.00	0.00			
14	0.00	0.00	32	0.00	0.00	14	-0.02	0.02	32	0.00	0.00			
15	0.00	0.00	33	0.00	0.00	15	-0.04	-0.01	33	0.00	0.00			
16	0.00	0.00	34	0.00	0.00	16	0.05	0.05	34	0.00	0.00			
17	-0.01	0.00	SUM	0.06	0.06	17	0.00	0.00	SUM	-8.25	-2.55			

Table S9. Contributions (cm^{-1}) to the spin-orbit coupling of **2** as calculated with SA-NEVPT2(6,5) averaged over 5 quintet, 11 triplet, and 13 singlet states [SA(5,11,13)-NEVPT2(6,5)].

	$S = 0$						$S = 1$						$S = 2$	
Root	D	E	Root	D	E	Root	D	E	Root	D	E	Root	D	E
0	0.00	0.00	7	-1.51	1.51	0	-6.49	-6.50	7	0.00	0.00	0	0.00	0.00
1	18.98	0.00	8	1.62	0.00	1	-129.89	-0.05	8	0.06	-0.06	1	0.00	0.00
2	-1.97	-1.97	9	-0.02	0.02	2	31.98	-31.98	9	-0.14	0.10	2	0.00	0.00
3	-8.09	8.09	10	0.00	0.00	3	-0.14	-0.07	10	0.09	-0.09	3	0.00	0.00
4	-0.13	-0.49	11	-0.30	-0.30	4	0.02	-0.02				4	0.00	0.00
5	-4.47	-4.57	12	-2.46	-2.47	5	0.12	0.15						
6	-0.05	-0.10				6	-0.01	0.04						

Table S10. Discrepancy between the SA(5,45,50)-NEVPT2(6,5) and SA(5,11,13)-NEVPT2(6,5) contributions to the ZFS (cm^{-1}) for **2**.

	$S = 0$						$S = 1$						$S = 2$	
Root	ΔD	ΔE	Root	ΔD	ΔE	Root	ΔD	ΔE	Root	ΔD	ΔE	Root	ΔD	ΔE
0	0.01	-0.01	7	-0.03	0.03	0	0.30	0.29	18	0.00	0.00	0	0.00	0.00
1	0.84	0.00	8	-0.05	0.00	1	-26.78	-0.01	19	-0.03	0.03	1	0.00	0.00
2	0.02	0.03	9	0.00	0.00	2	5.11	-5.10	20	0.00	0.01	2	0.00	0.00
3	-0.32	0.32	10	0.00	0.00	3	-0.02	0.01	21	0.02	-0.02	3	0.00	0.00
4	-0.15	-0.25	11	-0.19	-0.19	4	0.00	0.00	SUM	-21.36	-4.76	4	0.00	0.00
5	0.02	0.00	12	0.18	0.17	5	0.02	0.03						
6	-0.04	-0.03	SUM	0.28	0.07	6	0.02	0.01						

Table S11. Contributions (cm^{-1}) to the spin-orbit coupling of **2** as calculated with SA-NEVPT2(6,5) averaged over 3 triplet states [SA(3)-NEVPT2(6,5)] and discrepancy with SA(5,45,50)-NEVPT2(6,5).

	Root 0	Root 1	Root 2
D	-0.00	-143.06	37.26
E	-0.00	0.004	-37.26
ΔD	6.79	-39.95	10.39
ΔE	6.79	0.04	-10.38

Table S12. SH parameters for **2** based on different averaging regimes. All ZFS parameters in cm^{-1}.

CASSCF(6,5)	D	E	g_1	g_2	g_3	g_{iso}
SA(5,45,50)	-75.78	-24.59	1.96	2.34	2.70	2.33
SA(5,35,35)	-83.28	-25.90	1.95	2.37	2.77	2.36
SA(5,11,13)	-97.32	-28.36	1.95	2.39	2.87	2.40
SA(3)	-97.65	-27.55	1.93	2.43	2.92	2.43

Table S13. Relative energies of the $^3B_2$ and $^3B_3$ for **2** in cm^{-1}.

NEVPT2(6,5)	$^3B_2$	$^3B_3$
SA(5,45,50)	2412.7	4868.2
SA(5,35,35)	2208.9	4534.7
SA(5,11,13)	1931.1	4185.4
SA(3)	1768.0	3646.7

Table S14. SH parameters for **2** based on different active spaces averaged over 5 quintet states, 11 triplet states, and 13 singlet states (top) and 3 triplet states (bottom). All ZFS parameters in cm^{-1}.

SA(5,11,13)	D	$\|E\|$	g_1	g_2	g_3	g_{iso}
NEVPT2(6,5)	-97.32	28.36	1.95	2.39	2.87	2.40
NEVPT2(8,6)	-98.79	28.61	1.95	2.41	2.90	2.42
NEVPT2(8,8)	-93.29	30.49	1.93	2.47	2.91	2.44
NEVPT2(8,11)	92.08	30.24	1.94	2.49	2.92	2.45
NEVPT2(12,10)	79.74	23.23	1.97	2.41	2.75	2.37
NEVPT2(12,13)	72.83	17.56	1.98	2.41	2.67	2.35
SA(3)						
NEVPT2(12,10)	77.10	20.44	1.95	2.43	2.72	2.37
NEVPT2(12,13)	65.85	13.58	1.97	2.40	2.60	2.32

Table S15. Relative energies of the $^3B_2$ and $^3B_3$ in cm^{-1} with different active spaces for **2**.

SA(5,11,13)	$^3B_2$	$^3B_3$
NEVPT2(6,5)	1931.1	4185.4
NEVPT2(8,6)	1856.8	3955.7
NEVPT2(8,8)	1793.0	3283.3
NEVPT2(8,11)	1720.8	3235.1
NEVPT2(12,10)	2223.2	3883.2
NEVPT2(12,13)	2490.3	4068.0
SA(3)		
NEVPT2(12,10)	2272.8	38016
NEVPT2(12,13)	2793.1	4185.8

Table S16. Contributions (cm^{-1}) to the spin-orbit coupling as calculated with SA-NEVPT2(12,10) averaged over 5 quintet, 11 triplet, and 13 singlet states [SA(5,11,13)-NEVPT2(12,10)].

	$S=0$						$S=1$						$S=2$	
Root	*D*	*E*	Root	*D*	*E*	Root	*D*	*E*	Root	*D*	*E*	Root	*D*	*E*
0	-0.05	0.05	7	-0.30	-0.37	0	8.12	-0.14	7	0.89	-0.89	0	0.00	0.00
1	-0.25	-0.25	8	0.15	-0.04	1	55.47	55.44	8	-2.61	0.14	1	0.00	0.00
2	-5.09	-8.40	9	-0.12	0.12	2	31.92	-31.92	9	0.01	-0.01	2	0.00	0.00
3	-7.45	7.45	10	2.68	-0.03	3	-0.16	-0.01	10	-0.66	0.01	3	0.00	0.00
4	10.38	-0.50	11	1.65	-0.07	4	-0.00	0.00				4	0.00	0.00
5	1.72	-0.47	12	-0.03	0.03	5	-0.51	0.07						
6	-1.67	1.67				6	0.51	0.53						

Table S17. Contributions (cm^{-1}) to the spin-orbit coupling as calculated with SA-NEVPT2(12,13) averaged over 5 quintet, 11 triplet, and 13 singlet states [SA(5,11,13)-NEVPT2(12,13)].

	$S=0$						$S=1$						$S=2$	
Root	*D*	*E*	Root	*D*	*E*	Root	*D*	*E*	Root	*D*	*E*	Root	*D*	*E*
0	-0.04	0.04	7	-0.56	-0.56	0	8.62	-0.03	7	0.01	-0.01	0	0.00	0.00
1	-0.23	-0.42	8	0.02	-0.09	1	47.67	47.67	8	-1.87	0.49	1	0.00	0.00
2	-8.37	-8.38	9	-0.04	0.04	2	30.40	-30.40	9	0.76	-0.76	2	0.00	0.00
3	-7.45	7.45	10	4.36	-0.00	3	0.09	-0.01	10	-0.23	0.00	3	0.00	0.00
4	7.97	-0.04	11	0.25	-0.05	4	0.00	-0.00				4	0.00	0.00
5	5.56	-0.17	12	-0.05	0.05	5	-0.29	0.05						
6	-1.51	1.51				6	-0.16	0.21						

Table S18. Contributions (cm^{-1}) to the spin-orbit coupling as calculated with SA-NEVPT2(12,10) averaged over 3 triplet states [SA(3)-NEVPT2(12,10)].

	Root 0	Root 1	Root 2
D	0.000	54.515	34.080
E	-0.000	54.515	-34.080

Table S19. Contributions (cm^{-1}) to the spin-orbit coupling as calculated with SA-NEVPT2(12,13) averaged over 3 triplet states [SA(3)-NEVPT2(12,13)].

	Root 0	Root 1	Root 2
D	-0.000	43.449	29.866
E	0.000	43.449	-29.866

Table S20. SH parameters for **2** with different basis sets, active spaces, averaging, scalar relativistic considerations, and expanded structural models. All ZFS parameters in cm^{-1}.

SA(5,11,13)-NEVPT2(6,5)	*D*	*E*	g_1	g_2	g_3	g_{iso}
cc-pVDZ	-114.74	-26.11	1.93	2.36	2.95	2.42
cc-pVTZ	-114.72	-27.15	1.93	2.39	2.97	2.43
def2-SVP	-119.74	-24.32	1.92	2.38	3.02	2.44
def2-TZVP	-111.89	-27.57	1.93	2.39	2.96	2.43
def2-QZVPP	-115.71	-27.84	1.93	2.40	2.98	2.44
DKH-def2-SVP	-90.383	-26.80	1.95	2.37	2.83	2.38
DKH-def2-TZVP	-97.347	-28.36	1.95	2.39	2.87	2.40
DKH-def2-QZVPP	-100.51	-28.44	1.94	2.40	2.89	2.41
SA(5,11,13)-NEVPT2(8,6)	*D*	*E*	g_1	g_2	g_3	g_{iso}
cc-pVTZ	-119.33	-27.63	1.93	2.41	3.02	2.45
DKH-def2-TZVP	-98.791	-28.61	1.95	2.41	2.90	2.42
SA(5,11,13)-NEVPT2(8,8)	*D*	*E*	g_1	g_2	g_3	g_{iso}
cc-pVTZ	-112.21	-33.48	1.91	2.50	3.02	2.48
DKH-def2-TZVP	-93.290	-30.49	1.93	2.47	2.91	2.44
SA(5,11,13)-NEVPT2(8,11)	*D*	*E*	g_1	g_2	g_3	g_{iso}
cc-pVTZ	-110.14	-31.21	1.92	2.51	3.04	2.49
DKH-def2-TZVP	92.078	30.24	1.94	2.49	2.92	2.45
SA(5,45,50)-NEVPT2(6,5)	*D*	*E*	g_1	g_2	g_3	g_{iso}
cc-pVTZ	-85.226	-23.46	1.95	2.33	2.76	2.35
DKH-def2-TZVP	-75.783	-24.59	1.96	2.34	2.70	2.33
Full Structure SA(5,11,13)-NEVPT2(12,10)	*D*	*E*	g_1	g_2	g_3	g_{iso}
cc-pVTZ	83.447	27.38	1.96	2.41	2.80	2.39
DKH-def2-TZVP	78.126	22.22	1.97	2.40	2.73	2.37
Full Structure SA(3)-NEVPT2(12,10)	*D*	*E*	g_1	g_2	g_3	g_{iso}
DKH-def2-TZVP	75.159	19.32	1.96	2.42	2.70	2.36
SA(3)-NEVPT2(6,5)	*D*	*E*	g_1	g_2	g_3	g_{iso}
cc-pVTZ	-120.82	-27.43	1.91	2.43	3.05	2.46
DKH-def2-SVP	-90.493	-25.92	1.94	2.41	2.88	2.41
DKH-def2-TZVP	-96.419	-28.18	1.93	2.43	2.91	2.42
DKH-def2-QZVPP	-102.93	-28.03	1.93	2.44	2.95	2.44

SA(5,11,13)-NEVPT2(12,10)	D	E	g_1	g_2	g_3	g_{iso}
cc-pVTZ	-85.254	-28.09	1.96	2.41	2.82	2.39
DKH-def2-SVP	65.535	15.74	1.99	2.36	2.59	2.31
DKH-def2-TZVP	79.740	23.23	1.97	2.41	2.75	2.37
SA(3)-NEVPT2(12,10)	D	E	g_1	g_2	g_3	g_{iso}
cc-pVTZ	83.893	24.61	1.95	2.44	2.78	2.39
DKH-def2-SVP	62.421	14.30	1.97	2.37	2.58	2.31
DKH-def2-TZVP	77.099	20.44	1.95	2.43	2.72	2.37
DKH-def2-QZVPP	78.721	20.65	1.95	2.43	2.73	2.37

Table S21. Equilibrium geometry for ^{1}**2**.

Co	-3.46901123013918	1.04871971576520	0.00382468866709
O	-4.78066908327011	0.24071806849354	-0.82725643712512
O	-2.18465942822852	0.10393669472038	-0.94258340623135
O	-2.15843523725788	1.86580345784872	0.82696622259859
O	-4.75221642568326	1.99453605373564	0.95049213341847
C	-6.04945221434626	0.47540089586424	-0.32939400919730
C	-5.97044449304455	1.93165163552842	0.36131387022666
C	-0.96480855568773	0.17481839777347	-0.35730631068666
C	-0.89013437779390	1.63452211680520	0.32638329310296
C	-7.04527735201407	2.24298897983210	1.46039850120910
C	-6.04574116049279	3.08554983886463	-0.70982480731866
C	-7.05827943637330	0.27720312510449	-1.50940838855413
C	-6.29180218750971	-0.67618510832071	0.71013338561335
C	-0.88212688204243	-0.97423934913952	0.71870655578723
C	0.10826438355936	-0.13726521321457	-1.45773432940179
C	-0.65406997445920	2.78293363867442	-0.71822170166643
C	0.12010173327216	1.84182126011524	1.50363427164356
F	-6.87581862479508	1.48582631686783	2.53936256374663
F	-8.30130033001840	2.06484560044308	1.03551579827410
F	-6.95217095552754	3.50944663470158	1.87231026411601
F	-5.20106332139295	2.86681410337303	-1.71871144911244
F	-5.68525278819401	4.24796640752550	-0.17151035500059
F	-7.26994372985248	3.25476385557499	-1.22999907793899
F	-7.13171007439843	-1.00084615867078	-1.88987957592872
F	-8.29410711049483	0.65584801278999	-1.18232600291572
F	-6.69022621916259	0.96558189876947	-2.58423108648927
F	-5.50427471409352	-0.55563408553370	1.77104756965624
F	-6.01237594545584	-1.86278442966154	0.17258648396295
F	-7.56104530010100	-0.71909593268859	1.12738755330271
F	-1.72663275119540	-0.75510595976082	1.72775164037882
F	0.34326558456270	-1.13588136539060	1.23825884021362
F	-1.23798447476691	-2.14060011211108	0.18569110978632
F	-0.06355177880117	0.61739879558695	-2.53804380510592
F	0.01607555878070	-1.40460791776708	-1.86688218689126
F	1.36474425766621	0.04343145735816	-1.03501674192337
F	-1.44042667786955	2.65389611684884	-1.77889108097062
F	0.61529014322828	2.83039766787600	-1.13506606171281
F	-0.93966627373978	3.97038087230141	-0.18578577345186
F	1.35635247611061	1.46476515136804	1.17657261459847
F	-0.24461044654252	1.15809210892773	2.58262853711727
F	0.19060541756487	3.12206675682071	1.87713668620282

Table S22. Equilibrium geometry for ^{3}**2**.

Co	-3.46869589907124	1.05477681210015	-0.00002621648651
O	-4.81051301333300	0.25701009034337	-0.90757968373531
O	-2.20700941626942	0.08233898223530	-0.84293882496671
O	-2.12693017294578	1.85234081856205	0.90771311624119
O	-4.73037756740030	2.02736461510427	0.84269875903488
C	-6.05656119550008	0.47808859340561	-0.37620721719330
C	-5.98652379441965	1.93428941905704	0.29560080050278
C	-0.95084977725713	0.17546160866628	-0.29603895034440
C	-0.88076278255512	1.63146910594076	0.37649173222565
C	-7.00712133876326	2.24318842462854	1.44285153495835
C	-6.09662846628641	3.09370538370240	-0.76054857170912
C	-7.09908806867193	0.27715024006386	-1.52658324494034
C	-6.28424706690344	-0.66436654173126	0.67806953042599
C	-0.84032326270630	-0.98401786939197	0.75987055621331
C	0.06973433384065	-0.13281506466355	-1.44346195350030
C	-0.65297644630979	2.77446771927859	-0.67723293529455
C	0.16151397066604	1.83173291507129	1.52703265477453
F	-6.77017903117870	1.49969451863410	2.51812936359649
F	-8.27516501669814	2.03840398656687	1.07466409291632
F	-6.91914528777476	3.51464303553692	1.83992787403401
F	-5.29003463745653	2.88768252596005	-1.79919228896139
F	-5.72093527181159	4.25447023943288	-0.22719167476387
F	-7.34275503353719	3.25773642005416	-1.22458836721351
F	-7.13652636392695	-0.99060348198591	-1.94050106323045
F	-8.33840465598522	0.59824266691188	-1.14566125535389
F	-6.79967558524952	1.00673304230976	-2.59545944902996
F	-5.44003823427515	-0.55114971710952	1.70200949821696
F	-6.04785837742438	-1.85659316212930	0.13538863165914
F	-7.53015819559258	-0.69331082081242	1.16558007643606
F	-1.64612045957882	-0.77781254682254	1.79911537852067
F	0.40614658384237	-1.14815600021442	1.22305840451324
F	-1.21653676086554	-2.14473300606972	0.22681661895886
F	-0.16795271802516	0.61069945276350	-2.51856048775053
F	-0.01760156754666	-1.40428956464660	-1.84067844814817
F	1.33773443909988	0.07255383643360	-1.07558354627591
F	-1.49745614934563	2.66178842276972	-1.70107563832706
F	0.59281974817265	2.80356521001452	-1.16498533520400
F	-0.88912669105007	3.96645219447774	-0.13393818967385
F	1.40094694849840	1.51132352123269	1.14581167143753
F	-0.13776495155981	1.10116917437473	2.59525066853884
F	0.19855723615528	3.09918479994458	1.94198237789835

Table S23. Equilibrium geometry for ^{5}**2**.

Co	-3.46717622627434	1.08093745641494	-0.01630672394061
O	-4.89761002275479	0.28862503819470	-0.93389523265160
O	-2.11904888365012	0.06207946410419	-0.80515096325087
O	-2.02884714689219	1.90569607095003	0.85580554451995
O	-4.82313085763614	2.04924789647651	0.81676038488714
C	-6.13632170556028	0.48225604126221	-0.41713840949923
C	-6.07931282704399	1.94902553203040	0.31451028325370
C	-0.87026672307533	0.15505271488608	-0.28466503881052
C	-0.78756703830911	1.65743810130444	0.36811111749629
C	-7.08975550691014	2.19516440173917	1.48246188033244
C	-6.23319735153814	3.12686255049796	-0.71373085192912
C	-7.19390337945297	0.31509890335746	-1.55563562398630
C	-6.35022320558862	-0.68264330016939	0.61361448612314
C	-0.76935756383287	-0.97036379297608	0.80747285012534
C	0.15530689599842	-0.18126225211237	-1.41638343879720
C	-0.52650634762634	2.76031367672818	-0.71799221624155
C	0.25671499277783	1.85671673824401	1.51446419934527
F	-6.81488896035612	1.42908930337532	2.53336026222906
F	-8.35960857594041	1.97183238862467	1.13227741753031
F	-7.02541885378227	3.45764319434549	1.91507740184519
F	-5.42697727493212	2.95568719708489	-1.76145926540071
F	-5.88079023690018	4.28839633692746	-0.16523402396603
F	-7.48423246780199	3.26943574619661	-1.16769104646863
F	-7.24784765256272	-0.94579267722471	-1.99329641262308
F	-8.42743134508244	0.63732525645416	-1.15608397193008
F	-6.89927308437935	1.06141122340405	-2.61497896530753
F	-5.48115650851670	-0.58507393477961	1.62185073682052
F	-6.12163085363427	-1.86441544906009	0.04533584346387
F	-7.58421986970758	-0.72526262515094	1.12733165833612
F	-1.59476670838702	-0.72465054108046	1.82498663610238
F	0.46559303250045	-1.12158544028805	1.30032338733776
F	-1.14004374832592	-2.14908657518524	0.30934307782395
F	-0.07723570855541	0.53719385872372	-2.51035775323990
F	0.06308987978308	-1.46268143689950	-1.78374771162657
F	1.42429063536302	0.02433040670860	-1.05252334450633
F	-1.37001041345701	2.62813030576272	-1.74304116999998
F	0.72091973830800	2.74767824596831	-1.19971415818619
F	-0.74263052426583	3.97667412342106	-0.22010658497799
F	1.48133175460710	1.45262547028792	1.16650468326081
F	-0.09260548489352	1.19841299681756	2.61479570606211
F	0.36115412828833	3.14231838463360	1.86477235044465

Table S24. Results of ligand-field theory (Ligfield program) calculation for idealized $[Co^{III}(pin^{F})_2]^{1-}$, without spin-orbit coupling. Annotations have been added by hand for further explanation.

These matrices were generated from the following terms:
5D 3P1 3P2 3D 3F1 3F2 3G 3H 1S1 1S2 1D1 1D2 1F 1G1 1G2 1I of d6 In SLMSML-basis.
One electron parametrization was taken from: AOM
The AOM-parametrization were based on the following premises:
Maximum lambda (sigma,pi,delta) value included: pi. The AOM-matrices were not barycentered.

Ligator	Theta	Phi	Psi	Linear
O1	90.000000	44.070000	0.000000	No
O2	90.000000	-44.070000	0.000000	No
O1'	90.000000	135.930000	0.000000	No
O2'	90.000000	224.070000	0.000000	No

Parameter:	Value:	
esigma(O1)	9000.00000000	
epi-s(O1)	1000.00000000	
epi-c(O1)	5000.00000000	
esigma(O2)	9000.00000000	
epi-s(O2)	1000.00000000	
epi-c(O2)	5000.00000000	
esigma(O1')	9000.00000000	
epi-s(O1')	1000.00000000	
epi-c(O1')	5000.00000000	
esigma(O2')	9000.00000000	
epi-s(O2')	1000.00000000	
epi-c(O2')	5000.00000000	
Racah B	650.00000000	60% of free-ion values
Racah C	2740.00000000	

--------- Eigenvalues and eigenfunction labelling ----------
(degenerate listings removed)
Energy: 0.00000000
Spin labels: (2S+1)= 3.00000
Symmetry of eigenfunction: B1(D2)

theta	ksi	eta	zeta	epsilon	(x2-y2)2,(z2)2,(yz)1,(xz)1,(xy)0
z2	yz	xz	xy	x2-y2	(ground state)
1.973083	1.000719	0.999283	0.034927	1.991988	

Energy: 841.26653792
Spin labels: (2S+1)= 3.00000
Symmetry of eigenfunction: E(D4) B2(D2)

theta	ksi	eta	zeta	epsilon	(x2-y2)2,(z2)1,(yz)2,(xz)1,(xy)0
z2	yz	xz	xy	x2-y2	(major contributor to zfs via l_x)
1.022445	1.972408	1.012160	0.031923	1.961064	

Energy: 1061.81510332
Spin labels: (2S+1)= 3.00000
Symmetry of eigenfunction: E(D4) B3(D2)

theta	ksi	eta	zeta	epsilon	(x2-y2)2,(z2)1,(yz)1,(xz)2,(xy)0
z2	yz	xz	xy	x2-y2	(major contributor to zfs via l_y)
1.047144	1.012112	1.971894	0.032406	1.936445	

==========
Energy: 1302.00263132
Spin labels: (2S+1)= 5.00000
Symmetry of eigenfunction: E(O) A1(D2)
| theta | ksi | eta | zeta | epsilon | (x2-y2)2,(z2)1,(yz)1,(xz)1,(xy)1
| z2 | yz | xz | xy | x2-y2 |
---------- (quintet with extra e in x^2-y^2)
| 1.010030| 1.000000| 1.000000| 1.000000| 1.989970|

Energy: 6379.62731529
Spin labels: (2S+1)= 5.00000
Symmetry of eigenfunction: E(O) A1(D2)
| theta | ksi | eta | zeta | epsilon | (x2-y2)1,(z2)2,(yz)1,(xz)1,(xy)1
| z2 | yz | xz | xy | x2-y2 | (contributor to zfs via l_z)
---------- (quintet with extra e in z^2)
| 1.989970| 1.000000| 1.000000| 1.000000| 1.010030|

Energy: 7004.12567928
Spin labels: (2S+1)= 5.00000
Symmetry of eigenfunction: T2(O) E(D4) B3(D2)
| theta | ksi | eta | zeta | epsilon | (x2-y2)1,(z2)1,(yz)2,(xz)1,(xy)1
| z2 | yz | xz | xy | x2-y2 |
---------- (quintet with extra e in *yz*)
| 1.000000| 2.000000| 1.000000| 1.000000| 1.000000|
==========
Energy: 7533.38177118
Spin labels: (2S+1)= 1.00000
Symmetry of eigenfunction: A1(D2)
| theta | ksi | eta | zeta | epsilon |
| z2 | yz | xz | xy | x2-y2 |

| 0.384336| 1.916962| 1.685610| 0.030414| 1.982678|

Energy: 7577.32991021
Spin labels: (2S+1)= 1.00000
Symmetry of eigenfunction: E(D4) B2(D2)
| theta | ksi | eta | zeta | epsilon |
| z2 | yz | xz | xy | x2-y2 |

| 0.977653| 1.954838| 1.029638| 0.049429| 1.988441|
==========
Energy: 7653.27412901
Spin labels: (2S+1)= 5.00000
Symmetry of eigenfunction: T2(O) E(D4) B2(D2)
| theta | ksi | eta | zeta | epsilon | (x2-y2)1,(z2)1,(yz)1,(xz)2,(xy)1
| z2 | yz | xz | xy | x2-y2 |
---------- (quintet with extra e in *xz*)
| 1.000000| 1.000000| 2.000000| 1.000000| 1.000000|
==========
Energy: 7790.85728870
Spin labels: (2S+1)= 1.00000
Symmetry of eigenfunction: B1(D2)
| theta | ksi | eta | zeta | epsilon |
| z2 | yz | xz | xy | x2-y2 |

| 1.938168| 1.005472| 0.997325| 0.072051| 1.986983|

Energy: 7993.25834273
Spin labels: (2S+1)= 1.00000
Symmetry of eigenfunction: E(D4) B3(D2)
| theta | ksi | eta | zeta | epsilon |
| z2 | yz | xz | xy | x2-y2 |

| 0.986649| 1.032301| 1.951197| 0.052938| 1.976915|

Energy: 8695.91939276
Spin labels: (2S+1)= 1.00000
Symmetry of eigenfunction: A1(D2)
| theta | ksi | eta | zeta | epsilon |
| z2 | yz | xz | xy | x2-y2 |

| 1.892566| 1.072515| 1.007861| 0.056333| 1.970726|
==========
Energy: 9597.96761655
Spin labels: (2S+1)= 3.00000
Symmetry of eigenfunction: A1(D2)
| theta | ksi | eta | zeta | epsilon | (x2-y2)1,(z2)1,(yz)2,(xz)2,(xy)0
| z2 | yz | xz | xy | x2-y2 | (two electron transition, so ignore for zfs)

| 1.000939| 1.827202| 1.825829| 0.185523| 1.160506|

Energy: 12971.22801275
Spin labels: (2S+1)= 3.00000
Symmetry of eigenfunction: E(D4) B2(D2)
| theta | ksi | eta | zeta | epsilon | (x2-y2)1,(z2)2,(yz)2,(xz)1,(xy)0 (roughly)
| z2 | yz | xz | xy | x2-y2 | (contributor to zfs)

| 1.892686| 1.638192| 0.814570| 0.379043| 1.275509|

Energy: 13700.51513494
Spin labels: (2S+1)= 3.00000
Symmetry of eigenfunction: E(D4) B3(D2)
| theta | ksi | eta | zeta | epsilon | (x2-y2)1,(z2)2,(yz)1,(xz)2,(xy)0 (roughly)
| z2 | yz | xz | xy | x2-y2 | (contributor to zfs)

| 1.859984| 0.810131| 1.593701| 0.420823| 1.315361|
==========
Energy: 14333.30485778
Spin labels: (2S+1)= 1.00000
Symmetry of eigenfunction: A1(D2)
| theta | ksi | eta | zeta | epsilon |
| z2 | yz | xz | xy | x2-y2 |

| 1.562977| 1.029828| 1.288171| 0.215836| 1.903188|
==========
Energy: 16411.48008419
Spin labels: (2S+1)= 3.00000
Symmetry of eigenfunction: A1(D2)
| theta | ksi | eta | zeta | epsilon | (x2-y2)2,(z2)1,(yz)1,(xz)2,(xy)1
| z2 | yz | xz | xy | x2-y2 | (z^2 not connected to x^2-y^2, so ignore for zfs)

| 1.071067| 1.035731| 1.034569| 0.965549| 1.893084|

Energy: 16566.09761477
Spin labels: (2S+1)= 3.00000
Symmetry of eigenfunction: E(D4) B2(D2)
| theta | ksi | eta | zeta | epsilon |
| z2 | yz | xz | xy | x2-y2 |

| 1.544590| 1.198158| 0.704560| 0.813405| 1.739286|

Energy: 16941.79959067
Spin labels: (2S+1)= 3.00000
Symmetry of eigenfunction: B1(D2)
| theta | ksi | eta | zeta | epsilon |
| z2 | yz | xz | xy | x2-y2 |

| 1.102689| 1.093990| 0.907561| 0.998691| 1.897069|

Energy: 17062.63574061
Spin labels: (2S+1)= 3.00000
Symmetry of eigenfunction: E(D4) B3(D2)
| theta | ksi | eta | zeta | epsilon |
| z2 | yz | xz | xy | x2-y2 |

| 1.459408| 0.793390| 1.200514| 0.811918| 1.734771|

Energy: 17930.87871288
Spin labels: (2S+1)= 3.00000
Symmetry of eigenfunction: A1(D2)
| theta | ksi | eta | zeta | epsilon | (x2-y2)2,(z2)1,(yz)1,(xz)2,(xy)1
| z2 | yz | xz | xy | x2-y2 |

| 1.135094| 0.999498| 1.005264| 1.003948| 1.856196|
==========
Energy: 19024.64237624
Spin labels: (2S+1)= 1.00000
Symmetry of eigenfunction: E(D4) B2(D2)
| theta | ksi | eta | zeta | epsilon |
| z2 | yz | xz | xy | x2-y2 |

| 1.889372| 1.528436| 0.662632| 0.486587| 1.432973|

Energy: 19045.32560896
Spin labels: (2S+1)= 1.00000
Symmetry of eigenfunction: A1(D2)
| theta | ksi | eta | zeta | epsilon |
| z2 | yz | xz | xy | x2-y2 |

| 0.999699| 1.653760| 1.654081| 0.358690| 1.333771|

Energy: 19718.41488747
Spin labels: (2S+1)= 1.00000
Symmetry of eigenfunction: E(D4) B3(D2)
| theta | ksi | eta | zeta | epsilon |
| z2 | yz | xz | xy | x2-y2 |

| 1.867796| 0.668271| 1.516387| 0.498136| 1.449410|
==========

Energy: 19877.12404440
Spin labels: (2S+1)= 3.00000
Symmetry of eigenfunction: E(D4) B2(D2)
| theta | ksi | eta | zeta | epsilon |
| z2 | yz | xz | xy | x2-y2 |

| 0.760896| 1.013843| 1.726161| 0.987963| 1.511137|

Energy: 20071.82332348
Spin labels: (2S+1)= 3.00000
Symmetry of eigenfunction: B1(D2)
| theta | ksi | eta | zeta | epsilon | (x2-y2)1.5,(z2)1.5,(yz)1,(xz)1,(xy)1
| z2 | yz | xz | xy | x2-y2 |

| 1.500210| 0.998428| 1.090251| 1.004654| 1.406458|

Energy: 20082.20912213
Spin labels: (2S+1)= 3.00000
Symmetry of eigenfunction: E(D4) B3(D2)
| theta | ksi | eta | zeta | epsilon |
| z2 | yz | xz | xy | x2-y2 |

| 0.781908| 1.735899| 1.013186| 0.988527| 1.480480|

Energy: 21285.33094621
Spin labels: (2S+1)= 3.00000
Symmetry of eigenfunction: A1(D2)
| theta | ksi | eta | zeta | epsilon |
| z2 | yz | xz | xy | x2-y2 |

| 1.628460| 1.030420| 1.040965| 0.974978| 1.325178|

Energy: 22053.04322734
Spin labels: (2S+1)= 3.00000
Symmetry of eigenfunction: A1(D2)
| theta | ksi | eta | zeta | epsilon |
| z2 | yz | xz | xy | x2-y2 |

| 1.320524| 1.076520| 1.059935| 0.966752| 1.576269|

Energy: 22338.28646150
Spin labels: (2S+1)= 3.00000
Symmetry of eigenfunction: E(D4) B3(D2)
| theta | ksi | eta | zeta | epsilon |
| z2 | yz | xz | xy | x2-y2 |

| 1.025153| 1.947768| 1.025915| 1.001643| 0.999521|

Energy: 22791.37357550
Spin labels: (2S+1)= 3.00000
Symmetry of eigenfunction: E(D4) B2(D2)
| theta | ksi | eta | zeta | epsilon |
| z2 | yz | xz | xy | x2-y2 |

| 1.029929| 1.017641| 1.960168| 1.009048| 0.983214|

Energy: 22822.12567723
Spin labels: (2S+1)= 3.00000
Symmetry of eigenfunction: B1(D2)
| theta | ksi | eta | zeta | epsilon |
| z2 | yz | xz | xy | x2-y2 |

| 0.249321| 1.850900| 1.843211| 1.018852| 1.037716|
==========
Energy: 24304.46976583
Spin labels: (2S+1)= 5.00000
Symmetry of eigenfunction: T2(O) B2(D4) B1(D2)
| theta | ksi | eta | zeta | epsilon | (x2-y2)1,(z2)1,(yz)1,(xz)1,(xy)2
| z2 | yz | xz | xy | x2-y2 |
---------- (quintet with extra e in xy)
| 1.000000| 1.000000| 1.000000| 2.000000| 1.000000|
==========
Energy: 24496.83253135
Spin labels: (2S+1)= 3.00000
Symmetry of eigenfunction: A1(D2)
| theta | ksi | eta | zeta | epsilon | (x2-y2)1,(z2)2,(yz)1,(xz)1,(xy)1
| z2 | yz | xz | xy | x2-y2 | (possible source of band at 405 nm, $^3A \leftarrow {}^3B_1$, *z*-dipole allowed)
---------- (1-electron transition, so most likely)
| 1.863953| 0.998427| 1.004040| 1.025210| 1.108370|

Energy: 24859.72902390
Spin labels: (2S+1)= 3.00000
Symmetry of eigenfunction: E(D4) B3(D2)
| theta | ksi | eta | zeta | epsilon | (x2-y2)1,(z2)1,(yz)2,(xz)1,(xy)1 (roughly)
| z2 | yz | xz | xy | x2-y2 | (possible source of band at 405 nm, $^3B_3 \leftarrow {}^3B_1$, *y*-dipole allowed)
---------- (but 2-electron transition)
| 0.940470| 1.812921| 1.042402| 0.962040| 1.242167|

Energy: 25317.76458242
Spin labels: (2S+1)= 3.00000
Symmetry of eigenfunction: A1(D2)
| theta | ksi | eta | zeta | epsilon | (x2-y2)1,(z2)2,(yz)1,(xz)1,(xy)1
| z2 | yz | xz | xy | x2-y2 | (possible source of band at 405 nm, $^3A \leftarrow {}^3B_1$, *z*-dipole allowed)
----------(1-electron transition, so most likely)
| 1.927607| 1.010289| 0.990070| 1.014721| 1.057313|

Energy: 25414.16803736
Spin labels: (2S+1)= 3.00000
Symmetry of eigenfunction: E(D4) B2(D2)
| theta | ksi | eta | zeta | epsilon | (x2-y2)1,(z2)1,(yz)1,(xz)2,(xy)1 (roughly)
| z2 | yz | xz | xy | x2-y2 | (possible source of band at 405 nm, $^3B_2 \leftarrow {}^3B_1$, *x* -dipole allowed)
---------- (but 2-electron transition)
| 0.943977| 1.016649| 1.841396| 0.989913| 1.208065|

Energy: 26275.46446750
Spin labels: (2S+1)= 3.00000
Symmetry of eigenfunction: E(D4) B3(D2)
| theta | ksi | eta | zeta | epsilon | (x2-y2)1,(z2)1,(yz)2,(xz)1,(xy)1
| z2 | yz | xz | xy | x2-y2 |

| 1.061543| 1.890713| 1.028324| 1.048714| 0.970706|
==========

Energy: 26311.89471197
Spin labels: (2S+1)= 1.00000
Symmetry of eigenfunction: B1(D2)
| theta | ksi | eta | zeta | epsilon |
| z2 | yz | xz | xy | x2-y2 |

| 1.199688| 1.141261| 0.901247| 1.024098| 1.733706|
==========
Energy: 26633.68110429
Spin labels: (2S+1)= 3.00000
Symmetry of eigenfunction: E(D4) B2(D2)
| theta | ksi | eta | zeta | epsilon | (x2-y2)1,(z2)1,(yz)1,(xz)2,(xy)1
| z2 | yz | xz | xy | x2-y2 |

| 1.040238| 1.024127| 1.921041| 1.055107| 0.959488|
==========
Energy: 26945.17678487
Spin labels: (2S+1)= 1.00000
Symmetry of eigenfunction: B1(D2)
| theta | ksi | eta | zeta | epsilon |
| z2 | yz | xz | xy | x2-y2 |

| 1.692453| 0.943589| 1.092377| 1.018385| 1.253196|

Energy: 27009.56255025
Spin labels: (2S+1)= 1.00000
Symmetry of eigenfunction: A1(D2)
| theta | ksi | eta | zeta | epsilon |
| z2 | yz | xz | xy | x2-y2 |

| 1.365399| 1.221184| 1.216376| 0.789025| 1.408016|

Energy: 27139.57505866
Spin labels: (2S+1)= 1.00000
Symmetry of eigenfunction: E(D4) B2(D2)
| theta | ksi | eta | zeta | epsilon |
| z2 | yz | xz | xy | x2-y2 |

| 0.753427| 1.057764| 1.901441| 0.945729| 1.341639|

Energy: 27195.02311890
Spin labels: (2S+1)= 1.00000
Symmetry of eigenfunction: E(D4) B3(D2)
| theta | ksi | eta | zeta | epsilon |
| z2 | yz | xz | xy | x2-y2 |

| 0.750920| 1.962939| 1.025300| 0.979578| 1.281262|
==========
Energy: 27728.03765745
Spin labels: (2S+1)= 3.00000
Symmetry of eigenfunction: B1(D2)
| theta | ksi | eta | zeta | epsilon |
| z2 | yz | xz | xy | x2-y2 |

| 1.405705| 1.467106| 1.206389| 1.010654| 0.910146|
==========

Energy: 28599.16364768
Spin labels: (2S+1)= 1.00000
Symmetry of eigenfunction: E(D4) B2(D2)

theta	ksi	eta	zeta	epsilon
z2	yz	xz	xy	x2-y2
1.858436	1.290178	0.636139	0.733429	1.481818

Energy: 28712.15262164
Spin labels: (2S+1)= 1.00000
Symmetry of eigenfunction: A1(D2)

theta	ksi	eta	zeta	epsilon
z2	yz	xz	xy	x2-y2
1.642885	1.012385	1.025872	0.966529	1.352330

Energy: 28901.92989692
Spin labels: (2S+1)= 1.00000
Symmetry of eigenfunction: E(D4) B3(D2)

theta	ksi	eta	zeta	epsilon
z2	yz	xz	xy	x2-y2
1.858700	0.634518	1.315253	0.711569	1.479960

Energy: 28951.46179221
Spin labels: (2S+1)= 1.00000
Symmetry of eigenfunction: B1(D2)

theta	ksi	eta	zeta	epsilon
z2	yz	xz	xy	x2-y2
0.210009	1.860004	1.846835	1.000852	1.082300

states above 30 000 cm^{-1} truncated

Table S25. Results of ligand-field theory (Ligfield program) calculation for idealized $[Co^{III}(pin^{F})_2]^{1-}$, without spin-orbit coupling. Annotations have been added by hand for further explanation.

a) These matrices were generated from the following terms:
^5D $^3P_1$ $^3P_2$ ^3D $^3F_1$ $^3F_2$ ^3G ^3H $^1S_1$ $^1S_2$ $^1D_1$ $^1D_2$ ^1F $^1G_1$ $^1G_2$ ^1I of d^6 (**all free-ion terms**)

---
identical to Table 23 but with addition of:
| Parameter: | Value: |
|Spin-orbit coupling | 400.00000|

--------- Eigenvalues and eigenfunction labelling ----------
Energy: 0.00000000
Spin labels: (2S+1)= 3.01732
Symmetry of eigenfunction: A1(D2*)
| theta | ksi | eta | zeta | epsilon | (x2-y2)2,(z2)2,(yz)1,(xz)1,(xy)0
| z2 | yz | xz | xy | x2-y2 | (predominantly triplet ground state)

| 1.835487| 1.083862| 1.057870| 0.043878| 1.978903|

Energy: 68.67654957
Spin labels: (2S+1)= 3.00360
Symmetry of eigenfunction: B3(D2*)
| theta | ksi | eta | zeta | epsilon | D = (83.05 + 68.68)/2 = +75.86 cm^{-1}
| z2 | yz | xz | xy | x2-y2 | E = (83.05 - 68.68)/2 = 7.18 cm^{-1} (E/D = 0.095)

| 1.849216| 1.125793| 1.003657| 0.038656| 1.982678|

Energy: 83.04799553
Spin labels: (2S+1)= 3.01166
Symmetry of eigenfunction: B2(D2*)
| theta | ksi | eta | zeta | epsilon |
| z2 | yz | xz | xy | x2-y2 |

| 1.877121| 1.004714| 1.094713| 0.042851| 1.980600|
==========
Energy: 887.91865753
Spin labels: (2S+1)= 3.02483
Symmetry of eigenfunction: B1(D2*)
| theta | ksi | eta | zeta | epsilon |
| z2 | yz | xz | xy | x2-y2 |

| 1.030471| 1.735075| 1.231693| 0.050304| 1.952457|

Energy: 892.72529616
Spin labels: (2S+1)= 3.12843
Symmetry of eigenfunction: A1(D2*)
| theta | ksi | eta | zeta | epsilon |
| z2 | yz | xz | xy | x2-y2 |

| 1.037711| 1.611714| 1.296038| 0.098089| 1.956447|

Energy: 1106.22167965
Spin labels: (2S+1)= 3.35336
Symmetry of eigenfunction: B3(D2*)
| theta | ksi | eta | zeta | epsilon |
| z2 | yz | xz | xy | x2-y2 |

| 1.126051| 1.692319| 1.009528| 0.204925| 1.967177|

Energy: 1191.68970279
Spin labels: (2S+1)= 3.77251
Symmetry of eigenfunction: B1(D2*)
| theta | ksi | eta | zeta | epsilon |
| z2 | yz | xz | xy | x2-y2 |

| 1.029912| 1.101690| 1.502398| 0.407588| 1.958412|

Energy: 1277.02151204
Spin labels: (2S+1)= 3.61947
Symmetry of eigenfunction: B2(D2*)
| theta | ksi | eta | zeta | epsilon |
| z2 | yz | xz | xy | x2-y2 |

| 1.113587| 1.008768| 1.584857| 0.333857| 1.958932|

Energy: 1277.24127744
Spin labels: (2S+1)= 3.98357
Symmetry of eigenfunction: A1(D2*)
| theta | ksi | eta | zeta | epsilon |
| z2 | yz | xz | xy | x2-y2 |

| 1.104412| 1.095548| 1.315304| 0.513472| 1.971265|
==========
higher states truncated

b) These matrices were generated from the following terms:
^5D $^3P_1$ $^3P_2$ ^3D $^3F_1$ $^3F_2$ ^3G ^3H of d^6 **(triplets and quintet free-ion terms only; no singlets)**

--------- Eigenvalues and eigenfunction labelling ----------
Energy: 0.00000000
Spin labels: (2S+1)= 3.02156
Symmetry of eigenfunction: A1(D2*)
| theta | ksi | eta | zeta | epsilon |
| z2 | yz | xz | xy | x2-y2 |

| 1.842318| 1.079927| 1.054563| 0.043832| 1.979359|

Energy: 75.43659025 $D = (89.70 + 75.44)/2 = +82.57$ cm^{-1}
Spin labels: (2S+1)= 3.00954 $E = (89.70 - 75.44)/2 = 7.13$ cm^{-1} ($E/D = 0.086$)
Symmetry of eigenfunction: B3(D2*)
| theta | ksi | eta | zeta | epsilon |
| z2 | yz | xz | xy | x2-y2 |

| 1.853753| 1.123970| 1.000844| 0.038517| 1.982917|

Energy: 89.70340778
Spin labels: (2S+1)= 3.01805
Symmetry of eigenfunction: B2(D2*)
| theta | ksi | eta | zeta | epsilon |
| z2 | yz | xz | xy | x2-y2 |

| 1.881669| 1.001786| 1.092898| 0.042836| 1.980810|

Energy: 899.07814373
Spin labels: (2S+1)= 3.14263
Symmetry of eigenfunction: A1(D2*)
| theta | ksi | eta | zeta | epsilon |
| z2 | yz | xz | xy | x2-y2 |

| 1.034541| 1.598050| 1.309537| 0.102085| 1.955786|

Energy: 908.31626725
Spin labels: (2S+1)= 3.04934 (MS)=-0.00000
Symmetry of eigenfunction: B1(D2*)
| theta | ksi | eta | zeta | epsilon |
| z2 | yz | xz | xy | x2-y2 |

| 1.024370| 1.764122| 1.201286| 0.056547| 1.953676|

Energy: 1090.09360401
Spin labels: (2S+1)= 3.35826 (MS)= 0.00000
Symmetry of eigenfunction: B3(D2*)
| theta | ksi | eta | zeta | epsilon |
| z2 | yz | xz | xy | x2-y2 |

| 1.123615| 1.692596| 1.009434| 0.207084| 1.967271|

Energy: 1177.75263522
Spin labels: (2S+1)= 3.76500 (MS)= 0.00000
Symmetry of eigenfunction: B1(D2*)
| theta | ksi | eta | zeta | epsilon |
| z2 | yz | xz | xy | x2-y2 |

| 1.030101| 1.077821| 1.531282| 0.403330| 1.957467|

Energy: 1260.76373085
Spin labels: (2S+1)= 3.63105 (MS)=-0.00000
Symmetry of eigenfunction: B2(D2*)
| theta | ksi | eta | zeta | epsilon |
| z2 | yz | xz | xy | x2-y2 |

| 1.111314| 1.008603| 1.581640| 0.339232| 1.959211|

Energy: 1288.46300714
Spin labels: (2S+1)= 4.11894 (MS)=-0.00000
Symmetry of eigenfunction: A1(D2*)
| theta | ksi | eta | zeta | epsilon |
| z2 | yz | xz | xy | x2-y2 |

| 1.095289| 1.085946| 1.269189| 0.575749| 1.973827|
==========
higher states truncated

c) These matrices were generated from the following terms:
$^3P_1$ $^3P_2$ ^3D $^3F_1$ $^3F_2$ ^3G ^3H of d^6 **(triplets free-ion terms only; no quintet or singlets)**

--------- Eigenvalues and eigenfunction labelling ----------
Energy: 0.00000000
Spin labels: (2S+1)= 3.00000 (note pure triplet state, since triplet-only basis set)
Symmetry of eigenfunction: A1(D2*)

theta	ksi	eta	zeta	epsilon
z2	yz	xz	xy	x2-y2
1.853363	1.077605	1.050827	0.033488	1.984718

Energy: 62.35996651 $D = (81.39 + 62.36)/2 = +71.88$ cm^{-1}
Spin labels: (2S+1)= 3.00000 (MS)=-0.00000 $E = (81.39 – 62.36)/2 = 9.52$ cm^{-1} ($E/D = 0.132$)
Symmetry of eigenfunction: B3(D2*)

theta	ksi	eta	zeta	epsilon
z2	yz	xz	xy	x2-y2
1.859699	1.118677	1.000697	0.034002	1.986925

Energy: 81.39267215
Spin labels: (2S+1)= 3.00000
Symmetry of eigenfunction: B2(D2*)

theta	ksi	eta	zeta	epsilon
z2	yz	xz	xy	x2-y2
1.891618	1.001585	1.086758	0.034212	1.985828

Energy: 901.82027440
Spin labels: (2S+1)= 3.00000
Symmetry of eigenfunction: B1(D2*)

theta	ksi	eta	zeta	epsilon
z2	yz	xz	xy	x2-y2
1.026698	1.712659	1.273523	0.032690	1.954430

Energy: 926.63748771
Spin labels: (2S+1)= 3.00000
Symmetry of eigenfunction: A1(D2*)

theta	ksi	eta	zeta	epsilon
z2	yz	xz	xy	x2-y2
1.036407	1.622426	1.353756	0.032843	1.954567

Energy: 1169.29646502
Spin labels: (2S+1)= 3.00000
Symmetry of eigenfunction: B3(D2*)

theta	ksi	eta	zeta	epsilon
z2	yz	xz	xy	x2-y2
1.135935	1.854414	1.011232	0.033414	1.965005

==========
higher states truncated

d) These matrices were generated from the following terms:
$^3P_1$ $^3P_2$ ^3D $^3F_1$ $^3F_2$ ^3G ^3H $^1S_1$ $^1S_2$ $^1D_1$ $^1D_2$ ^1F $^1G_1$ $^1G_2$ ^1I of d^6 of d^6 **(triplets and singlets free-ion terms, no quintet)**

--------- Eigenvalues and eigenfunction labelling ----------
Energy: 0.00000000
Spin labels: (2S+1)= 2.99581
Symmetry of eigenfunction: A1(D2*)

theta	ksi	eta	zeta	epsilon
z2	yz	xz	xy	x2-y2
1.846829	1.081361	1.054025	0.033559	1.984226

Energy: 55.51812323 $D = (74.59 + 55.52)/2 = +65.06\ cm^{-1}$
Spin labels: (2S+1)= 2.99409 $E = (74.59 – 55.52)/2 = 9.54\ cm^{-1}$ ($E/D = 0.146$)
Symmetry of eigenfunction: B3(D2*)

theta	ksi	eta	zeta	epsilon
z2	yz	xz	xy	x2-y2
1.855081	1.120571	1.003526	0.034169	1.986653

Energy: 74.59254570
Spin labels: (2S+1)= 2.99386
Symmetry of eigenfunction: B2(D2*)

theta	ksi	eta	zeta	epsilon
z2	yz	xz	xy	x2-y2
1.886832	1.004539	1.088694	0.034369	1.985565

Energy: 878.75106394
Spin labels: (2S+1)= 2.98830
Symmetry of eigenfunction: B1(D2*)

theta	ksi	eta	zeta	epsilon
z2	yz	xz	xy	x2-y2
1.032632	1.691369	1.289150	0.033002	1.953846

Energy: 918.93168754
Spin labels: (2S+1)= 2.99374
Symmetry of eigenfunction: A1(D2*)

theta	ksi	eta	zeta	epsilon
z2	yz	xz	xy	x2-y2
1.039257	1.633141	1.339280	0.032870	1.955452

Energy: 1184.56285027
Spin labels: (2S+1)= 2.99956
Symmetry of eigenfunction: B3(D2*)

theta	ksi	eta	zeta	epsilon
z2	yz	xz	xy	x2-y2
1.138535	1.851635	1.011349	0.033494	1.964988

Energy: 1384.11291506
Spin labels: (2S+1)= 2.99928
Symmetry of eigenfunction: B2(D2*)

theta	ksi	eta	zeta	epsilon
z2	yz	xz	xy	x2-y2
1.131377	1.012161	1.881334	0.033797	1.941331

Energy: 1395.96029303
Spin labels: (2S+1)= 2.99919
Symmetry of eigenfunction: B1(D2*)
| theta | ksi | eta | zeta | epsilon |
| z2 | yz | xz | xy | x2-y2 |

| 1.043722| 1.291020| 1.692220| 0.032248| 1.940789|

Energy: 1517.21239208
Spin labels: (2S+1)= 2.98619
Symmetry of eigenfunction: A1(D2*)
| theta | ksi | eta | zeta | epsilon |
| z2 | yz | xz | xy | x2-y2 |

| 1.150852| 1.273180| 1.591554| 0.034547| 1.949868|
==========
higher states truncated

D′ for $D_{2(d,h)}$ d^6 in Strong Field

Here, we will use D_2 point group symmetry for $[Co^{III}(pin^F)_2]^-$ (**2**), although it is close to D_{2d}, and the inner coordination sphere, {CoO4}, is very close to D_{4h} (square planar) symmetry. The coordinate system for the angular overlap model (AOM) is as shown in Scheme S2, where θ = 90° (idealized angle) for all ligands and ϕ = ±44.07° for O1,2 and 180° ± 44.07° for O′1,2, as shown.

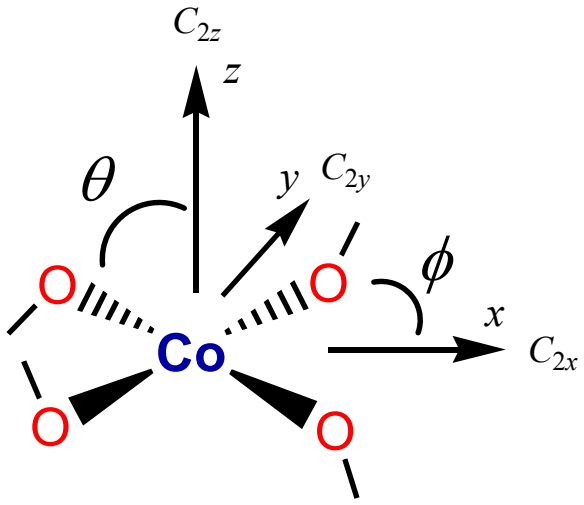

Scheme S2. Coordinate system for AOM on $[Co(pin^F)_2]^-$.

The Slater determinant orbitals for the $^3B_1$ ground state can be written as:

$$^3B_1(M_S=+1) = d^+_{x^2-y^2}d^-_{x^2-y^2}d^+_{z^2}d^-_{z^2}d^+_{yz}d^+_{xz}$$

$$^3B_1(M_S=0) = \frac{1}{\sqrt{2}}[d^+_{x^2-y^2}d^-_{x^2-y^2}d^+_{z^2}d^-_{z^2}d^+_{yz}d^-_{xz} + d^+_{x^2-y^2}d^-_{x^2-y^2}d^+_{z^2}d^-_{z^2}d^-_{yz}d^+_{xz}]$$

$$^3B_1(M_S=-1) = d^+_{x^2-y^2}d^-_{x^2-y^2}d^+_{z^2}d^-_{z^2}d^-_{yz}d^-_{xz}$$

There are four triplet excited states that are relatively low in energy; two each of $^3B_2$ and $^3B_3$. The corresponding functions for these lower lying excited states can be written as:

$$^3B_{2(a)}(M_S=+1) = d^+_{x^2-y^2} d^-_{x^2-y^2} d^+_{z^2} d^+_{yz} d^-_{yz} d^+_{xz}$$

$$^3B_{2(a)}(M_S=0) = \frac{1}{\sqrt{2}}[d^+_{x^2-y^2} d^-_{x^2-y^2} d^+_{z^2} d^+_{yz} d^-_{yz} d^-_{xz} + d^+_{x^2-y^2} d^-_{x^2-y^2} d^-_{z^2} d^+_{yz} d^-_{yz} d^+_{xz}]$$

$$^3B_{2(a)}(M_S=-1) = d^+_{x^2-y^2} d^-_{x^2-y^2} d^-_{z^2} d^+_{yz} d^-_{yz} d^-_{xz}$$

$$^3B_{3(a)}(M_S=+1) = d^+_{x^2-y^2} d^-_{x^2-y^2} d^+_{z^2} d^+_{yz} d^+_{xz} d^-_{xz}$$

$$^3B_{3(a)}(M_S=0) = \frac{1}{\sqrt{2}}[d^+_{x^2-y^2} d^-_{x^2-y^2} d^+_{z^2} d^-_{yz} d^+_{xz} d^-_{xz} + d^+_{x^2-y^2} d^-_{x^2-y^2} d^-_{z^2} d^+_{yz} d^+_{xz} d^-_{xz}]$$

$$^3B_{3(a)}(M_S=-1) = d^+_{x^2-y^2} d^-_{x^2-y^2} d^-_{z^2} d^-_{yz} d^+_{xz} d^-_{xz}$$

$$^3B_{2(b)}(M_S=+1) = d^+_{x^2-y^2} d^+_{z^2} d^-_{z^2} d^+_{yz} d^-_{yz} d^+_{xz}$$

$$^3B_{2(b)}(M_S=0) = \frac{1}{\sqrt{2}}[d^+_{x^2-y^2} d^+_{z^2} d^-_{z^2} d^+_{yz} d^-_{yz} d^-_{xz} + d^-_{x^2-y^2} d^+_{z^2} d^-_{z^2} d^+_{yz} d^-_{yz} d^+_{xz}]$$

$$^3B_{2(b)}(M_S=-1) = d^-_{x^2-y^2} d^+_{z^2} d^-_{z^2} d^+_{yz} d^-_{yz} d^-_{xz}$$

$$^3B_{3(b)}(M_S=+1) = d^+_{x^2-y^2} d^+_{z^2} d^-_{z^2} d^+_{yz} d^+_{xz} d^-_{xz}$$

$$^3B_{3(b)}(M_S=0) = \frac{1}{\sqrt{2}}[d^+_{x^2-y^2} d^+_{z^2} d^-_{z^2} d^-_{yz} d^+_{xz} d^-_{xz} + d^-_{x^2-y^2} d^+_{z^2} d^-_{z^2} d^+_{yz} d^+_{xz} d^-_{xz}]$$

$$^3B_{3(b)}(M_S=-1) = d^-_{x^2-y^2} d^+_{z^2} d^-_{z^2} d^-_{yz} d^+_{xz} d^-_{xz}$$

There is also a somewhat higher lying triplet excited state, ^{3}A, with Slater determinant given below (only for $M_S = +1$), but this involves a two-electron transition from the $^3B_1$ ground state and thus can be ignored.

$$^3A(M_S=+1) = d^+_{x^2-y^2} d^+_{z^2} d^+_{yz} d^-_{yz} d^+_{xz} d^-_{xz}$$

What we need to know are the matrix elements between the ground state and a given excited state for the spin orbit coupling (SOC) operator, H_{LS}.

$$H_{\mathrm{LS}} = \sum_i \zeta \left[l_{zi} s_{zi} + l_{xi} s_{xi} + l_{yi} s_{yi} \right]$$

where ζ is the single-electron SOC constant, which equals 619 cm^{-1} for free-ion Co^{3+}.[32] Using the relationships summarized in the following table, we can see how these ground and excited states can couple.

Table S26. Effect of orbital angular momentum operators on real d orbitals.

d orbital	$\hat{l}_x$	$\hat{l}_y$	$\hat{l}_z$
$d_{x^2-y^2}$	$-\mathrm{i}\left\|d_{yz}\right\rangle$	$-\mathrm{i}\left\|d_{xz}\right\rangle$	$2\mathrm{i}\left\|d_{xy}\right\rangle$
d_{xy}	$\mathrm{i}\left\|d_{xz}\right\rangle$	$-\mathrm{i}\left\|d_{yz}\right\rangle$	$-2\mathrm{i}\left\|d_{x^2-y^2}\right\rangle$
d_{xz}	$-\mathrm{i}\left\|d_{xy}\right\rangle$	$-\sqrt{3}\mathrm{i}\left\|d_{z^2}\right\rangle+\mathrm{i}\left\|d_{x^2-y^2}\right\rangle$	$\mathrm{i}\left\|d_{yz}\right\rangle$
d_{yz}	$\sqrt{3}\mathrm{i}\left\|d_{z^2}\right\rangle+\mathrm{i}\left\|d_{x^2-y^2}\right\rangle$	$\mathrm{i}\left\|d_{xy}\right\rangle$	$-\mathrm{i}\left\|d_{xz}\right\rangle$
d_{z^2}	$-\sqrt{3}\mathrm{i}\left\|d_{yz}\right\rangle$	$\sqrt{3}\mathrm{i}\left\|d_{xz}\right\rangle$	0

The spin angular momentum operators are as follows: $s_x = \frac{1}{2}[s_+ + s_-], s_y = -i\frac{1}{2}[s_+ - s_-], s_z = m_s$.

There are non-zero matrix elements between $^3B_1$ and both $^3B_2$ states because the $\hat{l}_x$ operator connects d_{yz} with both d_{z^2} and $d_{x^2-y^2}$ ($B_1 \times B_3$ (= R_x) × B_2 = A) and likewise between $^3B_1$ and both $^3B_3$ states because the $\hat{l}_y$ operator connects d_{xz} with both d_{z^2} and $d_{x^2-y^2}$ ($B_1 \times B_2$ (= R_y) × B_3 = A). We calculate the non-zero matrix elements as follows:

$$\left\langle {}^3B_1(+1)\middle| H_{\mathrm{LS}} \middle| {}^3B_{2(a)}(0)\right\rangle$$

$$= \left\langle d^+_{x^2-y^2} d^-_{x^2-y^2} d^+_{z^2} d^-_{z^2} d^+_{yz} d^+_{xz} \middle| H_{\mathrm{LS}} \middle| \frac{1}{\sqrt{2}} [d^+_{x^2-y^2} d^-_{x^2-y^2} d^+_{z^2} d^+_{yz} d^-_{yz} d^-_{xz} + d^+_{x^2-y^2} d^-_{x^2-y^2} d^-_{z^2} d^+_{yz} d^-_{yz} d^+_{xz}] \right\rangle$$

$$= \left\langle d^+_{x^2-y^2} d^-_{x^2-y^2} d^+_{z^2} d^-_{z^2} d^+_{yz} d^+_{xz} \middle| \frac{1}{\sqrt{2}} [d^+_{x^2-y^2} d^-_{x^2-y^2} d^+_{z^2} \left(\frac{1}{2}\right) \left\{\sqrt{3}\mathrm{i} \middle| d^-_{z^2}\right\rangle + \mathrm{i} \middle| d^-_{x^2-y^2}\right\rangle \Big\} d^-_{yz} d^-_{xz} + d^+_{x^2-y^2} d^-_{x^2-y^2} d^-_{z^2} d^+_{yz} \left(\frac{1}{2}\right) \left\{\sqrt{3}\mathrm{i} \middle| d^+_{z^2}\right\rangle + \mathrm{i} \middle| d^+_{x^2-y^2}\right\rangle \Big\} d^+_{xz}] \right\rangle$$

$$= \left\langle d^+_{x^2-y^2} d^-_{x^2-y^2} d^+_{z^2} d^-_{z^2} d^+_{yz} d^+_{xz} \middle| \frac{\sqrt{3}\mathrm{i}}{2\sqrt{2}} [d^+_{x^2-y^2} d^-_{x^2-y^2} d^+_{z^2} d^-_{z^2} d^-_{yz} d^-_{xz} + d^+_{x^2-y^2} d^-_{x^2-y^2} d^+_{z^2} d^-_{z^2} d^+_{yz} d^+_{xz}] \right\rangle$$

$$= \left\langle d^+_{x^2-y^2} d^-_{x^2-y^2} d^+_{z^2} d^-_{z^2} d^+_{yz} d^+_{xz} \middle| \frac{\sqrt{3}\mathrm{i}}{2\sqrt{2}} d^+_{x^2-y^2} d^-_{x^2-y^2} d^+_{z^2} d^-_{z^2} d^+_{yz} d^+_{xz} \right\rangle = \frac{\sqrt{3}\mathrm{i}}{2\sqrt{2}} \zeta$$

$$\left\langle {}^3B_1(0)\middle| H_{\mathrm{LS}} \middle| {}^3B_{2(a)}(+1)\right\rangle$$

$$= \left\langle \frac{1}{\sqrt{2}} [d^+_{x^2-y^2} d^-_{x^2-y^2} d^+_{z^2} d^-_{z^2} d^+_{yz} d^-_{xz} + d^+_{x^2-y^2} d^-_{x^2-y^2} d^+_{z^2} d^-_{z^2} d^-_{yz} d^+_{xz}] \middle| H_{\mathrm{LS}} \middle| d^+_{x^2-y^2} d^-_{x^2-y^2} d^+_{z^2} d^+_{yz} d^-_{yz} d^+_{xz} \right\rangle$$

$$= \left\langle \frac{1}{\sqrt{2}} [d^+_{x^2-y^2} d^-_{x^2-y^2} d^+_{z^2} d^-_{z^2} d^+_{yz} d^-_{xz} + d^+_{x^2-y^2} d^-_{x^2-y^2} d^+_{z^2} d^-_{z^2} d^-_{yz} d^+_{xz}] \middle| d^+_{x^2-y^2} d^-_{x^2-y^2} d^+_{z^2} \left(\frac{1}{2}\right) \left\{\sqrt{3}\mathrm{i} \middle| d^-_{z^2}\right\rangle + \mathrm{i} \middle| d^-_{x^2-y^2}\right\rangle \Big\} d^-_{yz} d^+_{xz} \right\rangle$$

$$= \left\langle \frac{1}{\sqrt{2}} [d^+_{x^2-y^2} d^-_{x^2-y^2} d^+_{z^2} d^-_{z^2} d^+_{yz} d^-_{xz} + d^+_{x^2-y^2} d^-_{x^2-y^2} d^+_{z^2} d^-_{z^2} d^-_{yz} d^+_{xz}] \middle| \frac{\sqrt{3}\mathrm{i}}{2} d^+_{x^2-y^2} d^-_{x^2-y^2} d^+_{z^2} d^-_{z^2} d^-_{yz} d^+_{xz} \right\rangle = \frac{\sqrt{3}\mathrm{i}}{2\sqrt{2}} \zeta$$

$$\left\langle {}^3B_1(-1)\middle| H_{\mathrm{LS}} \middle| {}^3B_{2(a)}(0)\right\rangle$$

$$= \left\langle d^+_{x^2-y^2} d^-_{x^2-y^2} d^+_{z^2} d^-_{z^2} d^-_{yz} d^-_{xz} \middle| H_{\mathrm{LS}} \middle| \frac{1}{\sqrt{2}} [d^+_{x^2-y^2} d^-_{x^2-y^2} d^+_{z^2} d^+_{yz} d^-_{yz} d^-_{xz} + d^+_{x^2-y^2} d^-_{x^2-y^2} d^-_{z^2} d^+_{yz} d^-_{yz} d^+_{xz}] \right\rangle$$

$$= \left\langle d^+_{x^2-y^2} d^-_{x^2-y^2} d^+_{z^2} d^-_{z^2} d^-_{yz} d^-_{xz} \middle| \frac{1}{\sqrt{2}} [d^+_{x^2-y^2} d^-_{x^2-y^2} d^+_{z^2} \left(\frac{1}{2}\right) \left\{\sqrt{3}\mathrm{i} \middle| d^-_{z^2}\right\rangle + \mathrm{i} \middle| d^-_{x^2-y^2}\right\rangle \Big\} d^-_{yz} d^-_{xz} + d^+_{x^2-y^2} d^-_{x^2-y^2} d^-_{z^2} d^+_{yz} \left(\frac{1}{2}\right) \left\{\sqrt{3}\mathrm{i} \middle| d^+_{z^2}\right\rangle + \mathrm{i} \middle| d^+_{x^2-y^2}\right\rangle \Big\} d^+_{xz}] \right\rangle$$

$$= \left\langle d^+_{x^2-y^2} d^-_{x^2-y^2} d^+_{z^2} d^-_{z^2} d^-_{yz} d^-_{xz} \middle| \frac{\sqrt{3}\mathrm{i}}{2\sqrt{2}} [d^+_{x^2-y^2} d^-_{x^2-y^2} d^+_{z^2} d^-_{z^2} d^-_{yz} d^-_{xz} + d^+_{x^2-y^2} d^-_{x^2-y^2} d^+_{z^2} d^-_{z^2} d^+_{yz} d^+_{xz}] \right\rangle$$

$$= \left\langle d^+_{x^2-y^2} d^-_{x^2-y^2} d^+_{z^2} d^-_{z^2} d^-_{yz} d^-_{xz} \middle| \frac{\sqrt{3}\mathrm{i}}{2\sqrt{2}} d^+_{x^2-y^2} d^-_{x^2-y^2} d^+_{z^2} d^-_{z^2} d^-_{yz} d^-_{xz} \right\rangle = \frac{\sqrt{3}\mathrm{i}}{2\sqrt{2}} \zeta$$

$$\left\langle {}^3B_1(0)\middle| H_{\mathrm{LS}} \middle| {}^3B_{2(a)}(-1)\right\rangle$$

$$= \left\langle \frac{1}{\sqrt{2}} [d^+_{x^2-y^2} d^-_{x^2-y^2} d^+_{z^2} d^-_{z^2} d^+_{yz} d^-_{xz} + d^+_{x^2-y^2} d^-_{x^2-y^2} d^+_{z^2} d^-_{z^2} d^-_{yz} d^+_{xz}] \middle| H_{\mathrm{LS}} \middle| d^+_{x^2-y^2} d^-_{x^2-y^2} d^-_{z^2} d^+_{yz} d^-_{yz} d^-_{xz} \right\rangle$$

$$= \left\langle \frac{1}{\sqrt{2}} [d^+_{x^2-y^2} d^-_{x^2-y^2} d^+_{z^2} d^-_{z^2} d^+_{yz} d^-_{xz} + d^+_{x^2-y^2} d^-_{x^2-y^2} d^+_{z^2} d^-_{z^2} d^-_{yz} d^+_{xz}] \middle| d^+_{x^2-y^2} d^-_{x^2-y^2} d^-_{z^2} d^+_{yz} \left(\frac{1}{2}\right) \left\{\sqrt{3}\mathrm{i} \middle| d^+_{z^2}\right\rangle + \mathrm{i} \middle| d^+_{x^2-y^2}\right\rangle \Big\} d^-_{xz} \right\rangle$$

$$= \left\langle \frac{1}{\sqrt{2}} [d^+_{x^2-y^2} d^-_{x^2-y^2} d^+_{z^2} d^-_{z^2} d^+_{yz} d^-_{xz} + d^+_{x^2-y^2} d^-_{x^2-y^2} d^+_{z^2} d^-_{z^2} d^-_{yz} d^+_{xz}] \middle| \frac{\sqrt{3}\mathrm{i}}{2} d^+_{x^2-y^2} d^-_{x^2-y^2} d^+_{z^2} d^-_{z^2} d^+_{yz} d^-_{xz} \right\rangle = \frac{\sqrt{3}\mathrm{i}}{2\sqrt{2}} \zeta$$

It can be seen that $M_S = \pm 1$ give the same results, as expected, so only the $M_S = +1$ elements will be done henceforth.

$$\left\langle {}^3B_1(+1)\middle| H_{\mathrm{LS}}\middle|{}^3B_{2(b)}(0)\right\rangle$$

$$=\left\langle d^+_{x^2-y^2}d^-_{x^2-y^2}d^+_{z^2}d^-_{z^2}d^+_{yz}d^+_{xz}\middle| H_{\mathrm{LS}}\middle|\frac{1}{\sqrt{2}}[d^+_{x^2-y^2}d^+_{z^2}d^-_{z^2}d^+_{yz}d^-_{yz}d^-_{xz}+d^-_{x^2-y^2}d^+_{z^2}d^-_{z^2}d^+_{yz}d^-_{yz}d^+_{xz}]\right\rangle$$

$$=\left\langle d^+_{x^2-y^2}d^-_{x^2-y^2}d^+_{z^2}d^-_{z^2}d^+_{yz}d^+_{xz}\middle|\frac{1}{\sqrt{2}}[d^+_{x^2-y^2}d^+_{z^2}d^-_{z^2}\left(\frac{1}{2}\right)\left\{\sqrt{3}\mathrm{i}\middle|d^-_{z^2}\right\rangle+\mathrm{i}\middle|d^-_{x^2-y^2}\right\rangle\Big\}d^-_{yz}d^-_{xz}+d^+_{x^2-y^2}d^+_{z^2}d^-_{z^2}d^+_{yz}\left(\frac{1}{2}\right)\left\{\sqrt{3}\mathrm{i}\middle|d^+_{z^2}\right\rangle+\mathrm{i}\middle|d^+_{x^2-y^2}\right\rangle\Big\}d^+_{xz}]\right\rangle$$

$$=\left\langle d^+_{x^2-y^2}d^-_{x^2-y^2}d^+_{z^2}d^-_{z^2}d^+_{yz}d^+_{xz}\middle|\frac{\mathrm{i}}{2\sqrt{2}}[d^+_{x^2-y^2}d^-_{x^2-y^2}d^+_{z^2}d^-_{z^2}d^-_{yz}d^-_{xz}+d^+_{x^2-y^2}d^-_{x^2-y^2}d^+_{z^2}d^-_{z^2}d^+_{yz}d^+_{xz}]\right\rangle$$

$$=\left\langle d^+_{x^2-y^2}d^-_{x^2-y^2}d^+_{z^2}d^-_{z^2}d^+_{yz}d^+_{xz}\middle|\frac{\mathrm{i}}{2\sqrt{2}}d^+_{x^2-y^2}d^-_{x^2-y^2}d^+_{z^2}d^-_{z^2}d^+_{yz}d^+_{xz}\right\rangle=\frac{\mathrm{i}}{2\sqrt{2}}\zeta$$

$$\left\langle {}^3B_1(0)\middle| H_{\mathrm{LS}}\middle|{}^3B_{2(b)}(+1)\right\rangle$$

$$=\left\langle\frac{1}{\sqrt{2}}[d^+_{x^2-y^2}d^-_{x^2-y^2}d^+_{z^2}d^-_{z^2}d^+_{yz}d^-_{xz}+d^+_{x^2-y^2}d^-_{x^2-y^2}d^+_{z^2}d^-_{z^2}d^-_{yz}d^+_{xz}]\middle| H_{\mathrm{LS}}\middle|d^+_{x^2-y^2}d^+_{z^2}d^-_{z^2}d^+_{yz}d^-_{yz}d^+_{xz}\right\rangle$$

$$=\left\langle\frac{1}{\sqrt{2}}[d^+_{x^2-y^2}d^-_{x^2-y^2}d^+_{z^2}d^-_{z^2}d^+_{yz}d^-_{xz}+d^+_{x^2-y^2}d^-_{x^2-y^2}d^+_{z^2}d^-_{z^2}d^-_{yz}d^+_{xz}]\middle|d^+_{x^2-y^2}d^+_{z^2}d^-_{z^2}\left(\frac{1}{2}\right)\left\{\sqrt{3}\mathrm{i}\middle|d^-_{z^2}\right\rangle+\mathrm{i}\middle|d^-_{x^2-y^2}\right\rangle\Big\}d^-_{yz}d^+_{xz}\right\rangle$$

$$=\left\langle\frac{1}{\sqrt{2}}[d^+_{x^2-y^2}d^-_{x^2-y^2}d^+_{z^2}d^-_{z^2}d^+_{yz}d^-_{xz}+d^+_{x^2-y^2}d^-_{x^2-y^2}d^+_{z^2}d^-_{z^2}d^-_{yz}d^+_{xz}]\middle|\frac{\mathrm{i}}{2}d^+_{x^2-y^2}d^-_{x^2-y^2}d^+_{z^2}d^-_{z^2}d^-_{yz}d^+_{xz}\right\rangle=\frac{\mathrm{i}}{2\sqrt{2}}\zeta$$

$$\left\langle {}^3B_1(+1)\middle| H_{\mathrm{LS}}\middle|{}^3B_{3(a)}(0)\right\rangle$$

$$=\left\langle d^+_{x^2-y^2}d^-_{x^2-y^2}d^+_{z^2}d^-_{z^2}d^+_{yz}d^+_{xz}\middle| H_{\mathrm{LS}}\middle|\frac{1}{\sqrt{2}}[d^+_{x^2-y^2}d^-_{x^2-y^2}d^+_{z^2}d^-_{yz}d^+_{xz}d^-_{xz}+d^+_{x^2-y^2}d^-_{x^2-y^2}d^-_{z^2}d^+_{yz}d^+_{xz}d^-_{xz}]\right\rangle$$

$$=\left\langle d^+_{x^2-y^2}d^-_{x^2-y^2}d^+_{z^2}d^-_{z^2}d^+_{yz}d^+_{xz}\middle|\frac{1}{\sqrt{2}}[d^+_{x^2-y^2}d^-_{x^2-y^2}d^+_{z^2}d^+_{yz}\left(\frac{\mathrm{i}}{2}\right)\left\{-\sqrt{3}\mathrm{i}\middle|d^-_{z^2}\right\rangle+\mathrm{i}\middle|d^-_{x^2-y^2}\right\rangle\Big\}d^-_{xz}+d^+_{x^2-y^2}d^-_{x^2-y^2}d^-_{z^2}d^+_{yz}d^+_{xz}\left(-\frac{\mathrm{i}}{2}\right)\left\{-\sqrt{3}\mathrm{i}\middle|d^+_{z^2}\right\rangle+\mathrm{i}\middle|d^+_{x^2-y^2}\right\rangle\Big\}\right\rangle$$

$$=\left\langle d^+_{x^2-y^2}d^-_{x^2-y^2}d^+_{z^2}d^-_{z^2}d^+_{yz}d^+_{xz}\middle|\frac{\sqrt{3}}{2\sqrt{2}}[-d^+_{x^2-y^2}d^-_{x^2-y^2}d^+_{z^2}d^-_{z^2}d^-_{yz}d^-_{xz}+d^+_{x^2-y^2}d^-_{x^2-y^2}d^+_{z^2}d^-_{z^2}d^+_{yz}d^+_{xz}]\right\rangle$$

$$=\left\langle d^+_{x^2-y^2}d^-_{x^2-y^2}d^+_{z^2}d^-_{z^2}d^+_{yz}d^+_{xz}\middle|\frac{\sqrt{3}}{2\sqrt{2}}d^+_{x^2-y^2}d^-_{x^2-y^2}d^+_{z^2}d^-_{z^2}d^+_{yz}d^+_{xz}\right\rangle=\frac{\sqrt{3}}{2\sqrt{2}}\zeta$$

$$\left\langle {}^3B_1(0)\middle| H_{\mathrm{LS}}\middle|{}^3B_{3(a)}(+1)\right\rangle$$

$$=\left\langle\frac{1}{\sqrt{2}}[d^+_{x^2-y^2}d^-_{x^2-y^2}d^+_{z^2}d^-_{z^2}d^+_{yz}d^-_{xz}+d^+_{x^2-y^2}d^-_{x^2-y^2}d^+_{z^2}d^-_{z^2}d^-_{yz}d^+_{xz}]\middle| H_{\mathrm{LS}}\middle|d^+_{x^2-y^2}d^-_{x^2-y^2}d^+_{z^2}d^+_{yz}d^+_{xz}d^-_{xz}\right\rangle$$

$$=\left\langle\frac{1}{\sqrt{2}}[d^+_{x^2-y^2}d^-_{x^2-y^2}d^+_{z^2}d^-_{z^2}d^+_{yz}d^-_{xz}+d^+_{x^2-y^2}d^-_{x^2-y^2}d^+_{z^2}d^-_{z^2}d^-_{yz}d^+_{xz}]\middle|d^+_{x^2-y^2}d^-_{x^2-y^2}d^+_{z^2}d^+_{yz}\left(\frac{\mathrm{i}}{2}\right)\left\{-\sqrt{3}\mathrm{i}\middle|d^-_{z^2}\right\rangle+\mathrm{i}\middle|d^-_{x^2-y^2}\right\rangle\Big\}d^-_{xz}\right\rangle$$

$$=\left\langle\frac{1}{\sqrt{2}}[d^+_{x^2-y^2}d^-_{x^2-y^2}d^+_{z^2}d^-_{z^2}d^+_{yz}d^-_{xz}+d^+_{x^2-y^2}d^-_{x^2-y^2}d^+_{z^2}d^-_{z^2}d^-_{yz}d^+_{xz}]\middle|-\frac{\sqrt{3}}{2}d^+_{x^2-y^2}d^-_{x^2-y^2}d^+_{z^2}d^-_{z^2}d^+_{yz}d^-_{xz}\right\rangle=-\frac{\sqrt{3}}{2\sqrt{2}}\zeta$$

$$\left\langle {}^3B_1(+1)\middle| H_{\rm LS}\middle|{}^3B_{3(b)}(0)\right\rangle$$

$$=\left\langle d^+_{x^2-y^2}d^-_{x^2-y^2}d^+_{z^2}d^-_{z^2}d^+_{yz}d^+_{xz}\middle| H_{\rm LS}\middle|\frac{1}{\sqrt{2}}[d^+_{x^2-y^2}d^+_{z^2}d^-_{z^2}d^-_{yz}d^+_{xz}d^-_{xz}+d^-_{x^2-y^2}d^+_{z^2}d^-_{z^2}d^+_{yz}d^+_{xz}d^-_{xz}]\right\rangle$$

$$=\left\langle d^+_{x^2-y^2}d^-_{x^2-y^2}d^+_{z^2}d^-_{z^2}d^+_{yz}d^+_{xz}\middle|\frac{1}{\sqrt{2}}[d^+_{x^2-y^2}d^+_{z^2}d^-_{z^2}d^-_{yz}\left(\frac{\rm i}{2}\right)\left\{-\sqrt{3}{\rm i}\middle|d^-_{z^2}\right\rangle+{\rm i}\middle|d^-_{x^2-y^2}\right\rangle\Big\}d^-_{xz}+d^-_{x^2-y^2}d^+_{z^2}d^-_{z^2}d^+_{yz}d^+_{xz}\left(-\frac{\rm i}{2}\right)\left\{-\sqrt{3}{\rm i}\middle|d^+_{z^2}\right\rangle+{\rm i}\middle|d^+_{x^2-y^2}\right\rangle\Big\}\right\rangle$$

$$=\left\langle d^+_{x^2-y^2}d^-_{x^2-y^2}d^+_{z^2}d^-_{z^2}d^+_{yz}d^+_{xz}\middle|\frac{1}{2\sqrt{2}}[d^+_{x^2-y^2}d^-_{x^2-y^2}d^+_{z^2}d^-_{z^2}d^-_{yz}d^-_{xz}-d^+_{x^2-y^2}d^-_{x^2-y^2}d^+_{z^2}d^-_{z^2}d^+_{yz}d^+_{xz}]\right\rangle$$

$$=\left\langle d^+_{x^2-y^2}d^-_{x^2-y^2}d^+_{z^2}d^-_{z^2}d^+_{yz}d^+_{xz}\middle|-\frac{1}{2\sqrt{2}}d^+_{x^2-y^2}d^-_{x^2-y^2}d^+_{z^2}d^-_{z^2}d^+_{yz}d^+_{xz}\right\rangle=-\frac{1}{2\sqrt{2}}\zeta$$

$$\left\langle {}^3B_1(0)\middle| H_{\rm LS}\middle|{}^3B_{3(b)}(+1)\right\rangle$$

$$=\left\langle\frac{1}{\sqrt{2}}[d^+_{x^2-y^2}d^-_{x^2-y^2}d^+_{z^2}d^-_{z^2}d^+_{yz}d^-_{xz}+d^+_{x^2-y^2}d^-_{x^2-y^2}d^+_{z^2}d^-_{z^2}d^-_{yz}d^+_{xz}]\middle| H_{\rm LS}\middle| d^+_{x^2-y^2}d^+_{z^2}d^-_{z^2}d^+_{yz}d^+_{xz}d^-_{xz}\right\rangle$$

$$=\left\langle\frac{1}{\sqrt{2}}[d^+_{x^2-y^2}d^-_{x^2-y^2}d^+_{z^2}d^-_{z^2}d^+_{yz}d^-_{xz}+d^+_{x^2-y^2}d^-_{x^2-y^2}d^+_{z^2}d^-_{z^2}d^-_{yz}d^+_{xz}]\middle| d^+_{x^2-y^2}d^+_{z^2}d^-_{z^2}d^+_{yz}\left(\frac{\rm i}{2}\right)\left\{-\sqrt{3}{\rm i}\middle|d^-_{z^2}\right\rangle+{\rm i}\middle|d^-_{x^2-y^2}\right\rangle\Big\}d^-_{xz}\right\rangle$$

$$=\left\langle\frac{1}{\sqrt{2}}[d^+_{x^2-y^2}d^-_{x^2-y^2}d^+_{z^2}d^-_{z^2}d^+_{yz}d^-_{xz}+d^+_{x^2-y^2}d^-_{x^2-y^2}d^+_{z^2}d^-_{z^2}d^-_{yz}d^+_{xz}]\middle| d^+_{x^2-y^2}d^-_{x^2-y^2}d^+_{z^2}d^-_{z^2}d^+_{yz}d^-_{xz}\right\rangle=\frac{1}{2\sqrt{2}}\zeta$$

We then use second order perturbation theory to calculate the contribution of the $^3B_{2,3(a,b)}$ states to $^3B_1(M_S)$ which is:

$$\Delta E'(+1)=$$

$$-\frac{\left\langle {}^3B_1(+1)\,|\,H_{\rm LS}\,|\,{}^3B_{2(a)}(0)\right\rangle\left\langle {}^3B_{2(a)}(0)\,|\,H_{\rm LS}\,|\,{}^3B_1(+1)\right\rangle}{\left(E\left({}^3B_{2(a)}\right)-E\left({}^3B_1\right)\right)}-\frac{\left\langle {}^3B_1(+1)\,|\,H_{\rm LS}\,|\,{}^3B_{2(b)}(0)\right\rangle\left\langle {}^3B_{2(b)}(0)\,|\,H_{\rm LS}\,|\,{}^3B_1(+1)\right\rangle}{\left(E\left({}^3B_{2(b)}\right)-E\left({}^3B_1\right)\right)}$$

$$-\frac{\left\langle {}^3B_1(+1)\,|\,H_{\rm LS}\,|\,{}^3B_{3(a)}(0)\right\rangle\left\langle {}^3B_{3(a)}(0)\,|\,H_{\rm LS}\,|\,{}^3B_1(+1)\right\rangle}{\left(E\left({}^3B_{3(a)}\right)-E\left({}^3B_1\right)\right)}-\frac{\left\langle {}^3B_1(+1)\,|\,H_{\rm LS}\,|\,{}^3B_{3(b)}(0)\right\rangle\left\langle {}^3B_{3(b)}(0)\,|\,H_{\rm LS}\,|\,{}^3B_1(+1)\right\rangle}{\left(E\left({}^3B_{3(b)}\right)-E\left({}^3B_1\right)\right)}=$$

$$-\frac{\left(\frac{\sqrt{3}{\rm i}}{2\sqrt{2}}\zeta\right)\left(-\frac{\sqrt{3}{\rm i}}{2\sqrt{2}}\zeta\right)}{\left(E\left({}^3B_{2(a)}\right)-E\left({}^3B_1\right)\right)}-\frac{\left(\frac{\rm i}{2\sqrt{2}}\zeta\right)\left(-\frac{\rm i}{2\sqrt{2}}\zeta\right)}{\left(E\left({}^3B_{2(b)}\right)-E\left({}^3B_1\right)\right)}$$

$$-\frac{\left(\frac{\sqrt{3}}{2\sqrt{2}}\zeta\right)\left(\frac{\sqrt{3}}{2\sqrt{2}}\zeta\right)}{\left(E\left({}^3B_{3(a)}\right)-E\left({}^3B_1\right)\right)}-\frac{\left(-\frac{1}{2\sqrt{2}}\zeta\right)\left(-\frac{1}{2\sqrt{2}}\zeta\right)}{\left(E\left({}^3B_{3(b)}\right)-E\left({}^3B_1\right)\right)}=$$

$$-\frac{\zeta^2}{8}\left[\begin{array}{l}\dfrac{3}{\left(E\left({}^3B_{2(a)}\right)-E\left({}^3B_1\right)\right)}+\dfrac{1}{\left(E\left({}^3B_{2(b)}\right)-E\left({}^3B_1\right)\right)}+\\ \dfrac{3}{\left(E\left({}^3B_{3(a)}\right)-E\left({}^3B_1\right)\right)}+\dfrac{1}{\left(E\left({}^3B_{3(b)}\right)-E\left({}^3B_1\right)\right)}\end{array}\right]$$

$$\Delta E'(0) =$$

$$-\frac{\left\langle {}^3B_1(0)\,|\,H_{\mathrm{LS}}\,|\,{}^3B_{2(a)}(+1)\right\rangle\left\langle {}^3B_{2(a)}(+1)\,|\,H_{\mathrm{LS}}\,|\,{}^3B_1(0)\right\rangle}{\left(E\left({}^3B_{2(a)}\right)-E\left({}^3B_1\right)\right)}-\frac{\left\langle {}^3B_1(0)\,|\,H_{\mathrm{LS}}\,|\,{}^3B_{2(b)}(+1)\right\rangle\left\langle {}^3B_{2(b)}(+1)\,|\,H_{\mathrm{LS}}\,|\,{}^3B_1(0)\right\rangle}{\left(E\left({}^3B_{2(b)}\right)-E\left({}^3B_1\right)\right)}$$

$$-\frac{\left\langle {}^3B_1(0)\,|\,H_{\mathrm{LS}}\,|\,{}^3B_{2(a)}(-1)\right\rangle\left\langle {}^3B_{2(a)}(-1)\,|\,H_{\mathrm{LS}}\,|\,{}^3B_1(0)\right\rangle}{\left(E\left({}^3B_{2(a)}\right)-E\left({}^3B_1\right)\right)}-\frac{\left\langle {}^3B_1(0)\,|\,H_{\mathrm{LS}}\,|\,{}^3B_{2(b)}(-1)\right\rangle\left\langle {}^3B_{2(b)}(-1)\,|\,H_{\mathrm{LS}}\,|\,{}^3B_1(0)\right\rangle}{\left(E\left({}^3B_{2(b)}\right)-E\left({}^3B_1\right)\right)}$$

$$-\frac{\left\langle {}^3B_1(0)\,|\,H_{\mathrm{LS}}\,|\,{}^3B_{3(a)}(+1)\right\rangle\left\langle {}^3B_{3(a)}(+1)\,|\,H_{\mathrm{LS}}\,|\,{}^3B_1(0)\right\rangle}{\left(E\left({}^3B_{3(a)}\right)-E\left({}^3B_1\right)\right)}-\frac{\left\langle {}^3B_1(0)\,|\,H_{\mathrm{LS}}\,|\,{}^3B_{3(b)}(+1)\right\rangle\left\langle {}^3B_{3(b)}(+1)\,|\,H_{\mathrm{LS}}\,|\,{}^3B_1(0)\right\rangle}{\left(E\left({}^3B_{3(b)}\right)-E\left({}^3B_1\right)\right)}$$

$$-\frac{\left\langle {}^3B_1(0)\,|\,H_{\mathrm{LS}}\,|\,{}^3B_{3(a)}(-1)\right\rangle\left\langle {}^3B_{3(a)}(-1)\,|\,H_{\mathrm{LS}}\,|\,{}^3B_1(0)\right\rangle}{\left(E\left({}^3B_{3(a)}\right)-E\left({}^3B_1\right)\right)}-\frac{\left\langle {}^3B_1(0)\,|\,H_{\mathrm{LS}}\,|\,{}^3B_{3(b)}(-1)\right\rangle\left\langle {}^3B_{3(b)}(-1)\,|\,H_{\mathrm{LS}}\,|\,{}^3B_1(0)\right\rangle}{\left(E\left({}^3B_{3(b)}\right)-E\left({}^3B_1\right)\right)}=$$

$$-\frac{\left(\frac{\sqrt{3}\mathrm{i}}{2\sqrt{2}}\zeta\right)\left(\frac{-\sqrt{3}\mathrm{i}}{2\sqrt{2}}\zeta\right)}{\left(E\left({}^3B_{2(a)}\right)-E\left({}^3B_1\right)\right)}-\frac{\left(\frac{\mathrm{i}}{2\sqrt{2}}\zeta\right)\left(\frac{-\mathrm{i}}{2\sqrt{2}}\zeta\right)}{\left(E\left({}^3B_{2(b)}\right)-E\left({}^3B_1\right)\right)}$$

$$-\frac{\left(\frac{\sqrt{3}\mathrm{i}}{2\sqrt{2}}\zeta\right)\left(\frac{-\sqrt{3}\mathrm{i}}{2\sqrt{2}}\zeta\right)}{\left(E\left({}^3B_{2(a)}\right)-E\left({}^3B_1\right)\right)}-\frac{\left(\frac{\mathrm{i}}{2\sqrt{2}}\zeta\right)\left(\frac{-\mathrm{i}}{2\sqrt{2}}\zeta\right)}{\left(E\left({}^3B_{2(b)}\right)-E\left({}^3B_1\right)\right)}$$

$$-\frac{\left(\frac{-\sqrt{3}}{2\sqrt{2}}\zeta\right)\left(\frac{-\sqrt{3}}{2\sqrt{2}}\zeta\right)}{\left(E\left({}^3B_{3(a)}\right)-E\left({}^3B_1\right)\right)}-\frac{\left(\frac{1}{2\sqrt{2}}\zeta\right)\left(\frac{1}{2\sqrt{2}}\zeta\right)}{\left(E\left({}^3B_{3(b)}\right)-E\left({}^3B_1\right)\right)}$$

$$-\frac{\left(\frac{-\sqrt{3}}{2\sqrt{2}}\zeta\right)\left(\frac{-\sqrt{3}}{2\sqrt{2}}\zeta\right)}{\left(E\left({}^3B_{3(a)}\right)-E\left({}^3B_1\right)\right)}-\frac{\left(\frac{1}{2\sqrt{2}}\zeta\right)\left(\frac{1}{2\sqrt{2}}\zeta\right)}{\left(E\left({}^3B_{3(b)}\right)-E\left({}^3B_1\right)\right)}=$$

$$-\frac{\left(\frac{3}{4}\zeta^2\right)}{\left(E\left({}^3B_{2(a)}\right)-E\left({}^3B_1\right)\right)}-\frac{\left(\frac{1}{4}\zeta^2\right)}{\left(E\left({}^3B_{2(b)}\right)-E\left({}^3B_1\right)\right)}$$

$$-\frac{\left(\frac{3}{4}\zeta^2\right)}{\left(E\left({}^3B_{3(a)}\right)-E\left({}^3B_1\right)\right)}-\frac{\left(\frac{1}{4}\zeta^2\right)}{\left(E\left({}^3B_{3(b)}\right)-E\left({}^3B_1\right)\right)}=$$

$$-\frac{\zeta^2}{4}\left[\begin{array}{l}\dfrac{3}{\left(E\left({}^3B_{2(a)}\right)-E\left({}^3B_1\right)\right)}+\dfrac{1}{\left(E\left({}^3B_{2(b)}\right)-E\left({}^3B_1\right)\right)}+\\ \dfrac{3}{\left(E\left({}^3B_{3(a)}\right)-E\left({}^3B_1\right)\right)}+\dfrac{1}{\left(E\left({}^3B_{3(b)}\right)-E\left({}^3B_1\right)\right)}\end{array}\right]$$

For the $S = 1$ system $E(M_S = \pm 1) - E(M_S = 0) = D$, therefore

$$D' = -\frac{\zeta^2}{8}\left[\frac{3}{\left(E\left({}^3B_{2(a)}\right) - E\left({}^3B_1\right)\right)} + \frac{1}{\left(E\left({}^3B_{2(b)}\right) - E\left({}^3B_1\right)\right)} + \frac{3}{\left(E\left({}^3B_{3(a)}\right) - E\left({}^3B_1\right)\right)} + \frac{1}{\left(E\left({}^3B_{3(b)}\right) - E\left({}^3B_1\right)\right)}\right] + \frac{\zeta^2}{4}\left[\frac{3}{\left(E\left({}^3B_{2(a)}\right) - E\left({}^3B_1\right)\right)} + \frac{1}{\left(E\left({}^3B_{2(b)}\right) - E\left({}^3B_1\right)\right)} + \frac{3}{\left(E\left({}^3B_{3(a)}\right) - E\left({}^3B_1\right)\right)} + \frac{1}{\left(E\left({}^3B_{3(b)}\right) - E\left({}^3B_1\right)\right)}\right]$$

$$D' = \frac{\zeta^2}{8}\left[\frac{3}{\left(E\left({}^3B_{2(a)}\right) - E\left({}^3B_1\right)\right)} + \frac{1}{\left(E\left({}^3B_{2(b)}\right) - E\left({}^3B_1\right)\right)} + \frac{3}{\left(E\left({}^3B_{3(a)}\right) - E\left({}^3B_1\right)\right)} + \frac{1}{\left(E\left({}^3B_{3(b)}\right) - E\left({}^3B_1\right)\right)}\right]$$

where $E\left({}^3B_{2(a)}\right) - E\left({}^3B_1\right)$ is the energy difference between $d^+_{x^2-y^2} d^-_{x^2-y^2} d^+_{z^2} d^-_{z^2} d^\pm_{yz} d^\pm_{xz}$ and $d^+_{x^2-y^2} d^-_{x^2-y^2} d^\pm_{z^2} d^+_{yz} d^-_{yz} d^\pm_{xz}$ (i.e., $d^\pm_{z^2} \rightarrow d^\pm_{yz}$), $E\left({}^3B_{2(b)}\right) - E\left({}^3B_1\right)$ is the energy difference between $d^+_{x^2-y^2} d^-_{x^2-y^2} d^+_{z^2} d^-_{z^2} d^\pm_{yz} d^\pm_{xz}$ and $d^+_{x^2-y^2} d^+_{z^2} d^-_{z^2} d^+_{yz} d^-_{yz} d^+_{xz}$ (i.e., $d^\pm_{x^2-y^2} \rightarrow d^\pm_{yz}$), $E\left({}^3B_{3(a)}\right) - E\left({}^3B_1\right)$ is the energy difference between $d^+_{x^2-y^2} d^-_{x^2-y^2} d^+_{z^2} d^-_{z^2} d^\pm_{yz} d^\pm_{xz}$ and $d^+_{x^2-y^2} d^-_{x^2-y^2} d^\pm_{z^2} d^\pm_{yz} d^+_{xz} d^-_{xz}$ (i.e., $d^\pm_{z^2} \rightarrow d^\pm_{xz}$), and $E\left({}^3B_{3(b)}\right) - E\left({}^3B_1\right)$ is the energy difference between $d^+_{x^2-y^2} d^-_{x^2-y^2} d^+_{z^2} d^-_{z^2} d^\pm_{yz} d^\pm_{xz}$ and $d^+_{x^2-y^2} d^+_{z^2} d^-_{z^2} d^+_{yz} d^+_{xz} d^-_{xz}$ (i.e., $d^\pm_{x^2-y^2} \rightarrow d^\pm_{xz}$). Because the energy difference between the d_{xz} and d_{yz} orbitals is small, and because the $d_{x^2-y^2}$ is much lower in energy than the d_{z^2} orbital (these two do mix in D_2 symmetry as both have A representation), we can further approximate this contribution to D as:

$$D' = \frac{\zeta^2}{4}\left[\frac{3}{\left(E\left({}^3B_{2,3(a)}\right) - E\left({}^3B_1\right)\right)} + \frac{1}{\left(E\left({}^3B_{2,3(b)}\right) - E\left({}^3B_1\right)\right)}\right] \approx \frac{3}{4}\frac{\zeta^2}{E\left(d_{z^2} \rightarrow d_{yz,xz}\right)}$$

i.e., ignoring the contribution from ${}^3B_{2,3(b)}$. The results of Ligfield (see Table S24) suggest that the relevant electronic transition energy is only ~1000 cm^{-1}, so use of $300 \leq \zeta \leq 330$ cm^{-1}, i.e., a

reduction to ~50% of the free-ion value, would give D' in the range of 70 – 80 cm^{-1}, with a positive value as seen experimentally. Note that the AOM bonding parameters used in the Ligfield calculations were chosen so as to be reasonable for the alkoxide donor perfluoropinacolate ligands. They are in no way meant to be definitive or a unique solution, but they do give the correct ground state, $^3B_1$, and orbital ordering, as well as electronic dipole-allowed transitions ($^3B_1 \rightarrow {}^3A$ (×2; z allowed); $\rightarrow {}^3B_2$ (x allowed); $\rightarrow {}^3B_3$ (y allowed)) all in the range 24 500 – 25 400 cm^{-1}, which correspond well with the observed band at 405 nm. The interelectronic repulsion (Racah) parameters were chosen to be 60% of the free-ion values for Co^{3+},[32] which is a reasonable reduction due to covalency., but is not meant to be other than illustrative.

We can also include the contribution from lower lying quintet excited states. These states are $^5A_{(a,b)}$ with Slater determinants as follows (only the highest M_S is given for $^5A_{(a)}$; the determinants for $M_S = -1, -2$ are also omitted for $^5A_{(b)}$):

$$^5A_{(a)}(M_S = +2) = d^+_{x^2-y^2} d^-_{x^2-y^2} d^+_{z^2} d^+_{yz} d^+_{xz} d^+_{xy}$$

...

$$^5A_{(b)}(M_S = +2) = d^+_{x^2-y^2} d^+_{z^2} d^-_{z^2} d^+_{yz} d^+_{xz} d^+_{xy}$$

$$^5A_{(b)}(M_S = +1) = \frac{1}{2}[d^+_{x^2-y^2} d^+_{z^2} d^-_{z^2} d^+_{yz} d^+_{xz} d^-_{xy} + d^+_{x^2-y^2} d^+_{z^2} d^-_{z^2} d^+_{yz} d^-_{xz} d^+_{xy} + d^+_{x^2-y^2} d^+_{z^2} d^-_{z^2} d^-_{yz} d^+_{xz} d^+_{xy} + d^-_{x^2-y^2} d^+_{z^2} d^-_{z^2} d^+_{yz} d^+_{xz} d^+_{xy}]$$

$$^5A_{(b)}(M_S = 0) = \frac{1}{\sqrt{6}}[d^+_{x^2-y^2} d^+_{z^2} d^-_{z^2} d^+_{yz} d^-_{xz} d^-_{xy} + d^+_{x^2-y^2} d^+_{z^2} d^-_{z^2} d^-_{yz} d^+_{xz} d^-_{xy} + d^-_{x^2-y^2} d^+_{z^2} d^-_{z^2} d^+_{yz} d^+_{xz} d^-_{xy} + d^+_{x^2-y^2} d^+_{z^2} d^-_{z^2} d^-_{yz} d^-_{xz} d^+_{xy} + d^-_{x^2-y^2} d^+_{z^2} d^-_{z^2} d^+_{yz} d^-_{xz} d^+_{xy} + d^-_{x^2-y^2} d^+_{z^2} d^-_{z^2} d^-_{yz} d^+_{xz} d^+_{xy}]$$

Other quintet excited states can be disregarded because they would involve two-electron transitions. The quintet excited state $^5A_{(b)}$ has non-zero matrix elements with the ground state because the $\hat{l}_z$ operator connects d_{xy} with $d_{x^2-y^2}$ ($B_1 \times B_1$ (= R_z) × A = A), but the lowest lying

quintet excited state, $^5A_{(a)}$, does not because no operator connects d_{xy} with d_{z^2}. The matrix elements between the $^3B_1$ ground state and $^5A_{(b)}$ excited state are as follows:

$$\left\langle {}^3B_1(+1)\middle|H_{\mathrm{LS}}\middle|{}^5A_{(a)}(+2)\right\rangle$$
$$=\left\langle d^+_{x^2-y^2}d^-_{x^2-y^2}d^+_{z^2}d^-_{z^2}d^+_{yz}d^+_{xz}\middle|H_{\mathrm{LS}}\middle|d^+_{x^2-y^2}d^+_{z^2}d^-_{z^2}d^+_{yz}d^+_{xz}d^+_{xy}\right\rangle=0$$

$$\left\langle {}^3B_1(+1)\middle|H_{\mathrm{LS}}\middle|{}^5A_{(a)}(+1)\right\rangle$$
$$=\left\langle d^+_{x^2-y^2}d^-_{x^2-y^2}d^+_{z^2}d^-_{z^2}d^+_{yz}d^+_{xz}\middle|H_{\mathrm{LS}}\middle|\frac{1}{2}[d^+_{x^2-y^2}d^+_{z^2}d^-_{z^2}d^+_{yz}d^+_{xz}d^-_{xy}+d^+_{x^2-y^2}d^+_{z^2}d^-_{z^2}d^+_{yz}d^-_{xz}d^+_{xy}+d^+_{x^2-y^2}d^+_{z^2}d^-_{z^2}d^-_{yz}d^+_{xz}d^+_{xy}+d^-_{x^2-y^2}d^+_{z^2}d^-_{z^2}d^+_{yz}d^+_{xz}d^+_{xy}]\right\rangle$$
$$=\left\langle d^+_{x^2-y^2}d^-_{x^2-y^2}d^+_{z^2}d^-_{z^2}d^+_{yz}d^+_{xz}\middle|\frac{1}{2}[d^+_{x^2-y^2}d^+_{z^2}d^-_{z^2}d^+_{yz}d^+_{xz}\left(-\frac{1}{2}\right)\left\{-2\mathrm{i}d^-_{x^2-y^2}\right\}+0+0+d^-_{x^2-y^2}d^+_{z^2}d^-_{z^2}d^+_{yz}d^+_{xz}\left(\frac{1}{2}\right)\left\{-2\mathrm{i}d^+_{x^2-y^2}\right\}]\right\rangle$$
$$=\left\langle d^+_{x^2-y^2}d^-_{x^2-y^2}d^+_{z^2}d^-_{z^2}d^+_{yz}d^+_{xz}\middle|\frac{\mathrm{i}}{2}[d^+_{x^2-y^2}d^-_{x^2-y^2}d^+_{z^2}d^-_{z^2}d^+_{yz}d^+_{xz}+d^+_{x^2-y^2}d^-_{x^2-y^2}d^+_{z^2}d^-_{z^2}d^-_{yz}d^+_{xz}]\right\rangle=\mathrm{i}\zeta$$
$$\left\langle {}^3B_1(+1)\middle|H_{\mathrm{LS}}\middle|{}^5A_{(a)}(0)\right\rangle$$
$$=\left\langle d^+_{x^2-y^2}d^-_{x^2-y^2}d^+_{z^2}d^-_{z^2}d^+_{yz}d^+_{xz}\middle|H_{\mathrm{LS}}\middle|\begin{array}{l}\frac{1}{\sqrt{6}}[d^+_{x^2-y^2}d^+_{z^2}d^-_{z^2}d^+_{yz}d^-_{xz}d^-_{xy}+d^+_{x^2-y^2}d^+_{z^2}d^-_{z^2}d^-_{yz}d^+_{xz}d^-_{xy}+d^-_{x^2-y^2}d^+_{z^2}d^-_{z^2}d^+_{yz}d^+_{xz}d^-_{xy}\\ \quad+d^+_{x^2-y^2}d^+_{z^2}d^-_{z^2}d^-_{yz}d^-_{xz}d^+_{xy}+d^-_{x^2-y^2}d^+_{z^2}d^-_{z^2}d^+_{yz}d^-_{xz}d^+_{xy}+d^-_{x^2-y^2}d^+_{z^2}d^-_{z^2}d^-_{yz}d^+_{xz}d^+_{xy}]\end{array}\right\rangle=0$$
$$\left\langle {}^3B_1(0)\middle|H_{\mathrm{LS}}\middle|{}^5A_{(a)}(0)\right\rangle$$
$$=\left\langle \frac{1}{\sqrt{2}}[d^+_{x^2-y^2}d^-_{x^2-y^2}d^+_{z^2}d^-_{z^2}d^+_{yz}d^-_{xz}+d^+_{x^2-y^2}d^-_{x^2-y^2}d^+_{z^2}d^-_{z^2}d^-_{yz}d^+_{xz}]\middle|H_{\mathrm{LS}}\middle|\begin{array}{l}\frac{1}{\sqrt{6}}[d^+_{x^2-y^2}d^+_{z^2}d^-_{z^2}d^+_{yz}d^-_{xz}d^-_{xy}+d^+_{x^2-y^2}d^+_{z^2}d^-_{z^2}d^-_{yz}d^+_{xz}d^-_{xy}+d^-_{x^2-y^2}d^+_{z^2}d^-_{z^2}d^+_{yz}d^+_{xz}d^-_{xy}\\ \quad+d^+_{x^2-y^2}d^+_{z^2}d^-_{z^2}d^-_{yz}d^-_{xz}d^+_{xy}+d^-_{x^2-y^2}d^+_{z^2}d^-_{z^2}d^+_{yz}d^-_{xz}d^+_{xy}+d^-_{x^2-y^2}d^+_{z^2}d^-_{z^2}d^-_{yz}d^+_{xz}d^+_{xy}]\end{array}\right\rangle$$
$$=\left\langle \frac{1}{\sqrt{2}}[d^+_{x^2-y^2}d^-_{x^2-y^2}d^+_{z^2}d^-_{z^2}d^+_{yz}d^-_{xz}+d^+_{x^2-y^2}d^-_{x^2-y^2}d^+_{z^2}d^-_{z^2}d^-_{yz}d^+_{xz}]\middle|\begin{array}{l}\frac{1}{\sqrt{6}}[d^+_{x^2-y^2}d^+_{z^2}d^-_{z^2}d^+_{yz}d^-_{xz}\left(-\frac{1}{2}\right)\left\{-2\mathrm{i}d^-_{x^2-y^2}\right\}+d^+_{x^2-y^2}d^+_{z^2}d^-_{z^2}d^-_{yz}d^+_{xz}\left(-\frac{1}{2}\right)\left\{-2\mathrm{i}d^-_{x^2-y^2}\right\}\\ +0+0+d^-_{x^2-y^2}d^+_{z^2}d^-_{z^2}d^+_{yz}d^-_{xz}\left(\frac{1}{2}\right)\left\{-2\mathrm{i}d^+_{x^2-y^2}\right\}+d^-_{x^2-y^2}d^+_{z^2}d^-_{z^2}d^-_{yz}d^+_{xz}\left(\frac{1}{2}\right)\left\{-2\mathrm{i}d^+_{x^2-y^2}\right\}]\end{array}\right\rangle$$
$$=\left\langle \frac{1}{\sqrt{2}}[d^+_{x^2-y^2}d^-_{x^2-y^2}d^+_{z^2}d^-_{z^2}d^+_{yz}d^-_{xz}+d^+_{x^2-y^2}d^-_{x^2-y^2}d^+_{z^2}d^-_{z^2}d^-_{yz}d^+_{xz}]\middle|\begin{array}{l}\frac{\mathrm{i}}{\sqrt{6}}[d^+_{x^2-y^2}d^-_{x^2-y^2}d^+_{z^2}d^-_{z^2}d^+_{yz}d^-_{xz}+d^+_{x^2-y^2}d^-_{x^2-y^2}d^+_{z^2}d^-_{z^2}d^-_{yz}d^+_{xz}\\ +d^+_{x^2-y^2}d^-_{x^2-y^2}d^+_{z^2}d^-_{z^2}d^+_{yz}d^-_{xz}+d^+_{x^2-y^2}d^-_{x^2-y^2}d^+_{z^2}d^-_{z^2}d^-_{yz}d^+_{xz}]\end{array}\right\rangle$$
$$=\left\langle \frac{1}{\sqrt{2}}[d^+_{x^2-y^2}d^-_{x^2-y^2}d^+_{z^2}d^-_{z^2}d^+_{yz}d^-_{xz}+d^+_{x^2-y^2}d^-_{x^2-y^2}d^+_{z^2}d^-_{z^2}d^-_{yz}d^+_{xz}]\middle|\frac{2\mathrm{i}}{\sqrt{6}}[d^+_{x^2-y^2}d^-_{x^2-y^2}d^+_{z^2}d^-_{z^2}d^+_{yz}d^-_{xz}+d^+_{x^2-y^2}d^-_{x^2-y^2}d^+_{z^2}d^-_{z^2}d^-_{yz}d^+_{xz}]\right\rangle=\frac{2\mathrm{i}}{\sqrt{3}}\zeta$$

The contribution to axial zero-field splitting is as follows:

$$\Delta E''(+1) =$$

$$-\frac{\left\langle {}^3B_1(+1) \left| H_{\mathrm{LS}} \right| {}^5A_{(a)}(+1) \right\rangle \left\langle {}^5A_{(a)}(+1) \left| H_{\mathrm{LS}} \right| {}^3B_1(+1) \right\rangle}{\left(E\left({}^5A_{(a)}\right) - E\left({}^3B_1\right)\right)}$$

$$-\frac{(\mathrm{i}\zeta)(-\mathrm{i}\zeta)}{\left(E\left({}^5A_{(a)}\right) - E\left({}^3B_1\right)\right)} = -\frac{\zeta^2}{\left(E\left({}^5A_{(a)}\right) - E\left({}^3B_1\right)\right)}$$

$$\Delta E''(0) =$$

$$-\frac{\left\langle {}^3B_1(0) \left| H_{\mathrm{LS}} \right| {}^5A_{(a)}(0) \right\rangle \left\langle {}^5A_{(a)}(0) \left| H_{\mathrm{LS}} \right| {}^3B_1(0) \right\rangle}{\left(E\left({}^5A_{(a)}\right) - E\left({}^3B_1\right)\right)}$$

$$-\frac{\left(\frac{2\mathrm{i}}{\sqrt{3}}\zeta\right)\left(-\frac{2\mathrm{i}}{\sqrt{3}}\zeta\right)}{\left(E\left({}^5A_{(a)}\right) - E\left({}^3B_1\right)\right)} = -\frac{4}{3}\frac{\zeta^2}{\left(E\left({}^5A_{(a)}\right) - E\left({}^3B_1\right)\right)}$$

$$D'' = \Delta E''(+1) - \Delta E''(0) =$$

$$-\frac{\zeta^2}{\left(E\left({}^5A_{(a)}\right) - E\left({}^3B_1\right)\right)} + \frac{4}{3}\frac{\zeta^2}{\left(E\left({}^5A_{(a)}\right) - E\left({}^3B_1\right)\right)} = \frac{1}{3}\frac{\zeta^2}{\left(E\left({}^5A_{(a)}\right) - E\left({}^3B_1\right)\right)}$$

So this quintet excited state adds another positive contribution to the overall zfs. The Ligfield calculation (see Table S24) suggests that this $^5A_{(b)}$ excited state is roughly 7000 cm^{-1} above the ground state, so its contribution to *D* is on the order of +4 cm^{-1}, using the same range of ζ values as above. As an aside, this is the total magnitude of *D* typically seen for high-spin d^4 complexes (e.g., 6-coordinate Mn(III)) wherein the ground state is similar to the $^5A_{(b)}$ excited state and the relevant excited state is similar to the $^3B_1$ ground state herein.[33] The *D* value calculated using the $^3B_{2,3(a,b)}$ and $^5A_{(b)}$ excited states is larger than that calculated by Ligfield using the entire d^6 basis set (see Table S25), e.g., ζ = 300 cm^{-1} gives $D \approx 70$ cm^{-1} by this perturbation theory, but only ~50 cm^{-1} using Ligfield; ζ = 400 cm^{-1} is needed to obtain $D \approx 75$ cm^{-1} in this exact calculation. Therefore, there are other excited states that play a role. For example, we have not considered the

triplet analogs to the five quintet states, which also involve electron occupation of the d_{xy} orbital, but maintaining triplet spin: $^3A_{(b,c)}$, $^3B_{1(b)}$, $^3B_{2(c)}$, $^3B_{3(c)}$. As can be seen in the Ligfield output (Table S24), these states, which are found at 16 000 – 18 000 cm^{-1} above the ground state, cannot be easily described by the expected, simple Slater determinants such as given below (only for M_S = +1):

$$^3B_{2(c)}(M_S = +1) = d^+_{x^2-y^2} d^-_{x^2-y^2} d^+_{z^2} d^-_{z^2} d^+_{yz} d^+_{xy}$$
$$^3B_{3(c)}(M_S = +1) = d^+_{x^2-y^2} d^-_{x^2-y^2} d^+_{z^2} d^-_{z^2} d^+_{xz} d^+_{xy}$$

The $^3B_{2,3(c)}$ (and to a lesser extent $^3A_{(b,c)}$) excited states do contribute to zfs, much less so than $^3B_{2,3(a,b)}$, but enough to be a possible source of the discrepancy between perturbation theory and an exact calculation. Singlet excited states have not been considered at all in the perturbation theory analysis, and these turn out to have a net *negative* contribution to zfs. This can be seen by comparison of Tables S24 (a) and (b), wherein the former uses the entire d^6 basis set, whilst the latter leaves out all of the free-ion singlet terms. For the same SOC, ζ = 400 cm^{-1}, D is ~7 cm^{-1} (~9%) larger when the singlets are omitted. The contribution of all of the quintet excited states can also be assayed in this manner. Table S25 (c) presents the results when only the triplet free-ion terms of d^6 are used. For completeness, Table S25 (d) gives the calculation using the free-ion triplet and singlet terms (i.e., leaving out only ^{5}D). The comparisons between (a) and (d) and between (b) and (c) show that the overall, positive contribution to D from the quintet excited states is ~10 cm^{-1}, indicating that the perturbation theory result for $^5A_{(a)}$ given above explains only about half of this effect. Nevertheless, the bulk of the D value arises from the contribution of only the $^3B_{2,3(b)}$ excited states. Thus this LFT model provides a reasonable and descriptive explanation for the large magnitude, positive zfs seen in $[Co^{III}(pin^F)_2]^-$ (**2**).

D′ for d^6 in Strong Field Based on CASSCF Wave Function

We can also use LFT and perturbation theory to rationalize the observed SH parameters using an electronic structure derived from the SA(3)-CASSCF(12,10) results. This technique allows for the inclusion of multi-configurational wave functions, and it allows for the A-symmetry orbitals ($3d_{z^2}$,$3d_{x^2-y^2}$) to mix. Here we only consider the $^3B_1$ ground state, and two of the triplet excited states ($^3B_2$, $^3B_3$). Taking only the dominant configurations in the CASSCF CI wave functions and approximating the CI coefficients, the wave functions can be defined as follows.

$$^3B_1\left(M_S=+1\right)=d^+_{x^2-y^2}d^-_{x^2-y^2}d^+_{z^2}d^-_{z^2}d^+_{xz}d^+_{yz}$$

$$^3B_1\left(M_S=0\right)=\frac{1}{\sqrt{2}}\left(d^+_{x^2-y^2}d^-_{x^2-y^2}d^+_{z^2}d^-_{z^2}d^+_{xz}d^-_{yz}+d^+_{x^2-y^2}d^-_{x^2-y^2}d^+_{z^2}d^-_{z^2}d^-_{xz}d^+_{yz}\right)$$

$$^3B_1\left(M_S=-1\right)=d^+_{x^2-y^2}d^-_{x^2-y^2}d^+_{z^2}d^-_{z^2}d^-_{xz}d^-_{yz}$$

$$^3B_2\left(M_S=+1\right)=-\sqrt{\frac{2}{3}}d^+_{x^2-y^2}d^-_{x^2-y^2}d^+_{z^2}d^+_{xz}d^-_{xz}d^+_{yz}+\sqrt{\frac{1}{3}}d^+_{x^2-y^2}d^+_{z^2}d^-_{z^2}d^+_{xz}d^-_{xz}d^+_{yz}$$

$$^3B_2\left(M_S=0\right)=\sqrt{\frac{1}{6}}\left(\begin{array}{l}-\sqrt{2}d^+_{x^2-y^2}d^-_{x^2-y^2}d^+_{z^2}d^+_{xz}d^-_{xz}d^-_{yz}-\sqrt{2}d^+_{x^2-y^2}d^-_{x^2-y^2}d^-_{z^2}d^+_{xz}d^-_{xz}d^+_{yz}\\+d^+_{x^2-y^2}d^+_{z^2}d^-_{z^2}d^+_{xz}d^-_{xz}d^-_{yz}+d^-_{x^2-y^2}d^+_{z^2}d^-_{z^2}d^+_{xz}d^-_{xz}d^+_{yz}\end{array}\right)$$

$$^3B_2\left(M_S=-1\right)=-\sqrt{\frac{2}{3}}d^+_{x^2-y^2}d^-_{x^2-y^2}d^-_{z^2}d^+_{xz}d^-_{xz}d^-_{yz}+\sqrt{\frac{1}{3}}d^-_{x^2-y^2}d^+_{z^2}d^-_{z^2}d^+_{xz}d^-_{xz}d^-_{yz}$$

$$^3B_3\left(M_S=+1\right)=-\sqrt{\frac{2}{3}}d^+_{x^2-y^2}d^-_{x^2-y^2}d^+_{z^2}d^+_{xz}d^+_{yz}d^-_{yz}-\sqrt{\frac{1}{3}}d^+_{x^2-y^2}d^+_{z^2}d^-_{z^2}d^+_{xz}d^+_{yz}d^-_{yz}$$

$$^3B_3\left(M_S=0\right)=-\sqrt{\frac{1}{6}}\left(\begin{array}{l}\sqrt{2}d^+_{x^2-y^2}d^-_{x^2-y^2}d^+_{z^2}d^-_{xz}d^+_{yz}d^-_{yz}+\sqrt{2}d^+_{x^2-y^2}d^-_{x^2-y^2}d^-_{z^2}d^+_{xz}d^+_{yz}d^-_{yz}\\+d^+_{x^2-y^2}d^+_{z^2}d^-_{z^2}d^-_{xz}d^+_{yz}d^-_{yz}+d^-_{x^2-y^2}d^+_{z^2}d^-_{z^2}d^+_{xz}d^+_{yz}d^-_{yz}\end{array}\right)$$

$$^3B_3\left(M_S=-1\right)=-\sqrt{\frac{2}{3}}d^+_{x^2-y^2}d^-_{x^2-y^2}d^-_{z^2}d^-_{xz}d^+_{yz}d^-_{yz}-\sqrt{\frac{1}{3}}d^-_{x^2-y^2}d^+_{z^2}d^-_{z^2}d^-_{xz}d^+_{yz}d^-_{yz}$$

With these wave functions, the non-zero matrix elements are as follows:

$$\left\langle {}^3B_2\left(0\right)\middle|\hat{H}_{SOC}\middle|{}^3B_1\left(+1\right)\right\rangle=\frac{\zeta}{12}\left(6+\sqrt{6}\right)$$

$$\left\langle {}^3B_3(0)\middle|\hat{H}_{SOC}\middle|{}^3B_1(+1)\right\rangle = -\frac{i\zeta}{12}\left(6+\sqrt{6}\right)$$

$$\left\langle {}^3B_2(+1)\middle|\hat{H}_{SOC}\middle|{}^3B_1(0)\right\rangle = -\frac{\zeta}{12}\left(6+\sqrt{6}\right)$$

$$\left\langle {}^3B_2(-1)\middle|\hat{H}_{SOC}\middle|{}^3B_1(0)\right\rangle = \frac{\zeta}{12}\left(6+\sqrt{6}\right)$$

$$\left\langle {}^3B_3(+1)\middle|\hat{H}_{SOC}\middle|{}^3B_1(0)\right\rangle = -\frac{i\zeta}{12}\left(6+\sqrt{6}\right)$$

$$\left\langle {}^3B_3(-1)\middle|\hat{H}_{SOC}\middle|{}^3B_1(0)\right\rangle = -\frac{i\zeta}{12}\left(6+\sqrt{6}\right)$$

$$\left\langle {}^3B_2(0)\middle|\hat{H}_{SOC}\middle|{}^3B_1(-1)\right\rangle = -\frac{i\zeta}{12}\left(6+\sqrt{6}\right)$$

We once again invoke second-order perturbation theory to include the contribution of the excited states into the ground state manifold.

$$\Delta E(+1) = \begin{pmatrix} -\dfrac{\left\langle {}^3B_1(+1)\middle|\hat{H}_{SOC}\middle|{}^3B_2(0)\right\rangle\left\langle {}^3B_2(0)\middle|\hat{H}_{SOC}\middle|{}^3B_1(+1)\right\rangle}{\Delta_{12}} \\ -\dfrac{\left\langle {}^3B_1(+1)\middle|\hat{H}_{SOC}\middle|{}^3B_3(0)\right\rangle\left\langle {}^3B_3(0)\middle|\hat{H}_{SOC}\middle|{}^3B_1(+1)\right\rangle}{\Delta_{13}} \end{pmatrix}$$

$$= -\frac{\frac{\zeta}{12}\left(6+\sqrt{6}\right)\frac{\zeta}{12}\left(6+\sqrt{6}\right)}{\Delta_{12}} - \frac{\left(\frac{i\zeta}{12}\left(6+\sqrt{6}\right)\right)\left(-\frac{i\zeta}{12}\left(6+\sqrt{6}\right)\right)}{\Delta_{13}}$$

$$= -\frac{\zeta^2}{144}\left(6+\sqrt{6}\right)^2\left(\frac{1}{\Delta_{12}}+\frac{1}{\Delta_{13}}\right)$$

$$\Delta E(0)=\begin{pmatrix} -\dfrac{\langle {}^3B_1(0)|\hat{H}_{SOC}|{}^3B_2(+1)\rangle\langle {}^3B_2(+1)|\hat{H}_{SOC}|{}^3B_1(0)\rangle}{\Delta_{12}} - \dfrac{\langle {}^3B_1(0)|\hat{H}_{SOC}|{}^3B_2(-1)\rangle\langle {}^3B_2(-1)|\hat{H}_{SOC}|{}^3B_1(0)\rangle}{\Delta_{12}} \\ -\dfrac{\langle {}^3B_1(0)|\hat{H}_{SOC}|{}^3B_3(+1)\rangle\langle {}^3B_3(+1)|\hat{H}_{SOC}|{}^3B_1(0)\rangle}{\Delta_{13}} - \dfrac{\langle {}^3B_1(0)|\hat{H}_{SOC}|{}^3B_3(-1)\rangle\langle {}^3B_3(-1)|\hat{H}_{SOC}|{}^3B_1(0)\rangle}{\Delta_{13}} \end{pmatrix}$$

$$= -\begin{pmatrix} \dfrac{\frac{-\zeta}{12}\left(6+\sqrt{6}\right)\frac{-\zeta}{12}\left(6+\sqrt{6}\right)}{\Delta_{12}} + \dfrac{\frac{\zeta}{12}\left(6+\sqrt{6}\right)\frac{\zeta}{12}\left(6+\sqrt{6}\right)}{\Delta_{12}} \\ + \dfrac{\left(\frac{i\zeta}{12}\left(6+\sqrt{6}\right)\right)\left(-\frac{i\zeta}{12}\left(6+\sqrt{6}\right)\right)}{\Delta_{13}} + \dfrac{\left(\frac{i\zeta}{12}\left(6+\sqrt{6}\right)\right)\left(-\frac{i\zeta}{12}\left(6+\sqrt{6}\right)\right)}{\Delta_{13}} \end{pmatrix}$$

$$= -\frac{\zeta^2}{72}\left(6+\sqrt{6}\right)^2\left(\frac{1}{\Delta_{12}}+\frac{1}{\Delta_{13}}\right)$$

We thus have the following expression for *D*:

$$D=\frac{\zeta^2}{144}\left(6+\sqrt{6}\right)^2\left(\frac{1}{\Delta_{12}}+\frac{1}{\Delta_{13}}\right)\approx\frac{\zeta^2}{2}\left(\frac{1}{\Delta_{12}}+\frac{1}{\Delta_{13}}\right)$$

If we ignore rhombicity such that we assume $\Delta_{12}=\Delta_{13}$, we thus can reduce the above expression to

$D\approx\frac{\zeta^2}{\Delta}$, thus making the ZFS inversely proportional to the energy gap between the ground state and the $^3B_{2,3}$ states.

Using the energies of the Δ_{12} and Δ_{13} gaps calculated at the SA(3)-NEVPT2(12,10) (2272.8/3801.6 cm^{-1}) level and the exact expression for the ZFS ($D=\frac{\zeta^2}{144}\left(6+\sqrt{6}\right)^2\left(\frac{1}{\Delta_{12}}+\frac{1}{\Delta_{13}}\right)$), a value of 300 cm^{-1} for ζ predicts a ZFS of 31 cm^{-1}. To get to a ZFS between 65 and 75 cm^{-1}, ζ must range between 435 and 465 cm^{-1}.

Turning to the rhombicity, using the above guidelines, the expression for the rhombic SH parameter *E* is as follows:

$$E = \frac{\zeta^2 \left(7 + 2\sqrt{6}\right)}{24} \left(\frac{1}{\Delta_{12}} - \frac{1}{\Delta_{13}} \right)$$

As expected, if $\Delta_{12} = \Delta_{13}$ this term is zero and there is no rhombicity expected. From the SA(3)-NEVPT2(12,10) results (and all computational protocols explored), there is a large difference between the Δ_{12} and Δ_{13} energies. If we plug in the SA(3)-NEVPT2(12,10) results using a SOC constant of 435 cm^{-1}, the rhombic SH parameter is 16.60 cm^{-1}, or $|E/D| = 0.252$.

We thus see here that it is also possible to use the wave functions derived from CASSCF results to obtain analytical expressions for the ZFS Spin-Hamiltonian parameters that can be connected to ligand field theory.